Quantifying the dynamics of viruses and the cellular immune response of the host

Cover © Bart van der Leck: "De storm" (The tempest), 1916, oil on canvas, c/o Pictoright Amsterdam 2009; Collection Kröller-Müller Museum, Otterlo.

Print Ipskamp Drukkers

ISBN 978-90-393-5039-3

Quantifying the dynamics of viruses and the cellular immune response of the host

Kwantificatie van de dynamiek van virussen en de cellulaire immuunreactie van de gastheer
(met een samenvatting in het Nederlands)

Quantifizierung der Dynamik von Viren und der zellulären Immunantwort des Wirtes
(mit einer Zusammenfassung in deutscher Sprache)

Proefschrift

ter verkrijging van de graad van doctor aan de Universiteit Utrecht op gezag van de rector magnificus, prof. dr. J.C. Stoof, ingevolge het besluit van het college voor promoties in het openbaar te verdedigen op vrijdag 26 juni 2009 des middags te 4.15 uur

door

Christian Lorenz Althaus

geboren op 2 november 1978 te Wattwil, Zwitserland

Promotor: Prof. dr. R.J. De Boer

The work in this thesis was financially supported by the Netherlands Organisation for Scientific Research (NWO) (VICI grant 016.048.603).

With your feet in the air and your head on the ground
Try this trick and spin it, yeah
Your head will collapse
If there is nothing in it
And you will ask yourself

Where is my mind
Where is my mind
Where is my mind

The Pixies (1988)

Contents

1 General Introduction **1**
- 1.1 Infectious diseases . . . 1
  - 1.1.1 Acute and chronic viral infections . . . 1
- 1.2 Immune responses . . . 2
  - 1.2.1 Cytotoxic T lymphocytes . . . 2
  - 1.2.2 Immune escape . . . 3
- 1.3 Mathematical and computational modeling . . . 4
  - 1.3.1 Historical overview . . . 4
  - 1.3.2 Integrating virus dynamics and immune responses . . . 6
  - 1.3.3 New challenges for modeling . . . 6
- 1.4 Outline of this thesis . . . 8

2 Intracellular transactivation of HIV and its influence on the virus dynamics during drug therapy **11**
- 2.1 Introduction . . . 12
- 2.2 Results . . . 13
  - 2.2.1 Viral activation and reversion into latency . . . 13
  - 2.2.2 Basal transcription rates govern activation of latently infected cells . . . 18
- 2.3 Discussion . . . 21
- 2.4 Methods . . . 22
  - 2.4.1 Intracellular transactivation circuit . . . 22
  - 2.4.2 From probability densities to age-dependent rates . . . 24
  - 2.4.3 Dynamics of virus and latently infected cells during drug therapy . . . 25

3 Reassessing the HIV-1 life cycle through age-structured modeling: lifespan of infected cells, viral generation time and R_0 **27**
- 3.1 Introduction . . . 28
- 3.2 Model . . . 29
  - 3.2.1 Drug treatment . . . 30
- 3.3 Results . . . 32
- 3.4 Discussion . . . 36
- 3.5 Appendix . . . 39
  - 3.5.1 The special case of protease inhibitors . . . 39
  - 3.5.2 Infected cell death: Rates, probability densities and survival 39
  - 3.5.3 Lifespan and generation time . . . 40
  - 3.5.4 Basic reproductive number R_0 . . . 42
- 3.6 Supplemental material . . . 44

4 Dynamics of CD8$^+$ T cell responses during acute and chronic lymphocytic choriomeningitis virus infection **49**
4.1 Introduction . . . 50
4.2 Materials and Methods . . . 51
4.3 Results . . . 53
4.3.1 CD8$^+$ T cell responses during acute and chronic LCMV infection . . . 53
4.3.2 Dynamics of CD8$^+$ T cell responses in thymectomized mice 56
4.3.3 Comparing data of CD8$^+$ T cell responses between laboratories . . . 57
4.4 Discussion . . . 61

5 Dynamics of immune escape during HIV/SIV infection **65**
5.1 Introduction . . . 66
5.2 Model . . . 66
5.3 Results . . . 69
5.3.1 Sequential escape from several CTL clones . . . 69
5.3.2 Rates of escape . . . 73
5.3.3 Immunodominance and viral evolution . . . 75
5.4 Discussion . . . 75
5.5 Methods . . . 78
5.5.1 Stochastic events . . . 78
5.5.2 Viral fitness . . . 79
5.5.3 Estimating rates of escape . . . 79
5.5.4 Killing terms . . . 80

6 Intracellular delays and multiple infection of cells impede immune evasion in HIV **83**
6.1 Introduction . . . 84
6.2 Model . . . 85
6.2.1 Multiple infections of cells . . . 85
6.2.2 Intracellular delay . . . 86
6.3 Results . . . 87
6.3.1 HIV dynamics with multiple infections of cells . . . 87
6.3.2 Emergence of immune escape . . . 88
6.3.3 Intracellular delay and the rate of escape . . . 90
6.4 Discussion . . . 92

7 CTL killing mediated early during the intracellular eclipse phase explains large variations in HIV set-point levels **95**
7.1 Introduction . . . 96
7.2 Model . . . 97
7.3 Results . . . 98
7.3.1 Early vs. late killing of HIV-infected cells . . . 98
7.3.2 Set-point viral load . . . 98

7.3.3 Reproducing experimental observations of HIV dynamics 101
7.4 Discussion 104
7.5 Appendix 107
7.5.1 Influence of cell death on virus production 107
7.5.2 Viral load decay slopes 107
7.5.3 CTL-mediated killing of infected cells 108
7.5.4 Proliferation of CTL effector cells 108
7.5.5 Non-cytotoxic mechanisms of $CD8^+$ T cells 108

8 Discussion and Outlook **111**
8.1 Estimating the turnover of HIV-1 111
8.2 CTL-mediated control of chronic infections 112
8.3 Quantifying immune escape in HIV 114
8.4 Of mice and men: some general principles 115

Bibliography **119**

Samenvatting **141**

Zusammenfassung **143**

Curriculum Vitæ **145**

List of Publications **147**

General Introduction

1

1.1 INFECTIOUS DISEASES

Infectious 'organisms' are capable of entering a susceptible host where they start to propagate and eventually spread to a new host. The causative agents of an infection can be diverse, ranging from viruses to microbes such as bacteria, fungi or parasites and even proteins known as prions. Relatively few of these infections cause host pathology because their virulence is low. However, some infections are detrimental to the hosts fitness and result in a clinically evident disease.

Viruses are unable to replicate on their own and therefore infect cells where they can manipulate the cellular machinery. They generate an adequate environment to make more copies of themselves or even integrate their genomic information into the host DNA. The viral life cycle begins with the infection of a cell where they replicate intracellularly before newly generated viral particles can be released to infect a secondary cell. To prevent the viruses from unlimited replication, the infected hosts have evolved diverse mechanisms of the immune system to counter against. All the different steps during the viral life cycle can be under attack by these defense mechanisms. Depending on the ability of the hosts immune response to fight the infectious agent, some viral infections are only acute and cleared shortly after they infected a host. Other viruses can persist in the host and cause a chronic state of infection.

1.1.1 *Acute and chronic viral infections*

Acute viral infections such as influenza or the common cold cause a more or less severe pathogenic state early after infection but are usually cleared by the hosts immune system. Often, they replicate so fast that they might run out of resources when the immune system starts to attack them. Very pathogenic viruses that frequently cause deadly diseases, such as severe acute respiratory syndrome (SARS) or Ebola, probably kill their infected hosts too rapidly before the infection can be controlled by the immune system. Generally, acute infections are transmitted easily because they experience only a short transmission period in an infected host.

On the other hand, chronic viral infections persist in the host through ongoing replication. Many humans are infected with different chronic viruses that can eventually cause a disease. For example, hepatitis can lead to a chronic infection that eventually causes liver disease. Human immunodeficiency virus (HIV) infection typically leads to acquired immunodeficiency syndrome (AIDS). To date, it is unclear what causes a virus to be acute or chronic. Chronic viruses

could have evolved strategies to evade the different attacks by the hosts immune system. But since chronic infections often cause a transient non-pathogenic (i.e., disease-free) period, it might be the immune system that decides to tolerate the infection, which would otherwise be hard to eradicate completely from the host.

1.2 IMMUNE RESPONSES

The vertebrate immune system[1] has evolved remarkable defense mechanisms that can counter against an infection. Through numerous molecules and cell types that act in a highly dynamic network, it is capable to recognize and eliminate invading pathogens. Innate immunity provides a range of evolutionary conserved defense mechanisms as a first rapid response upon the onset of an infection. They can range from non-specific physiological responses like fever, to more specific molecules such as toll-like receptors (TLRs) that recognize conserved structures on pathogens. In order to respond with a higher specificity to more subtle differences between pathogens, the adaptive immune system comes into play. It is capable of recognizing a much greater diversity of foreign molecules, so-called antigens, but only at the cost that the response builds up slowly upon infection.

Adaptive immunity is based on a large diversity of lymphocytes that are derived from stem cells in the bone marrow. B lymphocytes express a unique antigen-binding molecule on its membrane, the antibody. If a B lymphocytes recognizes a foreign structure with the antibody, it proliferates and maturates to secrete antibodies with an even higher affinity to the antigen. On the other hand, T lymphocytes only recognize antigen that has been processed, i.e., that was internalized or originates from a cell and is subsequently presented on the surface.

1.2.1 *Cytotoxic T lymphocytes*

After infection of a cell, small fragments of virus-derived peptides will be processed by the antigen presentation pathway and subsequently presented on the surface of an infected cell (Fig. 1.1). As a complex with the polymorphic major histocompatibility (MHC) class I molecule, different viral epitopes can then be recognized by specific receptors on T lymphocytes. After a naive $CD8^+$ T cell encounters antigen that is presented on an MHC class I molecule, it starts to proliferate and differentiate into various effector T cells. Cytotoxic T lymphocytes (CTLs) are one type of effector T cells that are crucial for the elimination of virus-infected cells. Different viral epitopes can be recognized by different CTL 'clones', depending on the affinity of their specific T-cell-receptor to the peptide-MHC complex. Upon recognizing an infected cell, a CTL can induce lysis of the cell through the release of cytotoxins such as perforin, which forms pores in the cell membrane and eventually induces apoptosis of the infected cell.

[1] For a detailed overview we refer to Goldsby et al. (2003).

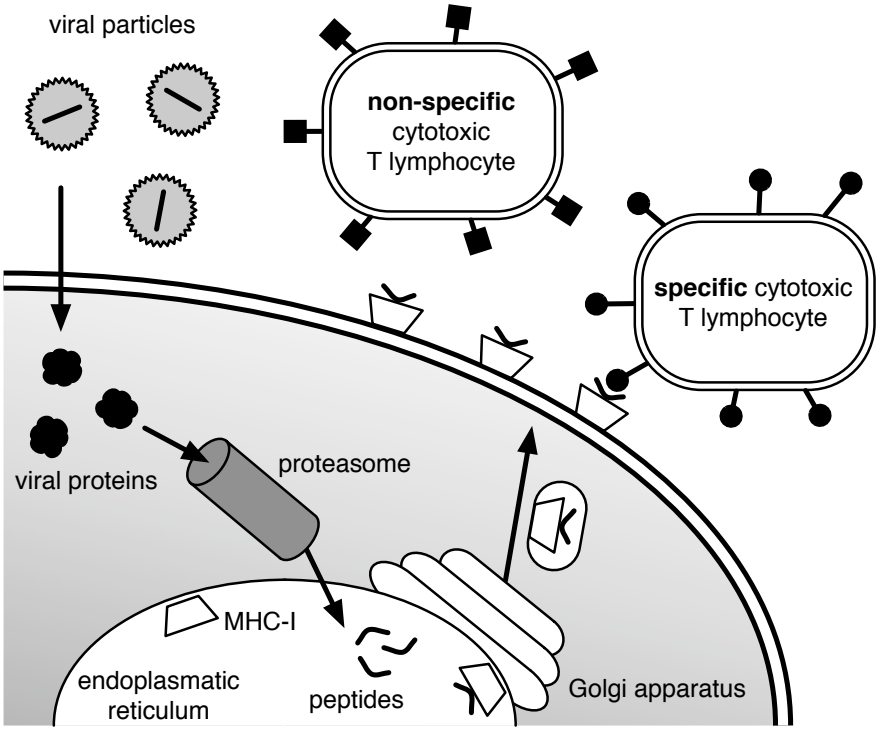

Figure 1.1 Illustration of the antigen presentation pathway and the recognition of virus-infected cells by cytotoxic T lymphocytes (CTLs). Viral proteins are cleaved by the (immuno-)proteasome into small fragments of 8 to 10 peptides and are transported into the endoplasmatic reticulum (ER) where they are loaded onto MHC class I molecules which are then transported through the Golgi apparatus to the cell surface. The peptide-MHC complexes can be recognized by antigen-specific CTLs that subsequently mediate cytotoxic killing of the virus-infected cells.

After a cell has been eliminated, the CTL swarms around in its neighborhood monitoring other infected cells to which it could deliver a lethal hit.

1.2.2 *Immune escape*

Viruses that can persist in the face of a strong CTL response often evade recognition by altering their epitopes. In the case of RNA viruses, the highly error prone transcription inevitably results in a high genetic variability (Holland et al., 1982). Mutations within or in proximity of epitopes can interfere with the processing of viral peptides and/or the antigen presentation. Many of these mutations are detrimental to the viral replication, but if they reduce the affinity or even prevent the recognition of the peptide-MHC complexes by the CTL

clones, they can become selected during the course of an infection. Viral escape from CTL responses was first demonstrated in mice that were infected with lymphocytic choriomeningitis virus (LCMV) (Pircher et al., 1990). Later and not surprisingly, the virus with the highest mutation rate found in nature, HIV (Mansky and Temin, 1995), has been observed to frequently evade immune recognition (Phillips et al., 1991). By now, immune escape in HIV is found to be strongly associated with progression to AIDS (Altfeld and Allen, 2006).

1.3 MATHEMATICAL AND COMPUTATIONAL MODELING

A model is an abstract representation of a system. Much like the painting "De storm" by the Dutch artist Bart van der Leck (Fig. 1.2), scientific models try to capture the relevant parts of a whole. As a founder of the De Stijl[2] art movement, van der Leck put emphasis on abstraction and universality in his paintings. He did so by a reduction to the essential forms and colors. A viewer only captures the main objects of the scenery: two people walking along a sand dune at the coast. It is stormy weather, illustrated by the seesawing ship and the waving coats of the people. However, the gender of the two persons cannot be identified. Apparently, this does not matter for the main purpose of the painting: to illustrate a storm at the Dutch coast. Models in biology and medicine follow a similar concept. Due to the vast complexity of the system under consideration, a model is a simplified abstraction of the components that are of interest. The purpose is to understand the relevant features of the system, not every detail. Universality is also an important concept of models. By using the formal language of mathematics or computational rules and algorithms, models can be generalized and applied to related systems. In the following, we give a historical overview of mathematical and computational models that have been successfully used in virology and immunology.

1.3.1 *Historical overview*

The dynamics of a replicating virus within a host can be described with models of population dynamics that originated from mathematical ecology and epidemiology. One of the first attempts to describe and understand the dynamics of natural populations was made in Italy after the First World War. Vito Volterra, a professor in mathematical physics in Rome, devised a simple model of ordinary differential equations (ODEs) to understand the change in fishing yield of the Adriatic sea during wartime (Volterra, 1926). The famous predator-prey dynamics was born, now known as the Lotka-Volterra equations[3]. Shortly afterwards, Kermack and McKendrick (1927) devised a related model to describe an epidemic disease outbreak. Known as the SIR model, they took into account a

[2] From the Dutch "The Style". Also known as neoplasticism, a Dutch artistic movement founded in 1917.

[3] Alfred J. Lotka was a US mathematician who published the same model in Lotka (1925) independently.

Figure 1.2 De storm (The tempest), 1916, oil on canvas; Collection Kröller-Müller Museum, Otterlo. The painting by the Dutch artist Bart van der Leck (1876, Utrecht - 1958, Blaricum) illustrates the nature of mathematical and computational modeling in biology and medicine: abstraction and universality.

population of susceptibles, infected and recovered hosts. Mathematical modeling of infectious diseases has since then established itself as an important field to study the spread of diseases in animal and human populations (Anderson and May, 1991; Diekmann and Heesterbeek, 2000; Keeling and Rohani, 2008).

Virus dynamics modeling

During the 1980's, HIV had been recognized as a new virus in the human population (Barre-Sinoussi et al., 1983). The elusive chronic nature of HIV that is reflected in the long infected period of a patient raised important questions about the within-host dynamics of viruses. The framework of population dynamics that has been developed for between-host studies proved to be suitable to study this new and deadly disease (Nowak et al., 1990; McLean and Kirkwood, 1990; Perelson et al., 1993). Eventually, this has led to the successful story of within-host virus dynamics modeling during the 1990's. Mathematical models of viral dynamics during drug therapy were used to derive the turnover of HIV-1 within infected patients (Ho et al., 1995; Wei et al., 1995)

and to describe the evolution of drug-resistant viral variants (Bonhoeffer et al., 1997). More recently, models have given insights into stochastic (Ribeiro and Bonhoeffer, 1999; Kouyos et al., 2006) and population genetic effects (Bretscher et al., 2004; Althaus and Bonhoeffer, 2005), rising questions about the evolution of recombination in retroviruses (Bonhoeffer et al., 2004).

Immune system modeling

Concurrently with the advanced understanding of the vertebrate immune system in the 1970's, the first conceptual models of the immune system were developed by Bell et al. (1978). For CTL responses, the notion became accepted that naive $CD8^+$ T cells become stimulated by viral antigen and follow a differentiation program. This implies that CTLs can be modeled as a set of growing populations which has ended in a series of models that describe the proliferation of $CD8^+$ T cells (De Boer and Perelson, 1995, 1998; Bocharov, 1998; Antia et al., 2003). Some of which have been applied to describe experimental data (De Boer et al., 2001, 2003; Kohler, 2007). The field of immune system modeling has since progressed substantially, exemplified by a recent computational model that describes the movement of T cells within lymph nodes (Beltman et al., 2007).

1.3.2 *Integrating virus dynamics and immune responses*

CTLs are considered to be one of the most important arms of the immune system to control viral infections. Hence, it is of interest to derive mathematical and computational models that integrate both the dynamics of a virus and the CTLs that can mediate killing of the infected cells (Nowak and May, 2000; Wodarz, 2007). This approach has given new insights into the nature of acute and chronic viral infections (Alizon and van Baalen, 2008), virus evolution (Regoes et al., 1998), the efficacy of $CD8^+$ T cell vaccination (De Boer, 2007) and the process of immune escape (Nowak et al., 1995).

Despite all progress, crucial questions remain open. The factors that determine clearance or control of viral infections are still not well understood. In the case of the chronic infection caused by HIV, it is still a matter of debate as to what extent the cellular immune response is able to control the viral replication. For example, although the virus frequently escapes recognition by the CTL response, this process appears to be slow, which suggests that the selective advantage of virus variants that are not recognized by a specific CTL clone is minor (Asquith et al., 2006). These discrepant findings call for a more quantitative approach to study the dynamical processes between viruses and the cellular immune response.

1.3.3 *New challenges for modeling*

In recent years, a deeper understanding of the molecular and cellular processes of virus replication and CTL-mediated killing has been gained. After viral entry,

an infected cell goes through several stages, such as viral transcription and translation, before new virus particles are released from the cell membrane. Although the detailed characterization of the HIV life cycle within an infected cell has given insights into the kinetics of virus replication, several of theses processes and how they affect the virus dynamics are ambiguous. For example, it is unclear at what time a cell is most prone to become a target for CTL-mediated killing after it was infected with a virus.

Intracellular reactions of the HIV life cycle have been investigated mathematically (Reddy and Yin, 1999). The influence of the intracellular kinetics on the extracellular dynamics, i.e., the virus dynamics within a host, is not well understood, however. Novel systems biology approaches that aim to decipher the intracellular regulation of HIV gene expression have become more popular within the last years (Weinberger et al., 2005; Burnett et al., 2009). These approaches have shown how intracellular reactions and molecular noise can determine the state of an infected cell. One goal of systems biology is to investigate and describe how processes within single cells give rise to the complex behavior of whole cell populations. In the case of virus dynamics, a higher resolution to describe infected cell populations can be achieved by splitting them into several stages. Separating an infected cell population into an 'early' and 'late' stage, e.g., by including an intracellular delay before the cell starts to produce viral particles, is one method to integrate intracellular properties of the viral life cycle. Partial differential equations (PDEs) are another framework that allows to structure a population according to its age, e.g., the time that has passed since a cell was infected (Kirschner and Webb, 1996; Nelson et al., 2004). In order to incorporate properties of the intracellular life cycle into virus dynamics models, both of these methods will be introduced and applied in this thesis.

To study the impact of the cellular immune response on the virus dynamics, it is necessary to quantify the process of CTL-mediated killing of infected cells. For example, the number of cells that belong to a specific CTL clone might be crucial to investigate the selective impact of a single clone on the viral replication. Numbers of $CD8^+$ T cells can be tracked with MHC tetramers. After a host has been infected with a virus, this method allows to follow the dynamics of single T cell clones that are subject to a proliferation program. It can be seen that the $CD8^+$ T cell clones exhibit an immunodominance pattern, i.e., the size of the clones is unequally distributed. This emphasizes the idea that CTL clones can induce different selection strength on the viral population. Adapting the notion mentioned above, that infected cells move through different stages of their life cycle, it is interesting to investigate which stages during the viral life cycle are most prone to CTL-mediated killing and how this would influence the virus dynamics.

All together, a series of open questions remain in the field of virus dynamics, especially to what extent the cellular immune response can control a chronic viral infection. Modeling approaches that aim for a higher resolution of individual processes, which can be achieved by structuring populations to different classes, are promising to bring new insights into the processes that affect the

dynamics of viruses and the role of the cellular immune response.

1.4 OUTLINE OF THIS THESIS

In this thesis, we use a series of mathematical and computational models to investigate the dynamics of viruses and the cellular immune responses they evoke. One attempted goal is to move towards a more quantified understanding of the process of viral replication and the interaction of viruses with the CTL responses of their hosts.

We start in **Chapter 2** with an intracellular description of the circuit that activates HIV-infected cells and renders them into virus-producing cells. Stochastic fluctuations within a cell influence the dynamics of virus replication within a host and we can show how this can give rise to the dynamics that has been observed in HIV-infected patients that are under antiretroviral drug therapy. To describe the different stages of a virus-infected cell, we use an age-structured model in **Chapter 3** to investigate the viral turnover within an infected host. By fitting the model to previously published data, we can derive new estimates of the turnover of HIV-1 within a patient and suggest that the rate at which an infected cell produces virus can increase with the age of the cell.

In order to discriminate between $CD8^+$ T cell responses against acute and chronic viral infections, we fit a mathematical model to previously published data of LCMV infection in mice (**Chapter 4**). We observe different dynamics of the T cell responses, depending on whether mice have been infected with acute or chronic LCMV, and estimate the kinetics of the response. Chronic viral infections are under constant selection pressure by the CTL response and we investigate this process during HIV and simian immunodeficiency virus (SIV) infection in **Chapter 5**. We show how the immunodominance pattern of different CTL clones affects the long-term dynamics of immune escape. Quantifying immune escape from the CTL responses gives important insights into the selective pressure they induce on the viral replication. In **Chapter 6**, we investigate the influence of specific properties of the HIV life cycle, such as multiple infection of cells and intracellular delays, on the process of immune escape. The stage of an infected cell at which it is prone to CTL-mediated killing is important for the ability to suppress the viral load. Based on recent experimental data, we illustrate in **Chapter 7** that if HIV-infected cells are killed early during the intracellular eclipse phase, CTLs can suppress the virus replication to very low levels.

In **Chapter 8**, we bring the results of the different chapters together and discuss our findings on quantitative aspects of virus dynamics and the impact of the cellular immune response on viral replication. First, we re-evaluate the rapid turnover of HIV-1-infected cells *in vivo*. Second, the possible impact of the CTL response on the viral dynamics and its potential to control an HIV-infection within a patient is critically discussed. Third, we shortly discuss the implications of our findings on the interpretation of immune escape and CTL-mediated killing in HIV. Lastly, we describe quantitative aspects of virus replication and

the cellular immune response in a broader sense and speculate about the nature of chronic viral infections in different host species.

Intracellular transactivation of HIV and its influence on the virus dynamics during drug therapy

2

C.L. Althaus and R.J. De Boer
Theoretical Biology, Utrecht University
Padualaan 8, 3584 CH Utrecht, The Netherlands.

manuscript submitted

ABSTRACT

Basic virus dynamics models have been essential in understanding quantitative issues of HIV replication. Several parts of the viral life cycle remain elusive, however. One of the most critical steps is the start of viral transcription, which is governed by the regulatory protein Tat that induces a positive feedback loop. It has been shown that this feedback loop can alternate between two states leading to a transient activation of viral transcription. Using Monte Carlo simulations, we integrate the transactivation circuit into a new virus dynamics model having an age-dependent transactivation rate and reversion into latency. The cycling of infected cells between an activated and latent state results in the typical decelerating decay of virus load following therapy. Further, we hypothesize that the activation of latently infected cells is governed by the basal transcription rate of the integrated provirus rather than the intra- or extracellular environment. Finally, the incorporation of intracellular reaction networks into the extracellular virus dynamics offers a promising new framework to analyze and understand the nature of viral infections.

2.1 INTRODUCTION

Within-host virus dynamics has traditionally been investigated with mathematical models that describe events happening between different compartments on the extracellular level. To analyze the population dynamics of infected cells and virus particles, ordinary differential equations (ODEs) are widely used, and have given important insight into the dynamics of viral infections within a host (Nowak and May, 2000; Perelson, 2002). In contrast, intracellular models have been used to describe the viral life cycle within a cell to analyze properties such as viral production or the interference of antiviral drugs with viral replication (Eigen et al., 1991; Reddy and Yin, 1999; Regoes et al., 2005). Connecting the dynamics of the intracellular virus replication with an extracellular description of virus dynamics is challenging and, to our knowledge, only recently came to attention (Haseltine et al., 2005, 2008).

It is of general interest to know how the intracellular dynamics of virus replication in a single cell affects the extracellular behavior of virus dynamics. Usually, one assumes populations to be homogeneous to model the dynamics of infected cells. However, theoretical and experimental studies have shown how intrinsic noise in single cells can give rise to heterogeneous cell populations (McAdams and Arkin, 1997; Elowitz et al., 2002). Stochasticity that arises when molecule numbers are low and their reaction rates are slow can result in delays and different intracellular states of a cell. Heterogeneous cell populations can, to a certain extent, be described with age-structured models that use partial differential equations (PDEs) in order to structure a cell population according to the age of the cells, e.g., the time that has passed since the cells were infected with a viral particle. Age-structured models have been used in virus dynamics modeling (Kirschner and Webb, 1996; Nelson et al., 2004) but the direct connection of intracellular reactions to the property of an infected cell has been difficult to achieve.

In HIV, the protein Tat (trans-activator of transcription) has been found to play a major role within an infected cell where it induces viral transcription through a positive feedback loop (Karn, 1999). Additionally, it has been shown that the feedback loop can alternate between two states, i.e., a cell that has been transactivated can revert back into a latent state (Weinberger et al., 2005). The viral reservoir of latent cells is considered to be one of the major barriers to eradicate HIV from an infected patient (Lassen et al., 2004a; Han et al., 2007). In patients on highly active antiretroviral therapy (HAART), the pool of latent infected cells declines very slowly (Siliciano et al., 2003), and low-level viremia persists over years (Palmer et al., 2008). Hence, it is critically important to understand the generation and maintenance of latent infected cells in order to propose treatment strategies that could eradicate this pool.

The majority of the pool of latently infected cells consists of resting $CD4^+$ T cells (Chun et al., 1997). It is unclear how viral latency is determined and it has been suggested that the availability of cellular transcription factors might play a role (Lassen et al., 2004a). However, different forms of viral transcripts have

also been found in resting $CD4^+$ T cells, highlighting that latency is not due to a complete transcriptional block but to an insufficient amount of transcripts and regulatory proteins, such as Tat (Lassen et al., 2004b). Since HIV mainly replicates in activated $CD4^+$ T cells, it is generally believed that resting $CD4^+$ T cells containing an HIV provirus need to be activated by extrinsic factors. Antigenic stimulation has been suggested as a mechanism at which latent infected cells can become activated (Gunthard et al., 2000) whereas the slow decay dynamics of the latent infected cell pool has been related to the long lifespan of resting and memory $CD4^+$ T cells (Finzi et al., 1999; Siliciano et al., 2003; Strain et al., 2003). Mathematical studies have investigated the dynamics of latent infected cells in HIV but could not decipher the mechanism of activation and reversion (Muller et al., 2002; Kim and Perelson, 2006; Sedaghat et al., 2008).

Here, we apply the intracellular model of HIV transactivation as presented in Weinberger et al. (2005) to understand the processes of viral activation and reversion into latency. We derive the transition rates of these processes to describe a heterogeneous cell population. We find that the basal transcription rate of the HIV provirus is the critical process that determines activation from viral latency. By taking into account a conventional distribution of basal transcription rates that can arise through insertion of the provirus at a random position, we can account for the typical decay dynamics of HIV after antiretroviral drug therapy. Thus, our results highlight that the activation of latent infected cells in HIV might be dictated by intrinsic viral factors rather than the intra- or extracellular environment.

2.2 RESULTS

2.2.1 *Viral activation and reversion into latency*

A central core of the HIV life cycle is the transactivation of viral transcription (Fig. 2.1). After a virus particle infects a cell, reverse transcription occurs and the provirus is integrated into the host DNA, where it becomes subject to basal transcription. Viral transcripts are translated into the regulatory protein Tat that gets re-imported into the nucleus where it elevates the transcription rate of the viral DNA (for a more detailed description see *Methods*). This circuit implies a positive feedback of viral transcription (transactivation) that can eventually result in a sufficient amount of viral proteins to generate new viral particles. A recent study has shown that this central core of the intracellular life cycle is critically important to activate viral transcription (Weinberger et al., 2005). It was shown in experiments, that depending on the intracellular concentration of the protein Tat, the cell is able to switch between a highly transactivated and a resting or latent state. Stochastic computer simulations of transactivation were used to analyze the intracellular circuit were found to agree with the experimental results (Weinberger et al., 2005).

We investigate a modified version of the computational model presented in Weinberger et al. (2005) to derive stochastic simulations for the transactivation

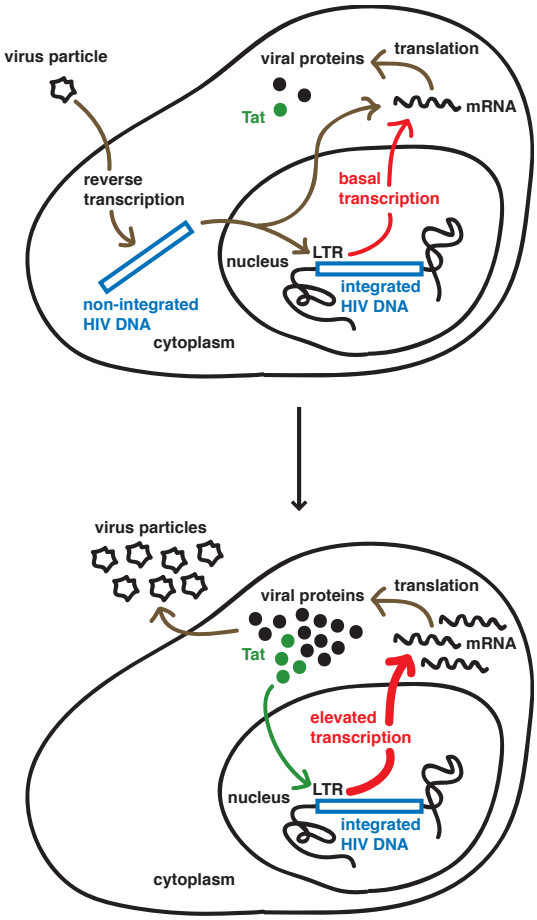

Figure 2.1 HIV replication life cycle. After infection of a cell, viral RNA is transcribed into a linear DNA provirus that is imported into the nucleus. Before integration at a semi-random position into the host DNA, pre-integration transcripts can be produced. After integration, the provirus is subject to basal transcription that generates RNA, which is translated into Tat and other viral proteins (top). In a positive feedback loop, Tat gets re-imported into the nucleus to elevate the transcription rate resulting in more mRNA and subsequently more viral proteins that can give rise to new viral particles which are budding of the cell membrane (bottom).

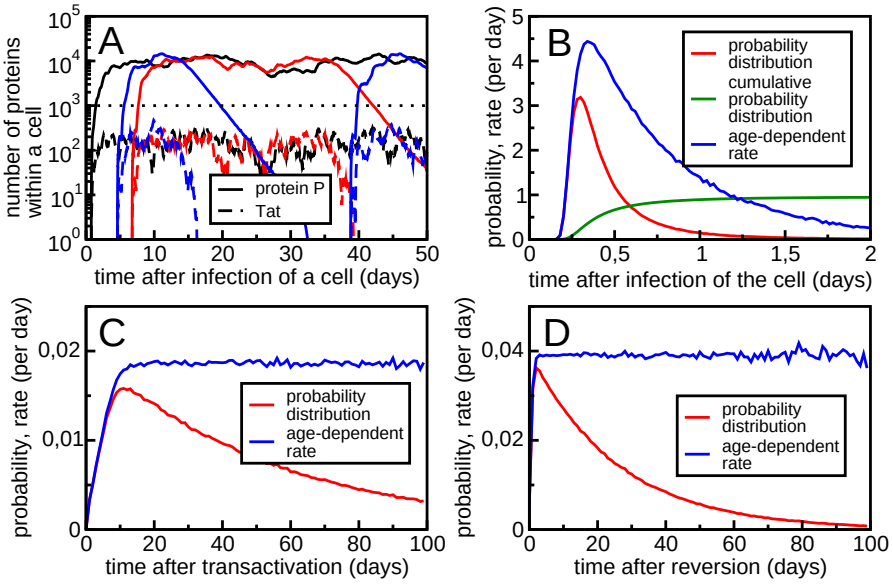

Figure 2.2 Tat induces transcriptional activation and reversion into latency. (A) Representative time plots from stochastic simulation runs of three HIV-infected cells. Each color depicts the concentration of protein P (solid lines) and protein Tat (dashed lines) within one infected cell. The dotted line indicates the threshold of transactivation. (B) Probability distribution and age-dependent rate of transactivation. A small amount of pre-integration transcripts ($mRNA_n(0) = 5$) results in early transactivation of HIV-infected cells. (C) Probability distribution and age-dependent rate of reversion. After a time window of a few days, the transactivated cells revert into a latent state at a constant rate (blue line). (D) Probability distribution and age-dependent rate of transactivation of latently infected cells. Reactivation of latently infected cells is determined by the slowest process in the transactivation circuit (basal transcription) and therefore occurs at a constant rate. $LTR = 1$ and all other species are zero except otherwise indicated. $k_b = 10^{-6}$ s^{-1} for all simulations.

and reversion of HIV-infected cells (see *Methods*). Time plots of representative simulations show the individual behavior of single cells infected with HIV (Fig. 2.2A). Concomitantly with the increase of the regulatory protein Tat, the concentration of the other viral proteins breaches a threshold where we assume that the cell is able to generate new viral particles. An infected cell can be transactivated for a long time period (e.g., black lines) whereas other cells quickly revert back into a latent state (e.g., blue lines).

Patients infected with HIV harbor on the order of millions or more infected $CD4^+$ T cells that are either in an activated or a resting (latent) state (Chun et al., 1997). The turnover of the total infected cell population within a patient

will be influenced by the stochastic fluctuations in single cells. To investigate the dynamics that arises from a large number of infected cells, we performed many simulations of single cells to derive the probability distribution of transactivation (Fig. 2.2B, red line). A small amount of pre-integration transcripts ($mRNA_n(0) = 5$, (Wu, 2004)) is sufficient for the early transactivation of an infected cell during the first 24 hours after integration of the provirus. Since the event of transactivation is ruled by a cascade of stochastic processes, it is not surprising that the probability distribution approximates a log-normal distribution. We can also derive the probability distribution of reversion into latency, i.e., the probability at which an activated cell that is producing viral particles will revert into a latent state (Fig. 2.2C, red line). Finally, latently infected cells can again become reactivated (Fig. 2.2D, red line).

Once we know the probability distribution of a transition into another state, we can derive the age-dependent rate at which it occurs (see *Methods*). As expected, we find that infected cells have a high probability of being transactivated early after infection. The age-dependent transactivation rate peaks a few hours after infection and decreases afterwards (Fig. 2.2B, blue line). Once an infected cell is activated, it can revert into a latent state. This age-dependent reversion rate, i.e., the reversion rate that depends on the age of the activated cell, reaches a constant value after an initial delay (Fig. 2.2C, blue line). The delay is caused by the threshold we set to discriminate between activated and latent cells. Overall, the rate at which the feedback loop is interrupted seems to be independent of the time the cell has spent in an activated state. Latent infected cells can become reactivated again and we also find a constant rate of transactivation that does not depend on the age of the latent cell (Fig. 2.2D, blue line). In our simulations, the process of transactivation in latent infected cells is indeed governed by a single process. The rate-limiting step of the transactivation circuit is given by the basal transcription rate of the long terminal repeat (LTR) that determines the rate at which latent cells become activated virus-producing cells.

Partial differential equations (PDEs) can be used to describe the transitions between compartments with rates that depend on the time a cell spends in a specific compartment. As observed in Fig. 2.2B, the transactivation of HIV-infected cells early after infection follows an age-dependent rate where the age a is given as the time that has passed since infection of the cell. This can be described as follows:

$$\begin{aligned} \frac{\partial I(a,t)}{\partial t} + \frac{\partial I(a,t)}{\partial a} &= -s(a)I(a,t), \\ \frac{dA}{dt} &= \int_0^\infty s(a)I(a,t)da - rA + \alpha L - \delta A, \\ \frac{dL}{dt} &= rA - \alpha L - \mu L, \end{aligned} \tag{2.1}$$

where $I(a,t)$ is defined as the time-density of infected cells of age a before they are transactivated with rate $s(a)$ and produce viral particles. We assume that activated cells A are subject to a constant reversion rate r and die at a rate δ per

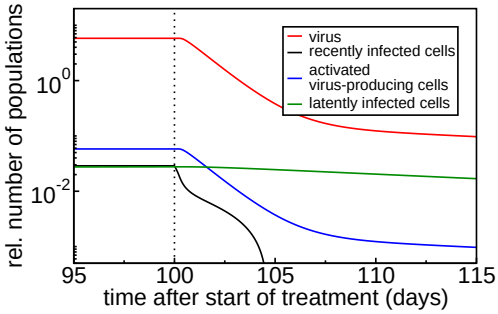

Figure 2.3 Virus load decline after antiretroviral drug therapy. Numerical simulations of the PDE model from Eq. 2.1 accurately describe the first two phases. Recently infected cells become transactivated (black line) causing the initial shoulder phase of the viral load after treatment (red line). The virus load decays proportional to the number of activated virus-producing cells (blue line). The first phase of decline is followed by a slower second phase, which is caused by reactivation of latently infected cells (green line). Initially, the simulation is run to approach an equilibrium before the number of new infections, $I(0,t)$, is set to zero (dotted line). Parameters are: $r = 0.019$ d^{-1}, $\alpha = 0.039$ d^{-1}, $\delta = 0.7$ d^{-1}, $\mu = 0.0$ d^{-1} and $p/\delta_V = 100$.

day that is independent of the age of the cell (CL Althaus, AS De Vos and RJ De Boer, in preparation). Latent infected cells L are generated through reversion of activated cells and can either become activated with rate α or die with rate μ. The boundary condition of the infected cells (i.e., the infection of cells) is simply given by $I(0,t)$. The dynamics of free virus particles can be described by the conventional $dV/dt = pA - cV$. Using the transition rates that we derived from the transactivation circuit (Fig. 2.2B, 2.2C and 2.2D, blue lines), we have run numerical simulations of the virus dynamics model given in Eq. 2.1 to model the chronic state of the infection (Fig. 2.3). The set-point level during chronic infection can be perturbed by the administration of antiretroviral drugs. Our model describes the typical shoulder phase during the first day after the start of treatment that is caused by the transactivation of recently infected cells I (Fig. 2.3, black line) into activated, virus-producing cells A (Fig. 2.3, blue line). During the first week after the start of treatment, the virus load (Fig. 2.3, red line) declines exponentially with a slope that approximates the death rate of activated cells A. Additionally, the dynamics is partly determined by the reversion of activated cells A into latent cells L and the reactivation of latently infected cells (Fig. 2.3, red line). After the first week during treatment, the virus decay is described by a slower second phase that is caused by the slow reactivation of cells in the latently infected cell pool.

To summarize, we have shown how stochastic fluctuations within the intracellular transactivation circuit of HIV-infected cells determine whether a cell is

activated and virus-producing, or whether it rests in a latent state. Using computer simulations, we derive the dynamics and turnover of the total infected cell population within a patient. We derive a new model where a small fraction of activated, virus-producing cells reverts into a latent state where they can become reactivated. This allows us to accurately describe the first two phases of virus decay after antiretroviral therapy. We hypothesize that the reactivation of latently infected cells is governed by the basal transcription rate of the long terminal repeat (LTR) of the provirus. In contrast to previous studies, this suggests that the turnover of the latent infected cell pool is dictated by intrinsic viral factors, rather than extracellular stimuli such as antigenic activation. A recent study provides supporting evidence that Tat can indeed prime and activate peripheral blood mononuclear cells (PBMCs) if cultured at physiological oxygen levels (Sahaf et al., 2008). Hence, the intracellular transactivation circuit might result in Tat levels that are sufficient to activate resting $CD4^+$ T cells for virus production.

2.2.2 *Basal transcription rates govern activation of latently infected cells*

We have shown above that activated, virus-producing cells revert into a latent state because the positive feedback loop of viral transactivation is switched off. Latently infected cells can get reactivated and become virus-producing cells again. Since the basal transcription rate of the viral promoter site (LTR) constitutes the slowest process of the intracellular transactivation circuit, we hypothesized that it is this rate that governs the activation of latently infected cells. By running stochastic simulations with different basal transcription rates, we obtain a linear relation between k_b and the activation rate of latently infected cells, α (Fig. 3.5).

The basal transcription rate of the provirus depends on the position where it is inserted into the host DNA. Generally, the HIV provirus appears to be inserted at positions that are under active transcription because of the free access for integration (Schroder et al., 2002). However, experiments have shown that the transcriptional profile of HIV proviruses obeys a distribution (Jordan et al., 2001), suggesting that the basal transcription rates of some proviruses are likely to be low. Because of the linear relation between basal transcription rates and activation rates, this suggests that activation rates are also heterogeneously distributed. The decelarating decay of virus load following drug therapy has indeed been linked to different activation rates of latently infected cells (Strain et al., 2003, 2005). A decelerating decay can also be found in a recent study by Chun et al. (2007) and has been suggested by mathematical modeling (Muller et al., 2002; Kim and Perelson, 2006). It has been speculated that the decelerating decay is a result of antigenic stimulation of resting $CD4^+$ T cells that have different specificities. Here, we hypothesize that the heterogeneous activation rates of latently infected cells derive from the integration of the provirus at different sites in the host DNA that results in a distribution of basal transcription rates. Once the latently infected cell pool gets depleted during drug treatment,

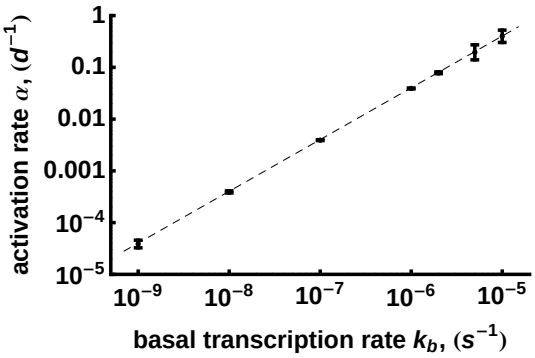

Figure 2.4 Relation between the basal transcription rate and the activation of latently infected cells. Since the basal transcription rate, k_b, is generally the slowest process of the transactivation circuit, we find a linear relation with the activation rate of latently infected cells, α. Activation rates are derived by simulations of the intracellular transactivation circuit as given in *Methods*.

the activation rates of the remaining cells shift towards low values that results in a decelerating decay. Since this affects the long-term behavior of the decay dynamics, we use a simplified HIV dynamics model that does not take into account the population of recently infected cells, i.e., we omit the integral of transactivation from Eq. 2.1. For the cycling between activated and latently infected cells, we devise the following integro-differential equations with different classes of latently infected cells, L_α:

$$\begin{aligned} \frac{dA}{dt} &= \int_0^{\alpha_{\max}} \alpha L_\alpha d\alpha - rA - \delta A \\ \frac{dL_\alpha}{dt} &= rf(\alpha)A - \alpha L_\alpha - \mu L_\alpha. \end{aligned} \tag{2.2}$$

Since we assume that *de novo* infections have stopped, activated cells A are only generated through activation of latently infected cells with a maximal activation rate $\alpha_{\max}$. They revert into latently infected cells with rate r or die with rate δ. Latently infected cells of type L_α are generated according to a distribution of activation rates, $f(\alpha)$, become activated with rate α and die with rate μ. By solving for the explicit solution (see *Methods*) and using parameters values from the literature, we can accurately describe the decay dynamics of the virus load (Fig. 2.5A and 2.5B) and the latently infected cells (Fig. 2.5C). We obtain similar decay dynamics for several distributions of activation rates, $f(\alpha)$, as long as they decrease and approach zero at low activation rates. Both, the concentration of virus and of latently infected cells falls below one copy per ml over a prolonged period of treatment, but the virus fails to become eradicated because some latently infected cells have very low activation rates, i.e., harbor an HIV provirus with a very low basal transcription rate.

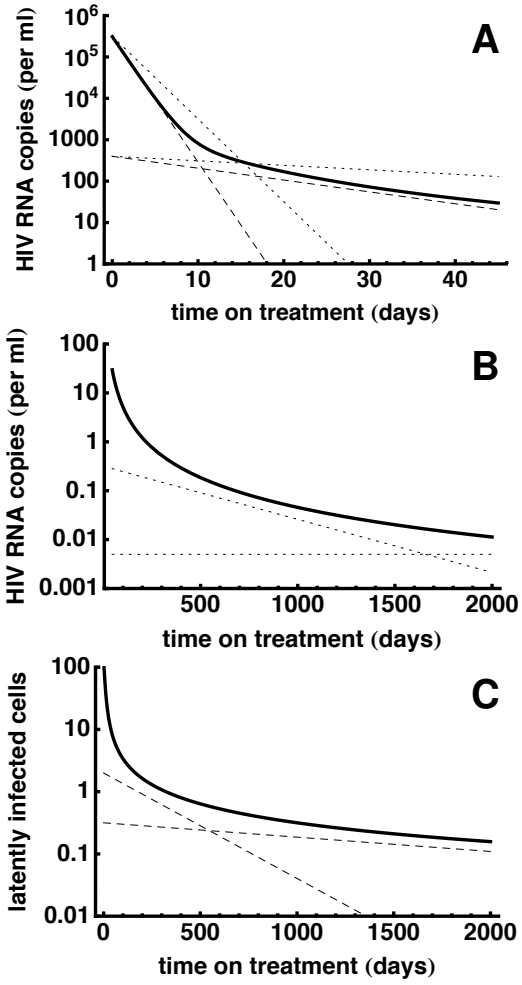

Figure 2.5 (A) Viral load decay during drug treatment. Within the first 45 days, the first phase results primarily from the death of activated, virus-producing cells whereas the second phase is determined by the reactivation of latently infected cells. Experimental estimates of the decay rates during the two phases are given by the dashed (Perelson et al., 1997) and dotted (Palmer et al., 2008) lines. (B) Decelerating decay during prolonged periods of treatment approximates experimental observations (dotted lines, (Palmer et al., 2008)). (C) Similarly, the pool of latently infected cells decays and approximates experimental estimates (dashed lines, (Zhang et al., 1999; Finzi et al., 1999; Ramratnam et al., 2000; Siliciano et al., 2003)). Parameters used: initial pool of activated, virus-producing cells $A_0 = 3.1 \times 10^7$ cells (Chun et al., 1997), initial pool of latently infected cells $L_0 = 1.4 \times 10^6$ cells (Chun et al., 1997), death rate of activated, virus-producing cells $\delta = 0.7$ d^{-1} (Perelson et al., 1997) and we for simplicity we assume lifelong persistence of the resting $CD4^+$ cells, i.e., $\mu = 0.0$ d^{-1} per day. In this figure, $f(\alpha)$ is a normal distribution with $\mu = 0.2$ and $\sigma = 0.1$, truncated at zero and renormalized.

2.3 DISCUSSION

It is challenging to investigate how the intracellular life cycle of a virus influences the virus dynamics within a host. So far, only few attempts have been made that combine the intra- and extracellular levels of virus dynamics (Haseltine et al., 2005, 2008). Here, we used a modified computational model of the intracellular transactivation circuit of HIV (Weinberger et al., 2005; Weinberger and Shenk, 2007) to elucidate the events of transactivation after infection, reversion into latency and reactivation of latently infected cells.

Early transcription of non-integrated proviruses has been observed in HIV-infected cells but the biological potential of pre-integration transcripts are unclear (Stevenson et al., 1990; Wu and Marsh, 2003; Wu, 2004). We find that a small amount of pre-integration transcripts of viral RNA can be sufficient to trigger the transactivation circuit that renders an infected cell into an activated, virus-producing cell. The cascade of the intracellular transactivation circuit generates a delay between the infection of a cell and the production of viral proteins that, at least in part, gives rise to the intracellular delay before virus production that is observed during the first day after antiretroviral drug treatment. Latently infected cells consist of resting $CD4^+$ T cells harboring an HIV provirus that does not provide sufficient transcription. Our simulations show, that a low basal transcription rate of the LTR can keep the infected cells in a latent state. Low basal transcription has been found to occur in resting $CD4^+$ T cells that are infected with HIV (Lassen et al., 2004b). As soon as a few Tat molecules have accumulated, the transactivation circuit may render a cell to become activated. Therefore, we postulate that the activation of latently infected cells is governed by the basal transcription rate of the provirus that is inserted in the host DNA. Interestingly, it has been shown recently that the molecule Tat can also act as an activator of PBMCs (Sahaf et al., 2008). Assuming a distribution of activation rates in latently infected cells that would arise from a distribution of basal transcription rates, we can show that a model with different classes of latently infected cells fully explains the long-term decay dynamics during drug treatment. The second (Perelson et al., 1997), third and fourth (Palmer et al., 2008) phase of virus decay may not just arise from different compartments of infected cells but may reflect the decay profile of latently infected cells with different activation rates, similar as was shown in Muller et al. (2002).

If the basal transcription rate indeed determined the activation rate of latently infected cells, complete eradication of the latent infected cell pool during antiretroviral therapy is unlikely to happen since the resting $CD4^+$ T cells may persist lifelong. However, strategies for purging the pool of latently infected cells with activating stimuli have been proposed (Kulkosky et al., 2001; Brooks et al., 2003). Our study suggests that elevating the transcription rate of the provirus might prove to be a new target to activate the latently infected cells. If the basal transcription rates could be increased with transcriptional activators, or even with the molecule Tat, eradication of the latently infected cell pool in a reasonable time span may become feasible.

The mechanisms behind the generation of viral latency have been difficult to assess so far (Lassen et al., 2004a). Li et al. (1996) proposed that HIV-infected cells have a 'shutdown' mechanism for virus production. Mathematical models have incorporated the process of reversion into latency (Bucy, 1999; Sedaghat et al., 2008) but a definite mechanism has not been further investigated. The transient gene expression for the transcriptional circuit in HIV that has been found by Weinberger et al. (2008) provides a model at which viral latency could be generated. One can speculate whether activated, virus-producing $CD4^+$ cells survive long enough to revert into a latent state (Han et al., 2007). The stochastic simulations of the intracellular transactivation circuit result in a reversion rate of ~ 0.019 per day. In the model that describes the long-term behavior of the decay dynamics, the reversion rate is determined by Eq. 2.9 and we obtain $r \sim 0.007$ per day. Since virus-producing cells follow a constant death rate (CL Althaus, AS De Vos and RJ De Boer, in preparation), these two estimates suggest that about $1 - 3\%$ of the cells becoming latent is sufficient to account for the characteristic dynamics.

Different host factors are likely to contribute to the nature of viral latency in HIV but we have illustrated that the properties of the intracellular transactivation circuit can account for many characteristics of the viral dynamics. Still, it needs to be determined which factors most directly govern viral transcription and virus production (Burnett et al., 2009). Also, we can only speculate about the definite role of the basal transcription rate and the HIV protein Tat in the generation and maintenance of viral latency but recent observations have given support that latency could be an intrinsic property of HIV (Jeeninga et al., 2008).

2.4 METHODS

2.4.1 *Intracellular transactivation circuit*

Viral transcription in HIV is under control of a transactivation circuit induced by the protein Tat. It has been shown that Tat can determine whether a cell is actively transcribing viral RNA and translating it into proteins, or is resting in a dormant state, the so-called clinical latency. Weinberger et al. (2005) and Weinberger and Shenk (2007) derived a mathematical model, which accurately describes the stochastic processes that occur during transactivation. Here, we adopt this model to simulate the transactivation of HIV-infected cells and their reversion into latency. For some additions of the model and parameters, we refer to the studies of Reddy and Yin (1999) and Kim and Yin (2005). Using

chemical kinetics, the model can be described as follows:

$$
\begin{aligned}
LTR &\xrightarrow{k_b} LTR + mRNA_n, \\
mRNA_n &\xrightarrow{k_e} mRNA_c, \\
mRNA_c &\xrightarrow{k_p} P + mRNA_c, \\
mRNA_c &\xrightarrow{k_t} Tat_c + mRNA_c, \\
Tat_c &\xrightarrow{k_i} Tat_n, \\
LTR + Tat_n &\underset{k_u}{\overset{k_b}{\rightleftharpoons}} pTEFb_d, \\
pTEFb_d &\underset{k_d}{\overset{k_a}{\rightleftharpoons}} pTEFb_a, \\
pTEFb_a &\xrightarrow{k_f} LTR + Tat_n + mRNA_n, \\
P &\xrightarrow{\delta_P}, \\
Tat_c &\xrightarrow{\delta_T}, \\
Tat_n &\xrightarrow{\delta_T}, \\
mRNA_n &\xrightarrow{\delta_R}, \\
mRNA_c &\xrightarrow{\delta_R} .
\end{aligned}
\tag{2.3}
$$

The promoter site of the HIV provirus consists of the long terminal repeat (LTR), which is under control of a low basal transcription rate k_b. mRNA is transcribed in the nucleus ($mRNA_n$) and exported into the cytoplasm ($mRNA_c$) at a rate k_e. There, protein translation takes place which generates the proteins for viral particle assembly, P, and at a lower rate the regulatory protein Tat_c. After import into the nucleus, Tat_n binds reversibly, together with co-factors, to the LTR resulting in the transcriptional elongation factor $pTEFb_d$. $pTEFb_d$ can reversibly become acetylated into the activated form $pTEFb_a$ that leads to a much higher transcription rate, k_f, of the provirus. mRNA, Tat and proteins P have different rates of decay. We do not take into account the processes of the HIV replication life cycle that occur before or after transactivation, such as reverse transcription or the viral particle assembly. For simplicity, we define an infected cell as activated and virus-producing when the intracellular concentration of the viral protein P breaches a threshold of 10^3 (Fig. 2.2A). The parameters are given in Table 2.1. For stochastic simulations of the transactivation circuit, we make use of the Gillespie algorithm (Gillespie, 1977). A program of the model was written in C and can be obtained freely on request from the authors.

Table 2.1 Reaction rates for the intracellular transactivation circuit of HIV. Depending on the proviral integration into the host DNA, the basal transcription rate can be given as a distribution (see *Results*). The translation rate and degradation rate of the viral protein P is adjusted that the level of intracellular protein in a fully activated cell saturates around 10^4 (Fig. 2.2A).

Reaction rate	Value	Unit	Reference
k_b: basal transcription rate	$f(k_b)$	s^{-1}	see legend
k_e: mRNA export into cytoplasm	7.2×10^{-4}	s^{-1}	Reddy and Yin (1999)
k_p: viral protein translation	1.0×10^{-2}	s^{-1}	see legend
k_t: Tat translation	1.32×10^{-3}	s^{-1}	Weinberger et al. (2005)
k_i: Tat import into nucleus	5.1×10^{-3}	s^{-1}	Kim and Yin (2005)
k_b: binding of elongation factor	1.5×10^{-4}	$mol^{-1}s^{-1}$	Weinberger et al. (2005)
k_u: dissociation of elongation factor	1.7×10^{-2}	s^{-1}	Weinberger et al. (2005)
k_a: acetylation of elongation factor	1.0×10^{-3}	s^{-1}	Weinberger et al. (2005)
k_d: deacetylation of elongation factor	1.3×10^{-1}	s^{-1}	Weinberger et al. (2005)
k_f: transactivated transcription rate	1.0×10^{-1}	s^{-1}	Weinberger et al. (2005)
δ_P: degradation rate of viral protein	5.0×10^{-6}	s^{-1}	see legend
δ_T: degradation rate of Tat	4.3×10^{-5}	s^{-1}	Reddy and Yin (1999)
δ_R: degradation rate of mRNA	4.8×10^{-5}	s^{-1}	Kim and Yin (2005)

2.4.2 *From probability densities to age-dependent rates*

To analyze the behavior of a large population of HIV-infected cells that are subject to stochastic processes, we perform many simulation runs of the transactivation circuit given in Eq. 2.3 within a single cell. For example, in the case of transactivation of recently infected cells, we initialize the simulation with a small amount of pre-integration transcripts (e.g., $mRNA_n(0) = 5$, which was chosen arbitrarily) and measure the time point at which the viral protein P exceeds the threshold of 10^3 (Fig. 2.2A). We define this time point as the time of transactivation and repeat the simulation 10^6 times to obtain the probability distribution of transactivation depending on the age of the infected cell (Fig. 2.2B, red line). Next, we derive the age-dependent transactivation rate $s(a)$, where a is the age of the cell after infection. The probability that an infected cell has not yet been transactivated until time t is given by

$$\exp\left[-\int_0^t s(a)da\right] = 1 - \int_0^t \hat{s}(a)da, \tag{2.4}$$

where $\hat{s}(a)$ is the probability density function and $\int_0^t \hat{s}(a)da$ the cumulative probability density function of transactivation. By taking the logarithm and differentiating over t we derive the age-dependent transactivation rate

$$s(a) = \frac{\hat{s}(a)}{1 - \int_0^t \hat{s}(a)da}. \tag{2.5}$$

Similarly, the reversion rate and transactivation rate of latently infected cells can be obtained. For numerical simulations of the partial differential equation

(PDE) model in Eq. 2.1, we use the age-dependent transactivation rate obtained in Fig. 2.2B and the constant rates from 2.2C and 2.2D to solve the equations using the *escalator boxcar train* model formulation as described in De Roos et al. (1992) (available on http://staff.science.uva.nl/∼aroos/Ebt.htm).

2.4.3 *Dynamics of virus and latently infected cells during drug therapy*

Based on the model given in Eq. 2.2, we derive an explicit mathematical solution for the dynamics of virus and latently infected cells during drug therapy. We extend a previous model by Muller et al. (2002) to account for the reversion of virus-producing cells into latency and additionally assume a distribution of activation rates of latently infected cells, $f(\alpha)$. For simplicity, we consider 100% drug efficacy and therefore assume that *de novo* infections have stopped.

First, we examine a simple case with only one class of latently infected cells, L_α, with a single activation rate α. Since the turnover of activated cells is much faster than that of latently infected cells, we can make a quasi steady-state assumption:

$$\bar{A}(t) = \frac{\alpha L_\alpha(t)}{r+\delta}. \tag{2.6}$$

The virus produced by activation of latently infected cells is then given by

$$V_L(t) = \frac{p}{c}\bar{A}(t) = \frac{p}{c(r+\delta)}\alpha L_\alpha(t) = \frac{p}{c(r+\delta)}\alpha L(0)e^{(\frac{r\alpha}{r+\delta}-\alpha-\mu)t}, \tag{2.7}$$

where p/c accounts for the virus production and clearance.

Second, we assume a distribution of latently infected cells and define the pre-treatment steady-state as

$$L_\alpha(0) = \frac{rf(\alpha)A(0)}{\alpha+\mu}, \tag{2.8}$$

with $A(0)$ being the pool of activated cells. The total pool of latently infected cells is then given by

$$L(0) = \int_0^{\alpha_{\max}} L_\alpha(0)d\alpha = rA(0)\int_0^{\alpha_{\max}} \frac{f(\alpha)}{\alpha+\mu}d\alpha. \tag{2.9}$$

Now, we can account for the virus production through activation of a heterogeneous pool of latently infected cells by simply substituting Eq. 2.9 into Eq. 2.7, which gives the final solution:

$$V_L(t) = \frac{prA(0)e^{-\mu t}}{c(r+\delta)}\int_0^{\alpha_{\max}} \frac{\alpha f(\alpha)}{\alpha+\mu}e^{(\frac{r\alpha}{r+\delta}-\alpha)t}d\alpha. \tag{2.10}$$

Similarly, the decay of latently infected cells is given by

$$L(t) = rA(0)e^{-\mu t}\int_0^{\alpha_{\max}} \frac{f(\alpha)}{\alpha+\mu}e^{(\frac{r\alpha}{r+\delta}-\alpha)t}d\alpha. \tag{2.11}$$

Additionally, the initial pool of activated virus producing cells is decaying rapidly and the virus load is given by

$$V_A(t) = \frac{p}{c}(A(0) - \bar{A}(0))e^{-(r+\delta)t}, \tag{2.12}$$

where $\bar{A}(0)$ represent the cells that are activated by latently infected cells at time 0 and therefore have been included in Eq. 2.10. The total concentration of virus over time is then given by $V(t) = V_L(t) + V_A(t)$. Numerical simulations of a full model without the quasi stead-state assumptions validate our explicit solution (results not shown).

ACKNOWLEDGMENTS

We would like to thank Vitaly Ganusov for discussions on technical aspects of the manuscript. Christian L. Althaus and Rob J. De Boer gratefully acknowledge financial support by the Netherlands Organisation for Scientific Research (VICI grant 016.048.603).

Reassessing the HIV-1 life cycle through age-structured modeling: lifespan of infected cells, viral generation time and R_0

3

C.L. Althaus, A.S. De Vos and R.J. De Boer
Theoretical Biology, Utrecht University
Padualaan 8, 3584 CH Utrecht, The Netherlands.

J Virol. in press (2009)

ABSTRACT

The rapid decay of viral load after drug treatment in patients infected with human immunodeficiency virus type 1 (HIV-1) has been shown to result from the rapid loss of infected cells due to their high turnover with a generation time of around 1-2 days. Traditionally, viral decay dynamics after drug treatment is investigated using models of differential equations in which both the death rate of infected cells and the viral production rate are assumed to be constant. Here, we describe an age-structured model of the viral decay dynamics in which viral production rates and death rates depend on the age of the infected cell. In order to investigate the effects of age-dependent rates, we compare these models with earlier descriptions of the viral load decay and fit them to previously published data. We find no supporting evidence for increasing infected cell death rates but we cannot reject the possibility of increasing viral production rates with the age of the cell. In particular, we demonstrate that an exponential increase in viral production with infected cell age is perfectly consistent with the data. Since an exponential increase in virus production can compensate for the exponential loss of infected cells, the death rates of HIV-1-infected cells might be higher than previously anticipated. We discuss the implications of these findings on the lifespan of infected cells, the viral generation time and the basic reproductive number R_0.

3.1 INTRODUCTION

An important step in the understanding of the replication dynamics of human immunodeficiency virus type 1 (HIV-1) was made in 1995 when Ho et al. (1995) and Wei et al. (1995) found that plasma concentrations of HIV-1 dropped rapidly after the administration of antiretroviral drugs. The fast exponential decline was associated with a rapid loss of virus producing cells, which suggested a fast turnover of HIV-1-infected cells. Later, more data points of the decrease in plasma concentrations of HIV-1 during the first week indicated a shoulder phase during the first day after treatment, which was explained with the decay of viral particles that had been released already at the start of treatment, and therefore were not affected by the administered protease inhibitor (Perelson et al., 1996). In 1999 however, Ramratnam et al. (1999) measured a very short half-life of viral particles, and the shoulder phase is now typically explained by the intracellular delay of virus production (Herz et al., 1996). The consensus view now is that the viral generation time consists of an intracellular delay of around 24 hours and a lifetime of virus producing cells of about one day, summing up to roughly two days (Dixit et al., 2004).

Traditionally, virus dynamics is investigated using models of ordinary differential equations (ODEs) in which both the death rate of infected cells and the viral production rate are assumed to be constant (Nowak and May, 2000; Perelson, 2002). In contrast to those assumptions, it is biologically plausible that the rate of virus production is initially low and increases with the age of the infected cell, where age is defined as the time that has passed since infection of the cell. Further, assuming a constant likelihood of the cell to die (i.e., a constant death rate) results in exponentially distributed lifespans of infected cells. However, it is known that lifespans of cells need not be necessarily exponentially distributed (Dowling et al., 2005) and previous studies have shown that assuming non-exponential lifespans of infected cells can cause problems in estimating parameters of the viral life cycle (Lloyd, 2001; Nelson and Perelson, 2002). The true dependence of infected cell death rates and viral production rates as a function of the age of the cell is unknown to date (Ho and Huang, 2002). Recently, Reilly et al. (2007) attempted to determine the total virus production of SIV-infected $CD4^+$ T cells in rhesus macaques and found supporting evidence for an exponential increase in the rate of virus production with the age of the infected cell. This behavior has already been indicated in a prior study with visna virus (Haase et al., 1982). In general, it is of great interest to know the kinetic profile of the viral production rate and the age-dependency of infected cell death rates in order to understand how much virus an infected cell produces and how long it lives *in vivo*.

Age-structured models of virus dynamics based on partial differential equations (PDEs) have come to attention more recently (Kirschner and Webb, 1996; Nelson et al., 2004; Gilchrist et al., 2004; Rong et al., 2007). There, infected cells are structured according to the time that has passed since they were infected with a viral particle. Each class of cells has a certain age with a corresponding

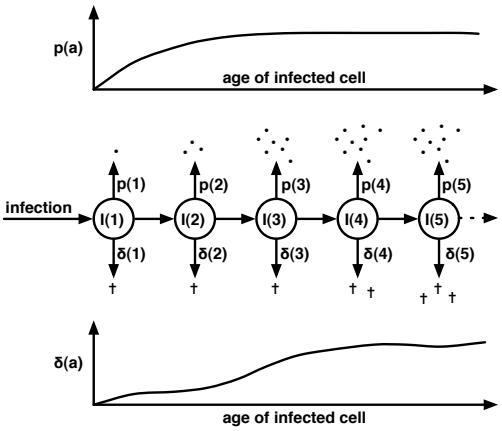

Figure 3.1 Illustration of an age-structured model of virus dynamics. After the event of infection, an infected cell moves through different classes of cell populations ($I(a)$) that are structured according to the time that has passed since infection. Each of these classes has its corresponding age-dependent viral production rate ($p(a)$, top) and infected cell death rate ($\delta(a)$, bottom) that can be defined arbitrarily.

age-dependent death rate and viral production rate (Fig. 3.1). In this paper, we derive a general framework for an age-structured virus dynamics model after drug treatment. We apply the model to previously published data of HIV-1 decay (Perelson et al., 1996) in order to investigate the effects of different kinetic profiles of viral production rates and age-dependent infected cell death rates. Generally, we find no evidence in this data for increasing infected cell death rates but we cannot reject the possibility of increasing viral production rates with the age of the infected cell. Interestingly, the exponential increase in the viral production rate indicated by Haase et al. (1982) and Reilly et al. (2007) is perfectly consistent with this data and would mask the death rates estimated from the HIV-1 decay after drug treatment. Our results indicate that the death rates of HIV-1-infected cells might be higher than previously anticipated and we discuss how the lifespan of infected cells, the viral generation time and the basic reproductive number, R_0, will be affected.

3.2 MODEL

We derive an age-structured model of virus dynamics based on partial differential equations (PDEs) similar to that in Nelson et al. (2004) (Fig. 3.1):

$$\frac{dT}{dt} = \lambda - \beta TV - \delta_T T, \tag{3.1}$$

$$\frac{\partial I(a,t)}{\partial t} + \frac{\partial I(a,t)}{\partial a} = -\delta(a)I(a,t). \tag{3.2}$$

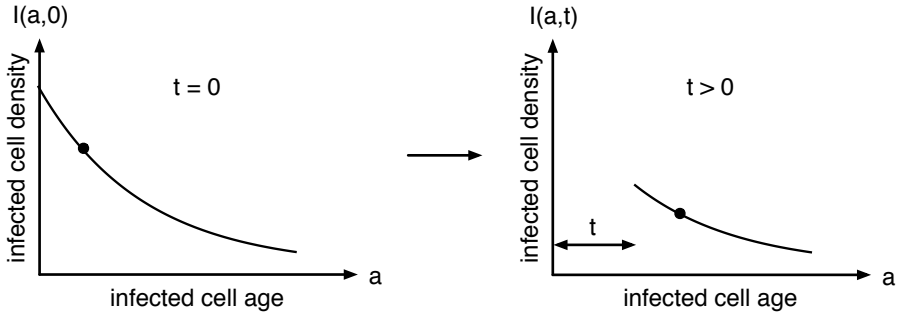

Figure 3.2 Density of infected cells $I(a,t)$ as a function of infected cell age a and the time t after drug treatment. At the start of treatment ($t = 0$, left panel), the infected cells will be in an equilibrium distribution that, assuming a constant death rate, declines exponentially with the age of the infected cell. During treatment ($t > 0$, right panel), *de novo* infections have stopped and all infected cells have age $a \geq t$. Thus, the density of infected cells that had a specific age at the start of treatment will further decrease during treatment and shift along the axis of infected cell age (black dot).

Non-infected $CD4^+$ target cells T are produced at a rate of λ cells per day, die at a rate δ_T and become infected by viral particles V at a rate β per day. $I(a,t)$ is defined as the time-density of infected cells of age a that die with an age-dependent death rate of $\delta(a)$ per day. New viral particles are produced according to

$$\frac{dV}{dt} = \int_0^\infty p(a)I(a,t)da - cV, \tag{3.3}$$

with $p(a)$ being the viral production kernel (i.e., the age-dependent viral production rate) and c the clearance rate of free viral particles. The boundary condition for the infected cells $I(a,t)$ is simply given as the infection of target cells T:

$$I(0,t) = \beta VT. \tag{3.4}$$

As viral decay is a fast process (Ramratnam et al., 1999), we can set the virus into a quasi-steady-state (De Boer and Perelson, 1998):

$$V(t) = \frac{1}{c}\int_0^\infty p(a)I(a,t)da. \tag{3.5}$$

3.2.1 *Drug treatment*

The rationale of antiretroviral drug treatment is to stop new infections by reducing β substantially. Protease inhibitors render the newly produced viral particles non-infectious so that the viral production rate is not affected but β is reduced. Viral particles that are already released from a virus-producing cell at the start of treatment will be unaffected by the protease inhibitor and cause

de novo infections of cells during drug treatment. However, since the free viral particles are cleared very rapidly, at a rate of approximately 23 per day (Ramratnam et al., 1999), we make the assumption that the influence of *de novo* infections becomes negligible. In the *Appendix*, we derive and discuss a full model that includes the viral particles that are unaffected by the protease inhibitors. For the matter of simplicity, we assume 100% drug efficacy and therefore set $\beta = 0$ after the start treatment. The boundary condition in Eq. 3.4 will change to $I(0,t) = 0$ except at the start of treatment where it is given by $I(0,0) = \beta V(0)T(0)$. Since we make the assumption that *de novo* infections have stopped, at any point in time during treatment, t, all infected cells have age $a \geq t$, and the density of the cells is given by

$$I(a,t) = I(a-t,0)e^{-\int_{a-t}^{a}\delta(s)ds} \qquad \text{for } a \geq t. \tag{3.6}$$

We further define $I(a,0)$ as the equilibrium distribution of infected cells with age a at time $t = 0$, i.e., at the beginning of treatment (Fig. 3.2):

$$I(a,0) = I(0,0)e^{-\int_{0}^{a}\delta(s)ds}. \tag{3.7}$$

Then,

$$I(a-t,0) = I(0,0)e^{-\int_{0}^{a-t}\delta(s)ds}, \tag{3.8}$$

and substituting $I(a-t,0)$ into Eq. 3.17 gives

$$I(a,t) = I(0,0)e^{-\int_{0}^{a-t}\delta(s)ds}e^{-\int_{a-t}^{a}\delta(s)ds} \tag{3.9}$$

that simplifies into

$$I(a,t) = I(0,0)e^{-\int_{0}^{a}\delta(s)ds}. \tag{3.10}$$

By substituting $I(a,t)$ into Eq. 3.5 and integrating from time t to ∞, we can account for the total viral production during drug treatment:

$$V(t) = \frac{I(0,0)}{c}\int_{t}^{\infty} p(a)e^{-\int_{0}^{a}\delta(s)ds}da \tag{3.11}$$

with $I(0,0)$ being the density of infected cells of age 0 at the start of treatment, i.e., the boundary condition as given in Eq. 3.4.

Using different types of infected cell death rates $\delta(a)$ and viral production kernels $p(a)$, Eq. 3.11 gives us a description of the viral load decay after the start of drug treatment. We therefore fit several models to previously published data of HIV-1 viral load decay (Perelson et al., 1996). The data consists of HIV-1 RNA concentrations in plasma from five infected patients that were administered a protease inhibitor (ritonavir) orally. We time-shifted the data to account for the pharmacokinetic delay as given in Perelson et al. (1996), and possibly allow for an additional intracellular delay τ corresponding to the viral eclipse phase. The model was fitted to the log-transformed data in Mathematica (version 6.0.1) using the FindMinimum routine to minimize the sum of squared residuals (SSR).

Table 3.1 Age-structured models describing HIV-1 decay after drug treatment. Infected cells produce virus after an intracellular delay, τ, according to their viral production kernels, i.e., $p(a) = 0$ for $a < \tau$. The age-dependent death rate, $\delta(a)$, can increase after the infected cells start to produce virus. Since the death rate of infected cells before the productive stage cannot be estimated, $\delta(a) = \delta'$ for $a < \tau$, where δ' can have any arbitrary value. Models 1 to 4 have different viral production kernels while the infected cell death rate is constant. Model 5 and 6 incorporate a linearly or exponentially increasing death rate, respectively, in combination with different viral production kernels. For model 1 to 3b, an explicit solution for the viral load decay is given while model 4 to 6 can only be described in integral form. During the intracellular delay, the viral load is constant and given as $V(\tau) = V(0)$.

Model	Viral production $p(a)$ for $a \geq \tau$	Infected cell death $\delta(a)$ for $a \geq \tau$	Viral load $V(t)$ for $t \geq \tau$
1	p_0	δ_0	$V(t) = V(\tau)e^{-\delta_0(t-\tau)}$
2	$x(a-\tau)$	δ_0	$V(t) = V(\tau)(1+\delta_0(t-\tau))e^{-\delta_0(t-\tau)}$
3a	$p_0 e^{x(a-\tau)}$	δ_0	$V(t) = V(\tau)e^{-(\delta_0-x)(t-\tau)}$
3b	$e^{xa}-1$	δ_0	$V(t) = \frac{V(\tau)}{x}((x-\delta_0)e^{-\delta_0 t} + \delta_0 e^{-(\delta_0-x)t})$
4	$p_0(1-e^{-\frac{a}{\tilde{x}}^2})$	δ_0	$V(t) = \frac{p_0 I(0,0)}{c}\int_t^\infty (1-e^{-\frac{a}{\tilde{x}}^2})e^{-\delta_0 a}da$
5	Model 1 to 4	$\delta_0(1+y(a-\tau))$	see Eq. 3.11 in *Model*
6	Model 1 to 4	$\delta_0 e^{y(a-\tau)}$	see Eq. 3.11 in *Model*

3.3 RESULTS

In order to investigate the effects of age-dependent viral production and infected cell death rates, we compare age-structured models to a standard model of HIV-1 decay after drug treatment. This allows us to build up complexity in the description of virus dynamics and test the hypotheses that viral production rates and infected cell death rates are increasing with the age of an infected cell. The mathematical equations underlying each model are provided in Table 3.1, and are graphically depicted in Fig. 3.3 and Fig. 3.5A from the *Appendix*. First, we evaluate the influence of different viral production kernels:

- In the standard model, the viral production kernel and the infected cell death rate is kept constant and does not depend on the infected cell age (Table 3.1: Model 1). After an intracellular delay τ, the virus dynamics follows a simple exponential decay with rate δ_0, i.e., is equal to the loss of infected cells (Fig. 3.3A).

- As a first extension of the model, we assume that the viral production rate is increasing linearly with the age of the infected cell (Table 3.1: Model 2). Interestingly, the slope of the linear increase in viral production, x, does not influence the slope of the viral load decay. The model fits the data well (Fig. 3.3C) but shows different properties. The estimated intracellular delay is much shorter (Table 3.2 and Fig. 3.3D), the decline slope is curved and eventually reaches an exponential with slope δ_0. Hence,

because the exponential decay is only approached later during treatment, the estimated death rates are higher than in the standard model (Table 3.2).

- Secondly, we test the hypothesis of an exponentially increasing viral production rate (Table 3.1: Model 3a and 3b). Surprisingly, model 3a results in exactly the same fit as the standard model since an exponential increase in viral production compensates for the exponential loss of infected cells (Table 3.1, Fig. 3.3A and 3.3B). The decline slope is now given as the difference between the death rate and the exponential increase in the production rate, $\delta_0 - x$, which makes it impossible to identify δ_0 or x alone. In model 3b, we change the function for an exponentially increasing production rate so that it starts at zero to account for an intracellular delay (Fig. 3.3F). This results in a bi-exponential decline (Table 3.1 and Fig. 3.3E) that is eventually approaching the same rate as given in model 3a. However, with model 3b we estimate infected cell death rates that are almost three times higher than those in the standard model (Table 3.2).

- In the standard model, virus production starts immediately at a constant rate after the intracellular delay. To describe the transition to virus production more realistically, we use a sigmoidally increasing virus production that is reaching a constant rate (Table 3.1: Model 4, Fig. 3.3H). Not surprisingly, the fits look very similar compared to the standard model with the exception of a smooth transition from the shoulder phase to the exponential decay of the viral load (Fig. 3.3G).

It is tempting to speculate whether increasing viral production rates with the age of the infected cell are mechanistically linked to increasing infected cell death rates with the age of the cell. The release of HIV-1 particles from the cell could cause disrupture of the cell membrane that might increase the likelihood of the cell to die and therefore would increase the rate at which an infected cell dies with the age of the cell. Thus, we also investigated the possibility of age-dependent infected cell death rates that are either linearly (Table 3.1: Model 5) or exponentially increasing with the age of the cell (i.e., following the Gompertz law (Gompertz, 1825), Table 3.1: Model 6). We combined these models with the different viral production kernels from model 1 to 4. Generally, increasing infected cell death rates with the age of the infected cell result in decay dynamics with an accelerating slope with ongoing treatment (Fig. 3.5C in the *Appendix*). Since the viral load decay data usually approximates an exponential slope after a few days, the fittings resulted in minuscule values for the relative increase in the infected cell death rates, y, indicating that a constant death rate of infected cells describes the viral load decay best.

To analyze the results from applying different viral production kernels to the viral load decay data, we can compare the quality of the fittings of the different models. The number of parameters for all our models is equal. It consists of an infected cell death rate for each patient ($5 \times \delta_0$), the individual viral load at

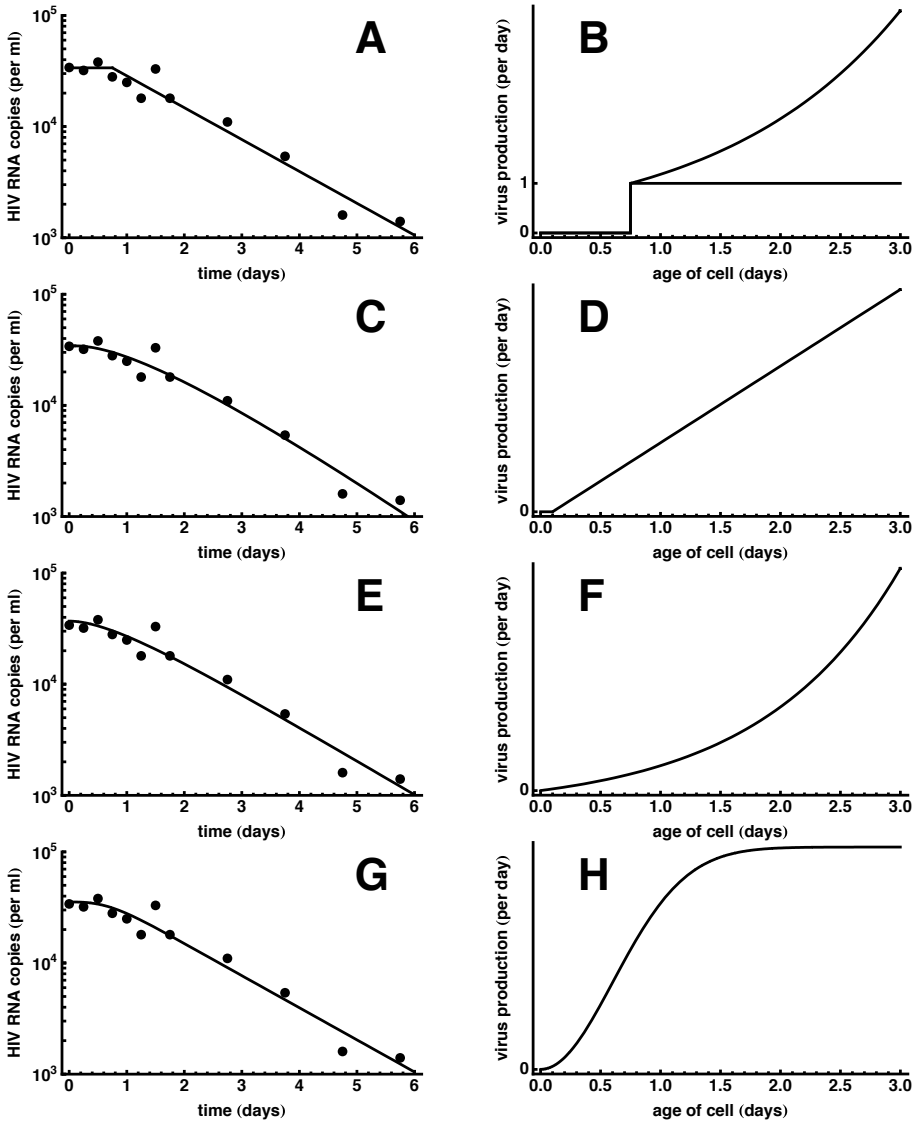

Figure 3.3 HIV-1 decay after drug treatment. The panels on the left side depict HIV-1 RNA concentrations (dots) as given in Perelson et al. (1996) for patient 103 together with the fit of different models to the data (solid lines). The panels on the right show the corresponding viral production kernels $p(a)$. Typically, viral production starts after the intracellular delay τ. (A, B) Constant production rate or exponentially increasing production rate yield the same decay dynamics. (C, D) Linearly increasing production. (E, F) Exponentially increasing production starting at zero. (G, H) Sigmoidally increasing production. For the mathematical description of the models see Table 3.1. Parameters are given in Table 3.2 and additional patient data is provided in the supplemental material.

Table 3.2 Estimated parameter values from model 1 to model 4 given in Table 3.1 to the data of 5 patients from Perelson et al. (1996). The mean and standard deviation of the death rate of infected cells are given together with the average lifespan, the mean generation time and the basic reproductive number R_0. For model 3a, only the difference between the death rate and the exponential increase in viral production can be estimated, which makes it impossible to calculate the lifespan. Model 1 to model 3a have an intracellular delay τ whereas model 3b and model 4 contain the parameter x defining the increase in the viral production rate (see Table 3.1). The models differ only slightly in their sum of squared residuals (SSR) with the standard model (model 1) together with model 3a yielding the lowest SSR. For the sigmoidally increasing production (model 4), the half-maximal viral production rate is reached at 17 hours after infection.

Patient	Parameter	Model 1	Model 2	Model 3a	Model 3b	Model 4
102	δ_0	0.27 d^{-1}	0.47 d^{-1}	-	1.14 d^{-1}	0.26 d^{-1}
103	δ_0	0.66 d^{-1}	0.93 d^{-1}	-	1.55 d^{-1}	0.67 d^{-1}
104	δ_0	0.48 d^{-1}	0.70 d^{-1}	-	1.36 d^{-1}	0.48 d^{-1}
105	δ_0	0.49 d^{-1}	0.72 d^{-1}	-	1.37 d^{-1}	0.49 d^{-1}
107	δ_0	0.49 d^{-1}	0.72 d^{-1}	-	1.37 d^{-1}	0.49 d^{-1}
	Mean of δ_0	0.48 d^{-1}	0.71 d^{-1}	-	1.36 d^{-1}	0.48 d^{-1}
	σ of δ_0	0.14 d^{-1}	0.16 d^{-1}	-	0.15 d^{-1}	0.15 d^{-1}
	τ	18 h	2 h	18 h	-	-
	x	-	-	-	0.86 d^{-1}	20 h
	Average lifespan	3.03 d	1.56 d	-	0.75 d	2.30 d
	Generation time	3.03 d	3.05 d	3.03 d	2.93 d	2.97 d
	R_0	13.6	11.4	-	8.7	10.1
	SSR	0.55	0.59	0.55	0.57	0.56

the start of treatment ($5 \times V(0)$) and either a single intracellular delay (τ) or a parameter that describes the increase of the viral production rate (x). Both, τ and x, are forced to be the same for all patients. Hence, we simply compare the sum of squared residuals (SSR) between our models (Table 3.2). Because the standard model fits the data well, we do not find supporting evidence for increasing viral production rates with the age of the cell. Still, the SSR are very similar for the models with different viral production kernels which indicates that all models describe the data well with an equal number of parameters. This observation is interesting as we cannot reject the hypothesis of increasing viral production rates. We find that models with increasing viral production rates can result in markedly higher estimates of the infected cell death rates (Table 3.2). Further, we find a special case of an exponentially increasing viral production rate (Table 3.1: Model 3a) that cannot be determined from viral load decay data because it might be hidden in the exponential slope of the viral load decay. This finding also indicates that the death rates of HIV-1-infected cells might be higher than it has been anticipated by fitting the standard model to the viral load decay data.

With the possibility for increasing viral production rates with the age of an infected cell, we investigate how those models affect the dynamics of the virus

replication and the viral turnover. Therefore, we calculated how the higher estimates of the infected cell death rate affect the average lifespan of an infected cell and the viral generation time (see in the *Appendix* for the mathematical definitions). Not surprisingly, models with increasing viral production rates result in much shorter average lifespans of the infected cells (Fig. 3.4A). In contrast, the viral generation time is hardly affected by the different models. Since the models resulting in higher estimates for the infected cell death rate have a viral production rate that is increasing with the age of the infected cell, the majority of viral particles are produced late during the viral life cycle which compensates for the shorter lifespans of infected cells. Another interesting property of the virus replication is the basic reproductive number R_0 (see also in the *Appendix* for the mathematical definitions). Due to different underlying distributions of the generation time between the different models (Fig. 3.6 in the *Appendix*), we find that our estimates for R_0 are generally smaller than the one derived from the standard model (Fig. 3.4B).

We can conclude that a constant viral production rate and infected cell death rate are appropriate assumptions to describe HIV-1 dynamics but we predict that infected cell death rates tend to be higher if viral production rates increase with the age of an infected cell. If that were the case, the lifespan of the infected cells tends to be shorter and the basic reproductive number decreases whereas the mean viral generation time is unaffected by the assumption of increasing viral production rates with the age of the infected cell.

3.4 DISCUSSION

In this paper, we have derived a general framework for age-structured virus dynamics after drug treatment. Our aim was to investigate the effects of age-dependent viral production rates and infected cell death rates in HIV-1-infected cells. By fitting different models to previously published data from Perelson et al. (1996), we tested the hypotheses of age-dependent viral production rates and infected cell death rates. We find no evidence for increasing cell death rates with the age of the infected cell. It is important to highlight, that due to the restrictions from viral load decay data, we are only able to infer the behavior of infected cells during the first seven days after infection. Additionally, we are unable to investigate the death of infected cells during the intracellular delay, since the removal of infected cells before they start to produce viral particles will not affect the dynamics of virus production. Still, the result is surprising as *in vitro* studies have shown that HIV-1-infection has cytopathic effects. For a summary of those studies we refer to Funk et al. (2006). Cytopathicity would likely result in an age-dependent increase of the infected cell death rate. However, the situation *in vivo* is likely to be different where the majority of infected cell death is imposed by cytotoxic T lymphocyte (CTL) mediated killing. In the case where CTLs have to search for infected target cells to deliver their lethal hit, a constant rate of death and therefore an exponentially distributed lifespan

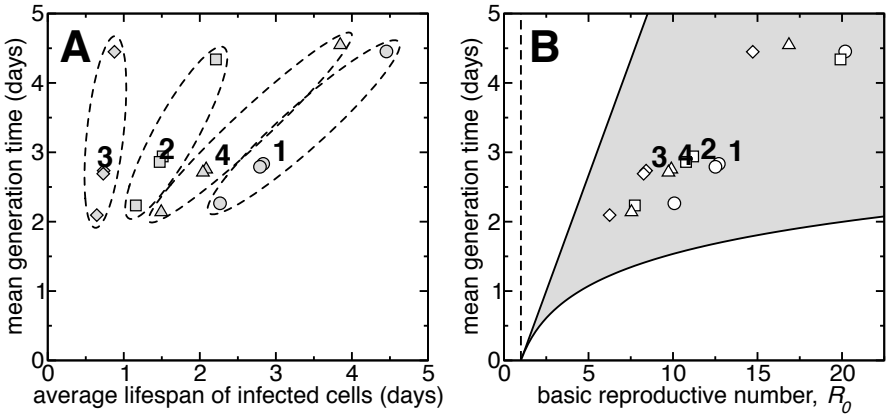

Figure 3.4 Lifespan of infected cells, viral generation time and the basic reproductive number R_0. (A) Each patient is plotted with the estimated average lifespan of infected cells and the mean viral generation time. The basic model (model 1, circles) with a constant viral production rate results in the lowest estimates for the death rate of infected cells and therefore yields the longest lifespans of infected cells. The models with increasing viral production rates that are either linearly (model 2, squares), exponentially (model 3b, diamonds) or sigmoidally increasing (model 4, triangles) result in shorter lifespans of infected cells. In contrast, the viral generation time is hardly affected by the different models. All patients given a certain model are surrounded by a dashed ellipse. (B) Models with increasing viral production rates with the age of the infected cell result in smaller basic reproductive numbers. The gray area depicts the range of the basic reproductive number given a certain viral generation time that can be either fixed or exponentially distributed (Wallinga and Lipsitch, 2007). The dashed line indicates the threshold of $R_0 = 1$. In both panels, each patient is indicated as a symbol. The mean of all patients given a certain model is shown as a bold number. Note that patient 105 and patient 107 overlap since their estimated parameters are equal.

of the cells might serve as an appropriate description of the virus dynamics (Regoes et al., 2007).

In contrast to the hypothesis of increasing infected cell death rates, we cannot reject the possibility of increasing viral production rates with the age of the infected cell. We have found that different models with increasing viral production rates describe the viral load decay data well and that they can result in markedly higher estimates of infected cell death rates. Since the true dependence of the kinetic profile of viral production is unknown, we can only speculate whether our different models with increasing viral production rates are adequate to describe the virus dynamics. For example, given the biology underlying the intracellular kinetics of HIV-1 replication (Reddy and Yin, 1999), it is questionable whether model 2 (τ = 2 h) and model 3b (no intracellular delay at all) describe the virus production realistically. The mathematical models

we present here try to capture a specific feature of the kinetic profile of virus production, such as the strength of the increase with the age of the cell or the smooth transition from the intracellular delay into the phase of virus production. Biological reality might be somewhere in between those models but since we generally find higher estimates for the infected cell death rates for increasing viral production rates with the age of the cell, we highlight that that the death rates of HIV-1-infected cells might be higher than previously anticipated. This would in turn imply shorter average lifespans of infected cells. Due to a different kinetic profile of virus production, we have also found that these models result in smaller values for the basic reproductive number. However, the mean viral generation time, i.e., the average time it takes from infection of a cell until a viral particle from that cell will infect a new cell, is not affected by the different models. Hence, the turnover rate of HIV-1 within a patient does not depend on the kinetic profile of virus production.

Maybe more interesting, we also found a special case with an exponential increase in the viral production rate that cannot be ruled out from viral load decay data because it provides an identical fit (Fig. 3.3A). It has been suggested recently, that viral production increases exponentially in SIV-infected cells from rhesus macaques. Reilly et al. (2007) estimate an exponential increase in viral production with an exponent of 0.1 d^{-1} for activated $CD4^+$ T cells. This finding is also supported by a study of visna virus that suggests an exponential increase in viral production that levels off after a few days (Haase et al., 1982). Because we cannot exclude that the viral production is indeed increasing exponentially, the observed exponential slope of viral load decay would represent the difference between infected cell death and the exponential increase in virus production. If the estimate from Reilly et al. (2007) were realistic, we would have to increase the previous estimates of HIV-1-infected cell death rates by 0.1 d^{-1}. It is important to note that the assumption of 100% drug efficacy also implies that the estimates of the infected cell death rates always have to be taken as minimal estimates (Perelson et al., 1996). Together, these two factors would result in much shorter lifespans of HIV-1-infected cells than previously thought. However, it remains to be ascertained whether exponentially increasing viral production rates also occur for HIV-1 *in vivo*, and if there was a leveling off, at what time it would take place.

Further analysis of the dynamics of virus production will be required to decipher the true kinetic profile of viral production. As there are limitations in measuring HIV-1-infected cells and viral production in a patient in closer detail, it is most likely that further *in vitro* studies that are close to an *in vivo* situation are required to shed new light on that question.

3.5 APPENDIX

3.5.1 *The special case of protease inhibitors*

In the main text, we made the assumption that the administration of antiretroviral drugs reduces the infection rate β. While this is true for reverse transcriptase inhibitors, protease inhibitors render newly produced viral particles non-infectious. Thus, the viral particles that have already been released from the virus-producing cell at the start of therapy will be unaffected by the protease inhibitor. We extend our model to include a population of infectious viral particles that cause *de novo* infections of cells during drug treatment.

The free viral particles at the start of treatment are simply given as $V(0)$. Since they are unaffected by the protease inhibitor and still infectious, we call them $V_i(0)$. Following therapy, they disappear with a clearance rate c, i.e., $V_i(t) = V_i(0)e^{-ct} = V(0)e^{-ct}$. Therefore, the boundary condition from Eq. 3.4 will not be zero but decreases according to $I(0,t) = \beta V(0)T(0)e^{-ct} = I(0,0)e^{-ct}$, where we have to assume that the number of target cells, T, stays constant during the very early period of drug treatment. Now, we describe the density of infected cells that have been produced *de novo* during treatment, i.e., the infected cells with age $a < t$:

$$I(a,t) = I(0,t-a)e^{-\int_0^a \delta(s)ds} \qquad \text{for } a < t. \tag{3.12}$$

Substituting the time-dependent boundary condition, $I(0,t)$, into Eq. 3.12 gives

$$I(a,t) = I(0,0)e^{-c(t-a)}e^{-\int_0^a \delta(s)ds}. \tag{3.13}$$

By substituting $I(a,t)$ into Eq. 3.5 and integrating from time o to t, we can account for the viral particles produced by cells being infected during treatment.

$$V(t) = \frac{I(0,0)}{c}\int_0^t e^{-c(t-a)}p(a)e^{-\int_0^a \delta(s)ds}da. \tag{3.14}$$

Together with Eq. 3.11, we can now describe the total viral production during drug treatment:

$$V(t) = \frac{I(0,0)}{c}\left(\int_0^t e^{-c(t-a)}p(a)e^{-\int_0^a \delta(s)ds}da + \int_t^\infty p(a)e^{-\int_0^a \delta(s)ds}da\right). \tag{3.15}$$

We also fitted the full model from Eq. 3.15 to the data of HIV-1 viral load decay. Since viral particles are cleared very rapidly, at a rate of approximately 23 per day (Ramratnam et al., 1999), the influence of new infections caused by viral particles that are not affected by the protease inhibitor is negligible and does not change our results and parameter estimates.

3.5.2 *Infected cell death: Rates, probability densities and survival*

Here, we want to illustrate the relation between age-dependent death rates of infected cells, the probability density of infected cell death and the survival of

infected cells. If a population of infected cells experiences an age-dependent death rate, $\delta(a)$ (Fig. 3.5A), we can derive the survival function of infected cells, i.e., the fraction of cells surviving until age a (Fig. 3.5C):

$$f(a) = e^{-\int_0^a \delta(s)ds}. \tag{3.16}$$

The age-dependent probability density function of infected cell death, which is equal to the lifespan distribution of infected cells, can then be given by the product of the probability that they die at age a (given by $\delta(a)$) and the survival of infected cells (Fig. 3.5B):

$$\hat{\delta}(a) = \delta(a)e^{-\int_0^a \delta(s)ds}. \tag{3.17}$$

Fig. 3.5C illustrates that if the death rate of infected cells increases with the age of the cell, the fraction of infected cells decreases with an accelerating slope (dashed and dotted line). Therefore, models with increasing death rates with the age of the infected cell cannot easily describe the observed HIV-1 viral load decay that typically approaches an exponential decline. Further, increasing viral production rates with the age of the infected cell cannot compensate for the more than exponential loss of infected cells.

3.5.3 *Lifespan and generation time*

Our findings that infected cell death rates might be higher than previously estimated suggests shorter lifespans for infected cells. The lifespan of an infected cell can be defined as the sum of the intracellular delay, τ, and the average lifespan of a cell in the phase of virus production. With $\hat{\delta}(a)$ being the lifespan distribution (see Eq. 3.17), the average lifespan of an infected cell can be written as

$$\bar{l} = \tau + \int_\tau^\infty a\hat{\delta}(a)da. \tag{3.18}$$

For the case where infected cell death rates are independent of the age of the cell, the lifespan is simply given by $\bar{l} = \tau + 1/\delta_0$, where δ_0 is the death rate of the infected cells.

We also want to investigate how the viral generation time is affected by our results. The viral generation time is given as the time between the onset of two consecutive productive phases of infected cells. This can be written as

$$\bar{g} = \tau + \frac{\int_0^\infty ap(a)f(a)da}{\int_0^\infty p(a)f(a)da}, \tag{3.19}$$

where $p(a)f(a)$ describes the amount of virus that is produced by cells that have reached age a. Note that for $a < \tau$, $p(a) = 0$. In principle, Eq. 3.19 needs to be expanded by the term $1/(\beta T)$ to account for the average time that a single viral particle needs to find a new target cell. Unfortunately, this time can hardly be estimated but, regarding the short lifetime of free viral particles, it is likely to be short. Moreover, this time is independent of age-dependent infected cell death rates or virus production rates.

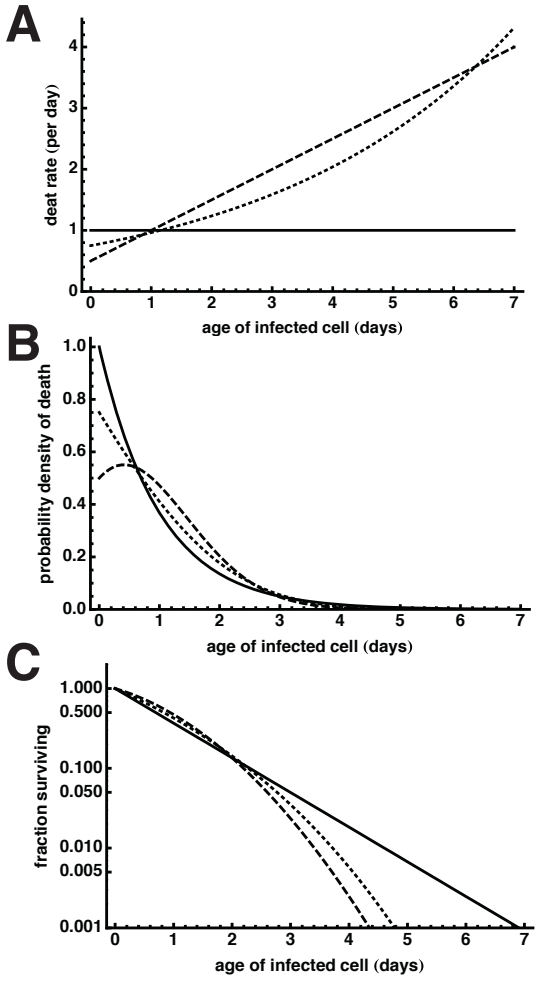

Figure 3.5 Relation between the death rate, the probability density of death and the fraction of cells surviving as a function of infected cell age. (A) Infected cell death rates can either be constant (straight line) or increase linearly (dashed line) or exponentially (dotted line) with the age of the infected cell. (B) This leads to a characteristic probability density function of infected cell death that is equal to the lifespan distribution of infected cells. Note, that if death rates increase with the age of the infected cell, the lifespan distributions can become humped. (C) The fraction of cells surviving until a certain age of the infected cell. Increasing infected cell death rates with the age of the cell lead to a decline of infected cells with an accelerating slope (dashed and dotted line).

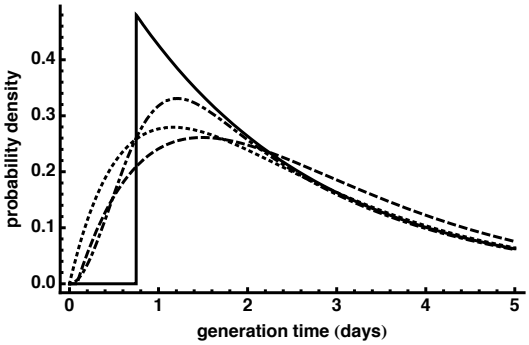

Figure 3.6 Generation time distributions resulting from different viral production kernels. Assuming increasing viral production rates with the age of an infected cell influences the shape of the generation time distribution. The standard model (model 1) follows an exponentially distributed generation time after the intracellular delay (solid line). Increasing viral production rates with the age of the infected cell result in shorter intracellular delays and a smoothing of the generation time distribution. Dashed line: Linearly increasing viral production rate (model 2). Dotted line: Exponentially increasing viral production rate (model 3a). Dash-dotted line: Sigmoidally increasing viral production rate (model 4). Note that the mean for all four distributions is roughly the same (see Table 3.2).

3.5.4 *Basic reproductive number R_0*

The basic reproductive number, R_0, of a viral infection within a host can be defined as the number of newly infected cells produced by one infected cell during its lifetime, assuming all other cells are susceptible. During the rapid viral replication early after HIV-1-infection, it is reasonable to make the assumption of maximal target cell availability, and the net growth rate of the virus during this phase has been estimated to be $\sim$1.5 per day (Little et al., 1999). For the standard model (model 1) with a fixed intracellular delay, τ, and a constant viral production rate and infected cell death rate, the basic reproductive number can be expressed as $R_0 = e^{r\tau}(1 + r/\delta_0)$, where r is the initial growth rate and δ_0 the death rate of the infected cells (Nowak et al., 1997). However, for the models that have age-dependent viral production kernels, the underlying distribution of the generation time can deviate from an exponential distribution and therefore differs from the standard model (Fig. 3.6). Generally, the generation time distribution of infected cells is defined as

$$g(a) = \frac{p(a)f(a)}{\int_0^\infty p(a)f(a)da}, \tag{3.20}$$

i.e., is given by the normalized product of the age-dependent viral production rate, $p(a)$, and the survival probability, $f(a)$, of an infected cell. Wallinga and

Lipsitch (2007) have recently shown how the distribution of generation times, $g(a)$, shapes the relationship between the growth rate, r, and the basic reproductive number, R_0, and obtained

$$R_0 = \frac{1}{\int_0^\infty e^{-ra} g(a) da}, \tag{3.21}$$

where the denominator can be defined as the Laplace transform of the generation time distribution $g(a)$. Hence, for the models with increasing viral production rates with the age of the infected cell, we use Eq. 3.21 to calculate R_0.

ACKNOWLEDGMENTS

We would like to thank Alan Perelson for kindly providing us the viral load data, Libin Rong for discussions about the derivation of the age-structured model, Vitaly Ganusov for providing a Mathematica notebook to fit multiple data sets and Jacco Wallinga, Henk-Jan van den Ham, Tendai Mugwagwa and Boris Schmid for critically reading the manuscript. We also thank two anonymous reviewers for helpful comments.

CLA and RJDB gratefully acknowledge financial support by the Netherlands Organisation for Scientific Research (VICI grant 016.048.603).

3.6 SUPPLEMENTAL MATERIAL

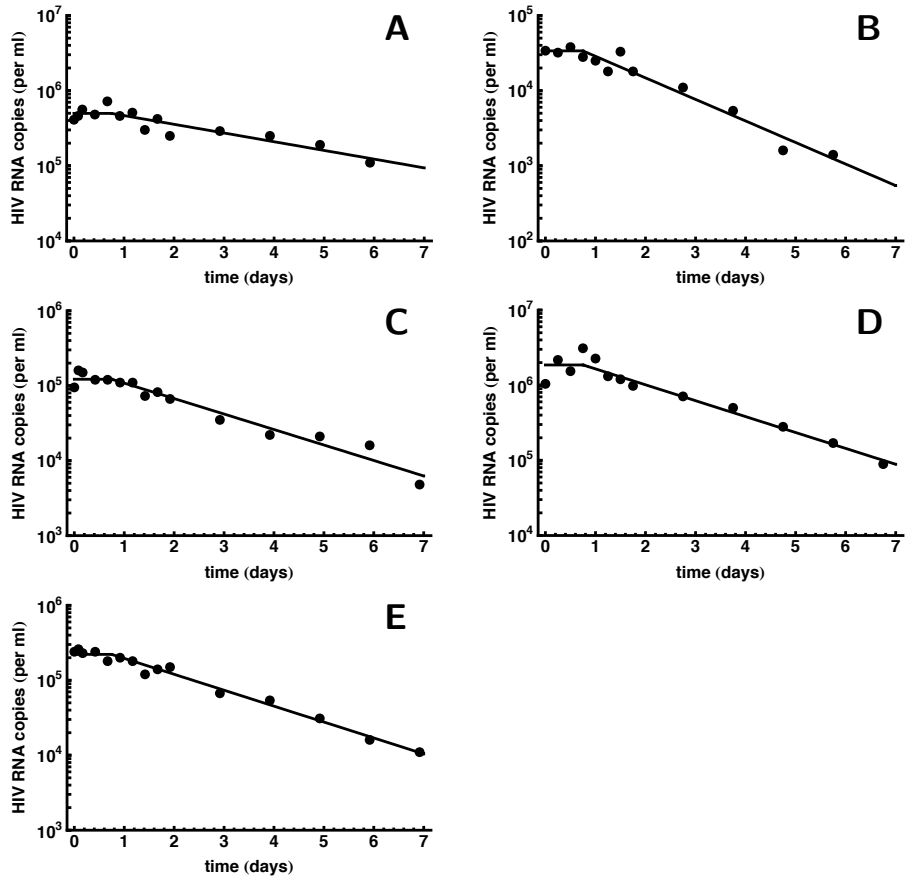

Figure 3.7 Plasma concentrations of HIV-1 RNA after drug treatment (black dots). The solid lines represent the best-fit of model 1 (constant viral production rate) to the data from Perelson et al. (1996). A: patient 102, B: patient 103, C: patient 104, D: patient 105 and E: patient 107.

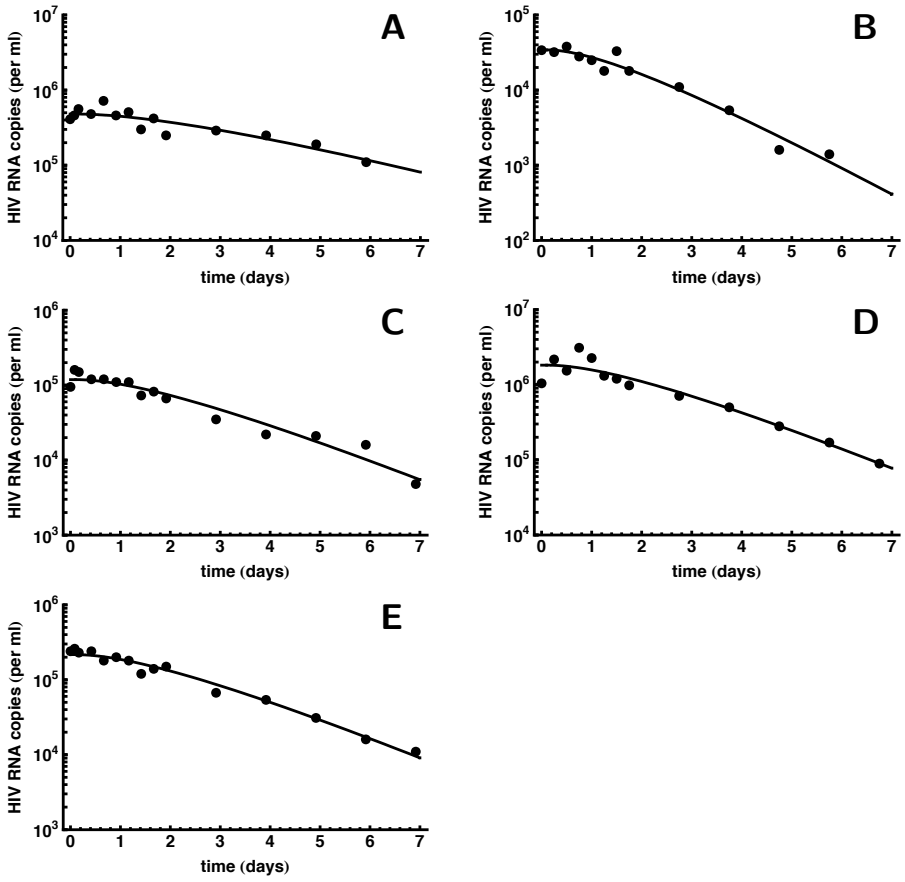

Figure 3.8 Plasma concentrations of HIV-1 RNA after drug treatment (black dots). The solid lines represent the best-fit of model 2 (linearly increasing viral production rate) to the data from Perelson et al. (1996). A: patient 102, B: patient 103, C: patient 104, D: patient 105 and E: patient 107.

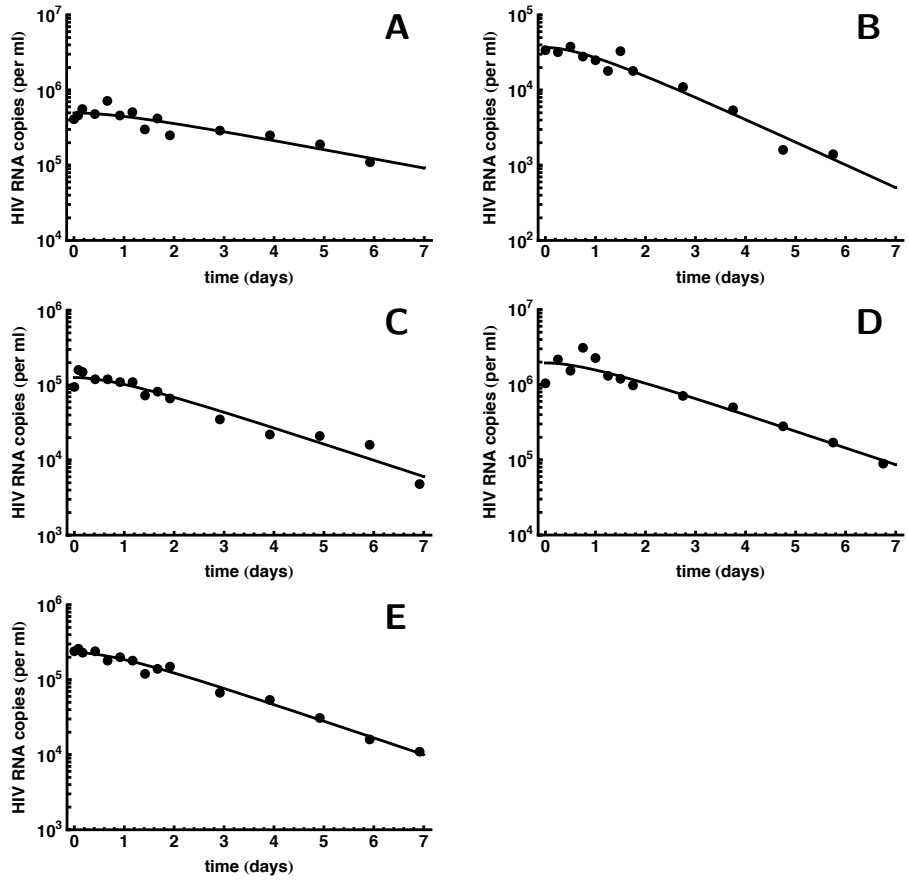

Figure 3.9 Plasma concentrations of HIV-1 RNA after drug treatment (black dots). The solid lines represent the best-fit of model 3b (exponentially increasing viral production rate starting at zero) to the data from Perelson et al. (1996). A: patient 102, B: patient 103, C: patient 104, D: patient 105 and E: patient 107.

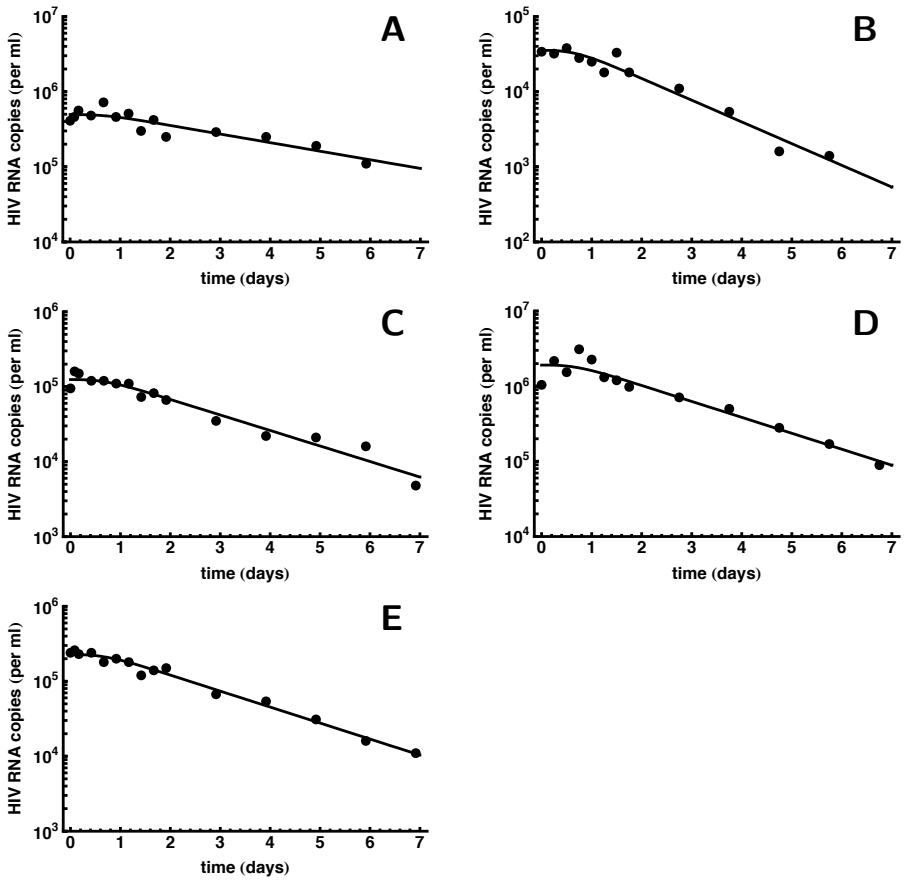

Figure 3.10 Plasma concentrations of HIV-1 RNA after drug treatment (black dots). The solid lines represent the best-fit of model 4 (sigmoidally increasing viral production rate) to the data from Perelson et al. (1996). A: patient 102, B: patient 103, C: patient 104, D: patient 105 and E: patient 107.

Dynamics of CD8$^+$ T cell responses during acute and chronic lymphocytic choriomeningitis virus infection

4

C.L. Althaus, V.V. Ganusov and R.J. De Boer
Theoretical Biology, Utrecht University
Padualaan 8, 3584 CH Utrecht, The Netherlands.

J Immunol. **179(5)**: 2944-51 (2007 Sep)

ABSTRACT

Infection of mice with lymphocytic choriomeningitis virus (LCMV) is frequently used to study the underlying principles of viral infections and immune responses. We fit a mathematical model to recently published data characterizing antigen-specific CD8$^+$ T cell responses during acute (Armstrong) and chronic (clone-13) LCMV infection. This allows us to analyze the differences in the dynamics of CD8$^+$ T cell responses against different types of LCMV infections. For the four CD8$^+$ T cell responses studied, we find that, compared to the responses against acute infection, responses against chronic infection are generally characterized by an earlier peak and a faster contraction phase thereafter. Furthermore, the model allows us to give a new interpretation of the effect of thymectomy on the dynamics of CD8$^+$ T cell responses during chronic LCMV infection: a smaller number of naive precursor cells is sufficient to account for the observed differences in the responses in thymectomized mice. Finally, we compare data characterizing LCMV-specific CD8$^+$ T cell responses from different laboratories. Although the data were derived from the same experimental model, we find quantitative differences that can be solved by introducing a scaling factor. Also, we find kinetic differences that are at least partly due to the infrequent measurements of CD8$^+$ T cells in the different laboratories.

4.1 INTRODUCTION

CD8$^+$ T cell (cytotoxic T lymphocyte) responses play an important role in the clearance of acute and control of chronic viral infections (Doherty and Christensen, 2000). The time course of a CD8$^+$ T cell response to an acute viral infection is typically separated into a rapid expansion phase and a contraction phase that is followed by the memory phase during which memory T cells are maintained by antigen-independent homeostatic proliferation (Lau et al., 1994; Murali-Krishna et al., 1998). The infection of mice with lymphocytic choriomeningitis virus (LCMV) is frequently used to study the dynamics of CD8$^+$ T cell responses. It is the nature of LCMV that makes it an excellent infection model since different strains of this virus can lead to distinct courses of infection. The Armstrong strain of LCMV causes acute infection where the virus is cleared 8 days post-infection (p.i.), whereas LCMV clone-13 causes chronic infection with the virus persisting in the brain and kidneys for more than three months (Wherry et al., 2003).

It is generally unknown how the nature of viral infection influences the different stages of CD8$^+$ T cell responses. Very little is known especially about the dynamics of CD8$^+$ T cell responses during chronic infections. Recent studies show that the time course of CD8$^+$ T cell responses following chronic LCMV infection look similar to responses following acute infection. However, during chronic infections, the cells that persist after the contraction phase are still antigen-dependent and often lose their effector functions, i.e. become exhausted (Zajac et al., 1998; Wherry et al., 2004). Recently, it was shown that PD-1 (programmed death 1) is selectively upregulated in functionally impaired cells during chronic LCMV infection and that blockage of this receptor can restore their effector functions (Barber et al., 2006).

The application of mathematical models has been useful to improve our understanding of the behavior of CD8$^+$ T cell responses (Antia et al., 2003, 2005). For example exhaustion of CD8$^+$ T cell responses was studied by mathematical modeling (Bocharov, 1998; Kesmir and De Boer, 2003). Fitting models to data characterizing immune responses can help to interpret the dynamics (De Boer et al., 2001). A previous study characterized the different dynamics of CD4$^+$ and CD8$^+$ T cell responses following acute LCMV infection (De Boer et al., 2003). Recently, two new studies measured CD8$^+$ T cell responses against LCMV infection in mice in order to investigate new aspects of those responses. Wherry et al. (2003) tracked CD8$^+$ T cell responses during acute and chronic LCMV infection, and Miller et al. (2005) measured CD8$^+$ T cell responses against chronic LCMV in sham-thymectomized (SThx) and thymectomized (Thx) mice to ascertain the role of thymic output on the dynamics of the response.

We fit these published data sets of CD8$^+$ T cell responses with a previously developed mathematical model of De Boer et al. (2001) and estimate its dynamical parameters. This not only allows us to analyze the differences between acute and chronic infection and the influence of thymic output on the immune

responses in detail, but also gives us the opportunity to compare data on the same LCMV infection model obtained from different laboratories.

For the epitope-specific $CD8^+$ T cell responses studied, our analysis shows distinct dynamics for responses against acute and chronic LCMV infection with the chronic infection having an earlier peak and a generally faster contraction phase. Further, our model allows us to give a reinterpretation of the thymectomy experiments of Miller et al. (2005). The influence of thymectomy on the development of $CD8^+$ T cell responses can simply be explained by different precursor frequencies of naive T cells. Finally, our analysis shows discrepancies between data obtained from different laboratories.

4.2 MATERIALS AND METHODS

The data used in our analysis have been published recently (Wherry et al., 2003; Miller et al., 2005). In the study of Wherry et al. (2003), four- to six-week-old female C57BL/6 mice were infected with LCMV Armstrong (2×10^5 PFU intraperitoneally) or LCMV clone-13 (2×10^6 PFU intravenously) causing acute and chronic infection, respectively. The numbers of antigen-specific $CD8^+$ T cells/spleen were determined by MHC tetramer staining at several time points after infection against the following epitopes: NP396, GP33, GP34 and GP276. Mice infected with LCMV Armstrong were able to control the virus effectively in serum and tissues, whereas in mice infected with LCMV clone-13 virus persisted at high levels in the brain and kidneys (Wherry et al., 2003). The study of Miller et al. (2005) used thymectomized (Thx) and sham-thymectomized (SThx) C57BL/6 mice. Surgeries were performed when the mice were approximately six weeks old. Two to three weeks after surgery, mice were infected with 2×10^6 PFU LCMV clone-13 intravenously. Specific $CD8^+$ T cells against the epitopes NP396, GP33 and GP276 were measured as cells/spleen by MHC tetramer staining. At day 80 p.i., virus was cleared in the liver but persisted in the lung. For a more detailed description of how data were obtained we refer to the original studies (Wherry et al., 2003; Miller et al., 2005). The data were kindly provided to us by the authors of these papers.

Different models have been proposed to describe the dynamics of $CD8^+$ T cells after viral infections (De Boer et al., 2001; Antia et al., 2003, 2005; Kohler, 2007). De Boer et al. (2001) published a mathematical model that was fitted to $CD8^+$ T cell responses following LCMV Armstrong infection. Here, we used the same model in order to estimate the dynamics of $CD8^+$ T cell responses during acute and chronic LCMV infection. The model considers "clones" of activated (A) and effector/memory (M) cells. Since the proliferation of T cells after antigenic stimulation seems to be programmed (Mercado et al., 2000; Van Stipdonk et al., 2001; Kaech and Ahmed, 2001; Badovinac et al., 2002), the dynamics are split into two distinct phases. Before the peak of the response at time T_{off}, there is rapid proliferation. After the peak, activated cells die or turn into effector/memory cells.

The dynamics can be described by a set of ordinary differential equations (ODEs). During the expansion phase, when $t \leq T_{\text{off}}$, we assume that there are no effector/memory cells and activated T cells A proliferate according to

$$\frac{dA}{dt} = \rho A, \tag{4.1}$$

where ρ is the net expansion rate, and A_0 is the initial number of cells at $t = 0$. More realistically, naive precursor cells should start proliferating after they have been recruited through antigenic stimulation. For simplicity, we lump these precursor numbers and the recruitment time together, and consider a proliferation that starts at $t = 0$. Therefore, our estimates of A_0 are lower than the precursor frequency of naive cells that has been estimated by Blattman et al. (2002). After the peak at time T_{off}, activated cells A die with a net death rate of δ_A (representing activation-induced cell death and normal death) and turn into effector/memory cells M at a rate r. Therefore, the dynamics of activated and effector/memory cells for $t > T_{\text{off}}$ can be described as follows:

$$\frac{dA}{dtt} = -(r + \delta_A)A, \tag{4.2}$$

$$\frac{dM}{dt} = rA - \delta_M M, \tag{4.3}$$

where δ_M represents the net death rate of effector/memory cells, consisting of a balance between cell renewal and death. This balance is maintained through ongoing cell division which has been shown with BrdU labeling for cells that persist after acute and chronic LCMV infection (Zajac et al., 1998; Miller et al., 2005).

Using the number of activated cells at the peak of the response, $A(T_{\text{off}})$, as the initial condition for equation 4.2, the solution of equation 4.1 - 4.3 gives a continuous function for the total cell number $N = A + M$. Parameter estimates of the differential equations were obtained by fitting the prediction of the total cell number, N, to the data (taking the natural logarithm) based on the Levenberg-Marquardt algorithm (Marquardt, 1963) for solving nonlinear least-squares problems. 95% confidence intervals for the inferred parameters were determined using a bootstrap method (Efron and Tibshirani, 1986), where the residuals to the optimal fit were resampled 500 times. When we compare a smaller model with restricted parameters to a bigger model with a higher number of free parameters we perform the partial F-test to compare the two nested models by the difference between their residual sum of squares per additional parameter, divided by the residual mean square of the larger of the two models (Armitage and Berry, 1994). Given this value the F distribution contains two parameters. The one in the numerator is the difference in the number of parameters between the two models. The one in the denominator is the number of degrees of freedom of the larger model (i.e., the number of data points minus the number of parameters). Throughout the paper we accepted the hypothesis

that the model with the larger number of parameters provides the best fit with a significance level of $p < 0.05$.

To compare data sets of $CD8^+$ T cell responses from different laboratories we introduced a scaling factor s. First, the mathematical model was fitted to a specific $CD8^+$ T cell response from laboratory 1. Then, the estimated total cell numbers N_1 were scaled and used as a prediction for the specific $CD8^+$ T cell response from laboratory 2 ($N_2 = sN_1$). Regression analysis and Student's t test were performed using Gnumeric (version 1.0.12) and the R statistical software package (R Development Core Team, 2005). Significance was defined as $p < 0.05$.

4.3 RESULTS

4.3.1 *$CD8^+$ T cell responses during acute and chronic LCMV infection*

We fit the data by Wherry et al. (2003) with a simple mathematical model described in *Materials and Methods* in order to detect differences between the dynamics of $CD8^+$ T cell responses during acute and chronic LCMV infection (Fig. 4.1, Table 4.1 and 4.2). Due to the limited number of data points before the peak of the response one cannot estimate the expansion rate, the time of the peak and the initial cell number from these data. We therefore employed previous estimates of the net expansion rate ρ that were obtained by fitting the same mathematical model to $CD8^+$ T cell responses against LCMV Armstrong in the same mouse strain (De Boer et al., 2003). The data used in that study had several measurements before the peak of the response and therefore allowed to estimate the expansion rates (Homann et al., 2001). Since clone-13 differs from LCMV Armstrong by two amino acids not affecting the relevant $CD8^+$ T cell epitopes (Matloubian et al., 1990, 1993), we consider the initial expansion rate of the corresponding $CD8^+$ T cell responses to be similar for both acute and chronic LCMV infection (see also in section 4.4: *Discussion*). We also force the number of naive precursor cells for each epitope to be the same for acute and chronic responses. As there are no data points during the expansion phase for the GP34-specific $CD8^+$ T cell response during acute infection, we only fit the contraction phase of this response.

Fitting the model to all data sets of $CD8^+$ T cell responses during acute and chronic infection gave reasonable fits (Fig. 4.1). As observed in De Boer et al. (2003), allowing the net death rate of effector/memory cells, δ_M, to be a free parameter failed to improve the quality of the fits and converged to a value close to zero for both acute and chronic infection. Therefore, we set δ_M to be zero. The time of the peak, T_{off}, appeared to be different between responses during acute and chronic infection but similar for the epitope-specific responses for one type of infection. Based on an F-test, we could indeed restrict the model to a single T_{off} for the responses during acute infection, and another single T_{off} for the responses during chronic infection. Furthermore, the responses during acute infection could be fitted with the same effector/memory formation rate r.

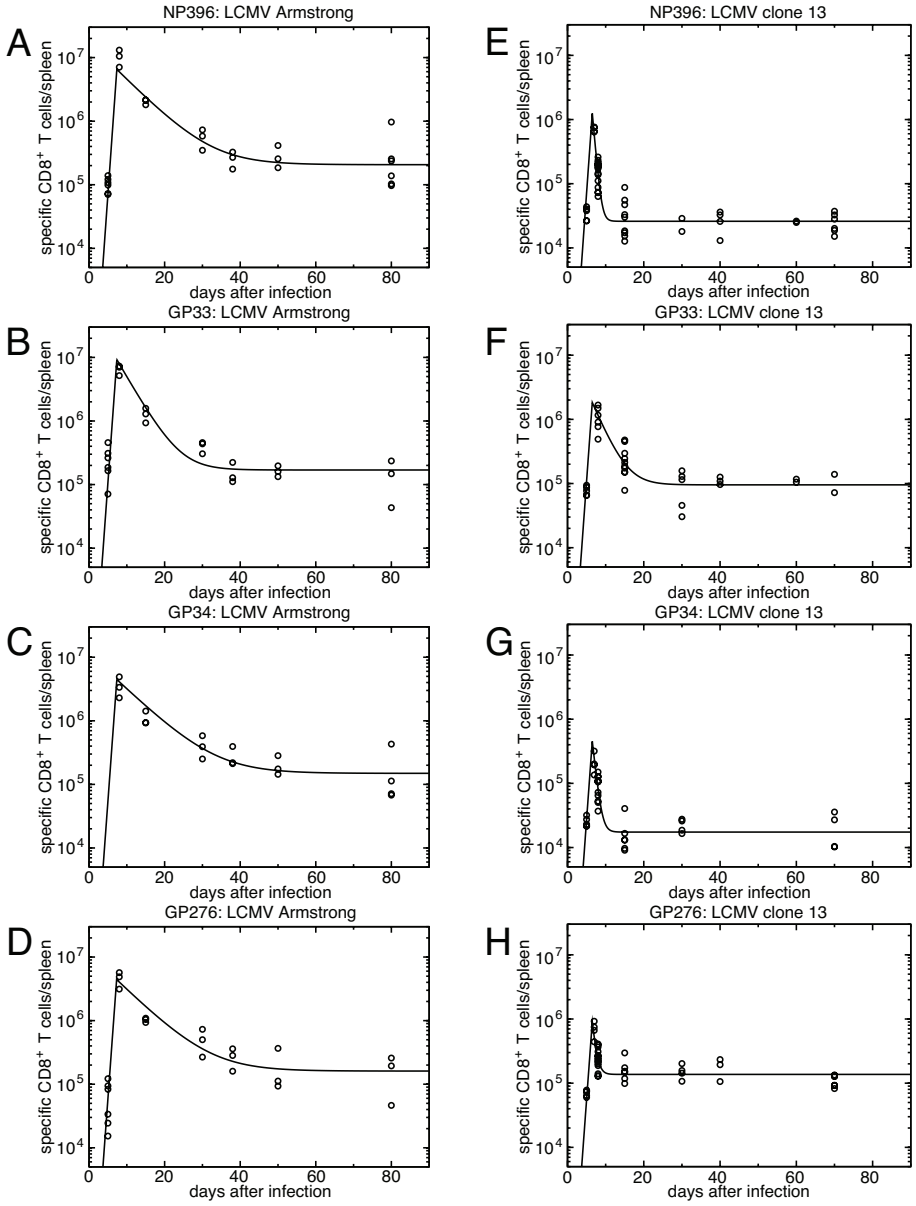

Figure 4.1 The epitope-specific CD8$^+$ T cell responses during acute (A-D) and chronic (E-H) LCMV infection against the following epitopes: NP396, GP33, GP34 and GP276. Each data point represents one mouse as measured in Wherry et al. (2003). The solid lines represent the best-fit of the model to the data. Compared to the CD8$^+$ T cell responses against acute infection, responses against chronic infection are generally characterized by an earlier peak (6.5 days for chronic and 7.3 days for acute infection) and a faster contraction phase thereafter. For parameters see Tables 4.1 and 4.2.

Table 4.1 Parameter estimates obtained by fitting the model to the data on $CD8^+$ T cell responses to four different epitopes during acute LCMV infection (Armstrong). Previous estimates of proliferation rates were used: 1.92 d^{-1} for NP396, 1.89 d^{-1} for GP33 and GP34, 1.87 d^{-1} for GP276 (De Boer et al., 2003). The death rate of effector/memory cells is $\delta_M = 0$.

		δ_A (day^{-1})	r (day^{-1})	T_{off} (days)	A_0 (cells)
NP396	Value	0.13	0.004	7.3	4.9
	95% CI	0.10–0.17	0.003–0.006	7.2–7.5	3.8–6.2
GP33	Value	0.23	0.004	7.3	8.6
	95% CI	0.18–0.13	0.003–0.006	7.2–7.5	6.9–11.1
GP34	Value	0.08	0.004	7.3	2.1
	95% CI	0.06–0.11	0.003–0.006	7.2–7.5	1.5–3.0
GP276	Value	0.13	0.004	7.3	4.8
	95% CI	0.10–0.17	0.003–0.006	7.2–7.5	3.8–6.2

Table 4.2 Parameter estimates obtained by fitting the model to the data on $CD8^+$ T cell responses to four different epitopes during chronic LCMV infection (clone-13). Previous estimates of proliferation rates were used: 1.92 d^{-1} for NP396, 1.89 d^{-1} for GP33 and GP34, 1.87 d^{-1} for GP276 (De Boer et al., 2003). The death rate of effector/memory cells is $\delta_M = 0$. The initial numbers of activated cells, A_0, are the same as for acute LCMV infection and given in Table 4.1.

		δ_A (day^{-1})	r (day^{-1})	T_{off} (days)
NP396	Value	1.52	0.032	6.5
	95% CI	1.16–1.86	0.024–0.041	6.4–6.6
GP33	Value	0.31	0.017	6.5
	95% CI	0.22–0.42	0.011–0.026	6.4–6.6
GP34	Value	1.21	0.048	6.5
	95% CI	0.85–1.63	0.032–0.066	6.4–6.6
GP276	Value	1.11	0.201	6.5
	95% CI	0.67–1.80	0.135–0.341	6.4–6.6

In combination this means that we restricted the model having 8 T_{off} parameters and 8 r parameters for the four responses against both types of infection to a smaller model having 5 r parameters and 2 T_{off} parameters (i.e., reducing the number of parameters by 9 which gives $F_{9,225} = 1.6, p = 0.13$).

$CD8^+$ T cell numbers specific for GP33 measured by intracellular cytokine staining for IFN-γ roughly correspond to the sum of GP33- and GP34-specific $CD8^+$ T cells obtained by MHC tetramer staining (Homann et al., 2001). In order to compare the dominance ranking for the four responses to the results in De Boer et al. (2003), that were obtained by fitting the model to $CD8^+$ T cell numbers measured by intracellular cytokine staining, we use the sum of GP33- and GP34-specific $CD8^+$ T cells. The results are in agreement with that study. For responses during acute LCMV infection, the data shows the same dominance ranking for the epitopes at the peak and in the memory phase, given as

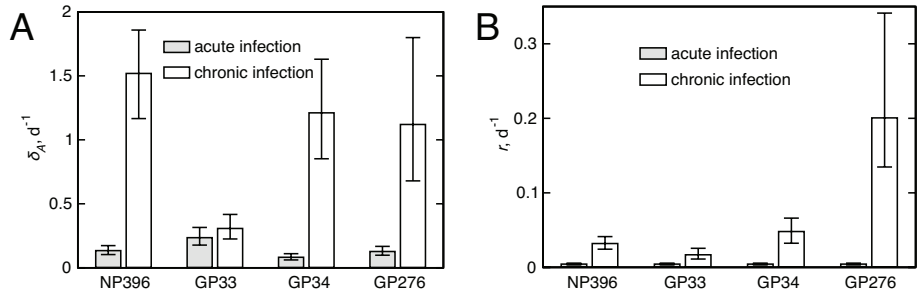

Figure 4.2 (A) Estimated death rates of activated cells, δ_A, and (B) estimates of the rate r at which effector/memory cells are formed for CD8$^+$ T cell responses during acute and chronic LCMV infection. Error bars represent 95% CI of parameter estimates. The rates are largely increased for responses during chronic infection except for the specific response against GP33.

GP33 + GP34 > NP396 > GP276. During chronic LCMV infection, the immunodominance at the peak of the response is the same as during acute infection but the hierarchy is changed after the peak and results in GP276 > GP33 + GP34 > NP396. We find the same hierarchy at the peak of the response during chronic LCMV infection, but the hierarchy is changed after the peak because the GP276 response becomes the largest, i.e. GP276 $\approx$ GP33 + GP34 > NP396. The change in immunodominance can be explained by different apoptosis rates and different effector/memory formation rates between the responses during chronic infection (Fig. 5.5 and Table 4.2). Apoptosis rates also differ between responses during acute infection, which is in contrast to the study by De Boer et al. (2003), however the differences are minor (Fig. 5.5A and Table 4.1). Comparing the obtained parameters between acute and chronic responses shows two major differences. The responses during chronic infection generally show an earlier peak (at day 6.5, compared to 7.3 for the responses during acute LCMV infection) and a faster contraction of the response after the peak. During the contraction phase of responses during chronic LCMV infection, both the death rate of activated cells, and the effector/memory formation rate are faster (Fig. 5.5A and 5.5B).

4.3.2 *Dynamics of CD8$^+$ T cell responses in thymectomized mice*

Miller et al. (2005) investigated the role of thymic output in the dynamics of antigen-specific CD8$^+$ T cell responses during chronic LCMV infection (Fig. 4.3). The authors argue that there is a transient CD8$^+$ T cell defect in Thx mice compared to SThx mice. The argument is based on the observation that there is a significantly lower CD8$^+$ T cell response in Thx mice at day 30 p.i. compared to SThx mice for all measured epitopes. Since there is no significant difference in the responses at later time points after day 30 p.i. Miller et al. (2005) conclude

that cells in Thx mice later rebound to levels similar to those in SThx mice, which suggests that there is an increase of the responses in Thx mice between day 30 and 80 p.i. BrdU labeling between day 15 and 25 p.i., and between day 30 and 40 p.i. with subsequent flow cytometry at the end of each pulse showed no difference in the proliferation rates between Thx and SThx mice, however. Another explanation for the reduced number of T cells in day 30 p.i. for Thx mice is that T cells are more sequestered to peripheral tissues because of higher viral load at these sites, compared to SThx mice (Miller et al., 2005).

To test the hypothesis of a transient $CD8^+$ T cell deficit in Thx mice, we performed a Student's t test to check whether the $CD8^+$ T cell numbers at day 30, 45 and 80 p.i. are significantly different from each other but found no evidence ($p > 0.05$). Furthermore, we performed a linear regression through all data points at day 30, 45 and 80 p.i., and found no evidence for a slope significantly different from zero ($p > 0.05$). Both these analysis argue against the increase in T cell responses in Thx mice from day 30 p.i.

This statistical analysis is in agreement with the results of our dynamical model: the stable phase of effector/memory cells given by $\delta_M = 0$ indicates that there is no $CD8^+$ T cell rebound after day 30 p.i. Therefore, we fit our model to the data describing $CD8^+$ T cell responses against three epitopes for SThx and Thx mice concurrently. Again, there is only one time point of measurements before the expected peak of the response (at day 5 p.i.). Hence, we set the proliferation rates to previously estimated parameters (De Boer et al., 2003), and assume the time of the peak, T_{off}, to be equal for Thx and SThx mice since both of them are infected with the same type of virus. The only parameters that can vary between Thx and SThx mice are the initial number of naive cells that become activated, A_0, the rate of effector/memory cell formation, r, and the net death rate of activated cells, δ_A. Since young Thx mice are expected to have markedly lower naive T cell numbers (about 50% compared to control mice, I. den Barber, manuscript in preparation), a basic hypothesis to test is whether we can account for the difference between the responses by assuming a difference in the initial number of T cells A_0 only. Indeed, the quality of the fit is not reduced when we restrict r and δ_A to be the same in Thx and Sthx mice ($F_{2,185} = 0.75, p = 0.48$), which is not the case for restricting identical A_0 with a free r. Further, we are able to estimate a constant fraction of 62% for the initial number of specific T cells in Thx mice compared to SThx mice (Table 4.3). Given this result, we are able to explain the differences in T cell responses for SThx only by a lower precursor frequency of naive T cells.

4.3.3 *Comparing data of $CD8^+$ T cell responses between laboratories*

The availability of data characterizing $CD8^+$ T cell responses against LCMV infections from different laboratories allows us to examine whether the published data are consistent with each other. We can compare the dynamics of T cell responses during acute LCMV infection between the study of Homann et al. (2001) and Wherry et al. (2003). Additionally, we have two studies that

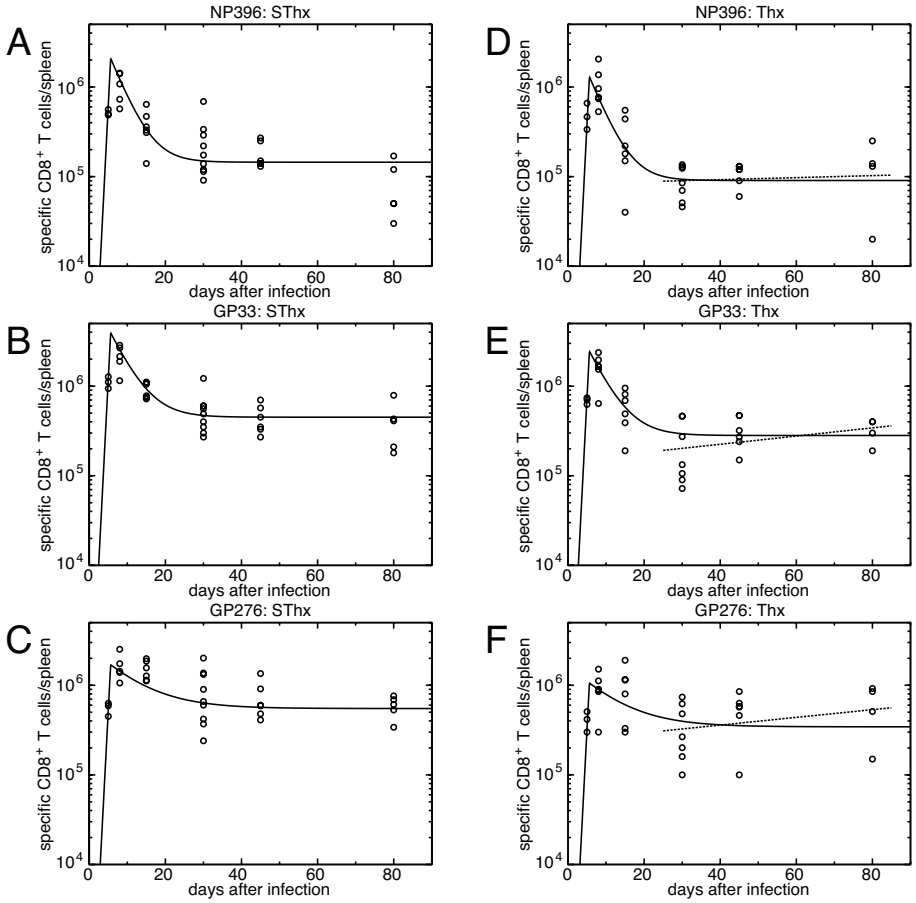

Figure 4.3 Comparison of CD8$^+$ T cell responses during chronic LCMV infection (clone-13) in sham-thymectomized (SThx, panels A-C) and thymectomized (Thx, panels D-F) mice. Each data point represents one mouse as measured in Miller et al. (2005). Statistical analysis using Student's t test and linear regression (dashed line) showed no significant change in T cell numbers after day 30 p.i. for Thx mice and therefore no evidence for a rebound. The solid lines represent the best-fit of the model to the data for each epitope. r and δ_A are restricted to be the same in SThx and Thx mice. $\delta_M = 0$ and $T_{\text{off}} = 5.6$ days. The difference in Thx mice can be explained by a reduced number of naive precursor cells (62%) compared to SThx mice. Other parameters are given in Table 4.3.

Table 4.3 Parameter estimates obtained by fitting the model to the data on $CD8^+$ T cell responses against three epitopes in sham-thymectomized mice (SThx) and thymectomized mice (Thx) during chronic LCMV infection (clone-13). The death rate of effector/memory cells, δ_M, is zero. The number of naive precursor cells in Thx mice are 62% of that in SThx mice. The fraction is given as α.

		NP396		GP33		GP276	
Name	Units	Value	95% CI	Value	95% CI	Value	95% CI
δ_A	d^{-1}	0.23	0.15–0.35	0.19	0.11–0.31	0.072	0.026–0.215
r	d^{-1}	0.017	0.012–0.026	0.024	0.015–0.035	0.035	0.010–0.080
T_{off}	d	5.6	5.4–5.8	5.6	5.4–5.8	5.6	5.4–5.8
A_0 in SThx	Cells	42.8	28.4–58.9	95.5	62.3–136.9	46.0	30.0–65.0
α		0.62	0.54–0.72	0.62	0.54–0.72	0.62	0.54–0.72

quantify T cell responses against chronic LCMV infection (Wherry et al., 2003; Miller et al., 2005). It is important to note that theses studies measure $CD8^+$ T cell responses after the same challenge with virus in the same mouse strain (see in section 4.2: *Materials and Methods*). The only difference is that, compared to normal C57BL/6 mice in Wherry et al. (2003), Miller et al. (2005) use SThx mice. However, it is typically assumed that $CD8^+$ T cell dynamics do not show a different behavior due to surgery without thymus removal.

First, we compared the data on $CD8^+$ T cell responses against NP396 and GP276 during acute LCMV infection from Wherry et al. (2003) to previously estimated parameters by De Boer et al. (2003). Those parameters were obtained by fitting the model to data from Homann et al. (2001) which resulted in very accurate fits. In Fig. 4.4A and 4.4B the data is shown together with the previously estimated dynamics depicted by the solid line. For both responses, the data is described well around the peak, whereas it drops below the previous estimate after 30 days p.i. We also compared responses during chronic infection. NP396- and GP276-specific $CD8^+$ T cell responses as measured in Miller et al. (2005) are shown together with the prediction of the model fitted to data by Wherry et al. (2003) (Fig. 4.4C and 4.4D). Here, the estimated dynamics are far below the data of $CD8^+$ T cell responses from the other laboratory.

This comparison raises the question why T cell measurements using the same experimental protocol lead to different results. On the one hand, it is important to note that the T cell measurements in Homann et al. (2001) were done using intracellular cytokine staining whereas the other studies used MHC tetramer technology. However, a previous study using both techniques to count antigen-specific $CD8^+$ T cells shows more consistent measurements (Murali-Krishna et al., 1998). On the other hand, it is likely that the total numbers of T cells that are measured depend on certain experimental procedures. For example, the preparation of a single-cell suspension of splenocytes is done by squeezing the spleen through a mesh. Here, some laboratories use stainless steel whereas others use meshes made of plastic. To account for problems with eliminating total cell numbers, we introduce a scaling factor where the prediction of cell

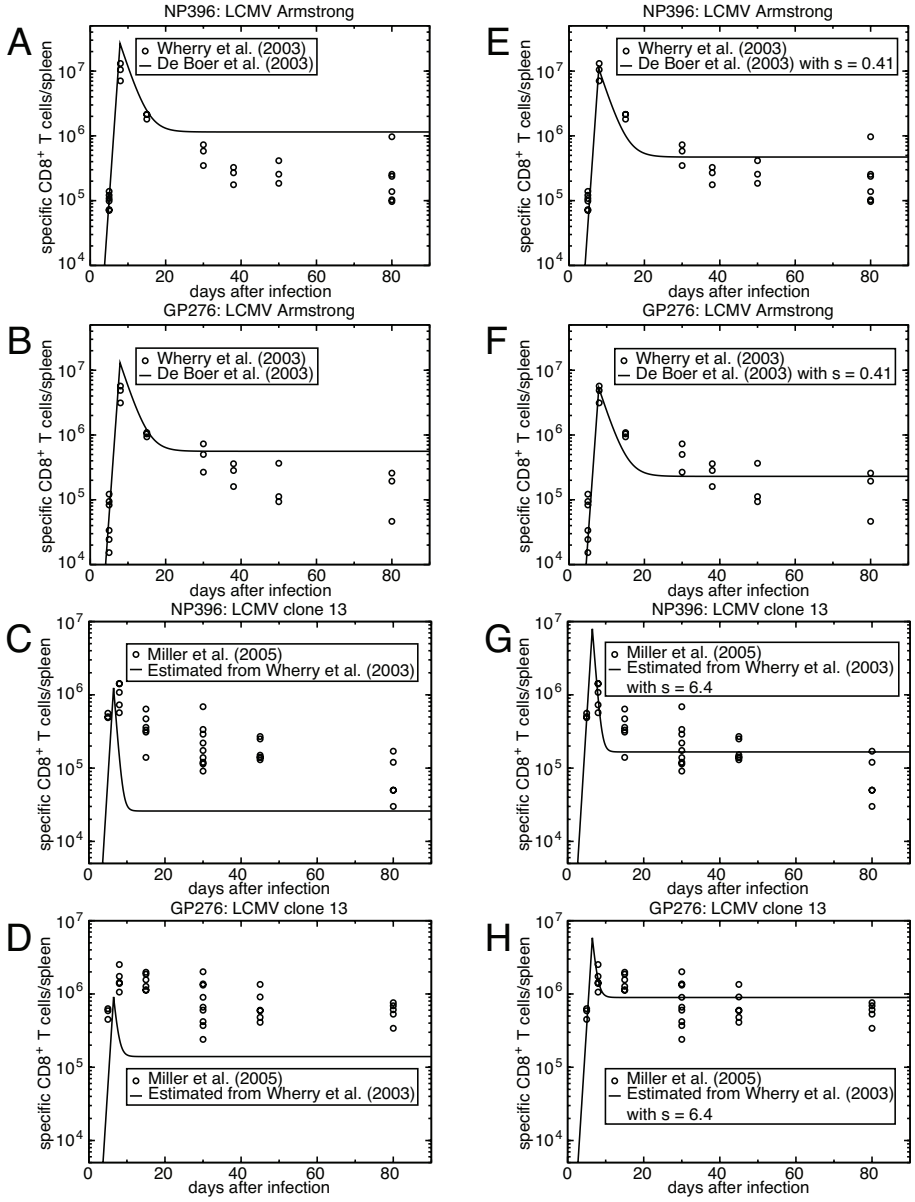

Figure 4.4 Comparing data of antigen-specific CD8$^+$ T cell responses between laboratories. Panels A-D show data on CD8$^+$ T cell responses together with the prediction of the model fitted to a data set from another laboratory. The data is described better by introducing a scaling factor s to account for differences in total T cell numbers between laboratories (panels E-H). In E and F, the predicted dynamics from De Boer et al. (2003) is scaled with $s = 0.41$. G and H are done using a scaling factor of $s = 6.4$.

numbers from one laboratory are given relative to the estimated cell numbers from another laboratory.

Fig. 4.4E and 4.4F again show data from Wherry et al. (2003) together with the $CD8^+$ T cell dynamics as estimated in De Boer et al. (2003). However, by fitting a scaling factor to account for differences in total numbers of T cells, the given lines describe the data much better ($s = 0.41$). Also in 4.4G and 4.4H the estimated parameters from one study describe the data from another study much better, given the application of a scaling factor ($s = 6.4$). Nevertheless, there are still kinetic differences in the data between laboratories as can be seen at 15 days p.i. in Fig. 4.4E and 4.4F, and at day 15 and 80 p.i. in Fig. 4.4H. Altogether, this comparison shows distinct differences between measurements of $CD8^+$ T cell responses from different laboratories.

4.4 DISCUSSION

Our analysis of $CD8^+$ T cell responses allowed us to get new insights into their dynamics. The parameter that differs between antigen-specific responses is the apoptosis rate δ_A. For responses during chronic infection, also the effector/memory formation rate r varies. Comparing acute to chronic infection, we observed that the time of the peak of the response, T_{off}, is different. All other parameters are the same. Zajac et al. (1998) already observed that immunodominance changes during chronic LCMV infection. We can now further discriminate the $CD8^+$ T cell responses between acute and chronic LCMV infection. The responses during chronic infection generally show an earlier peak and a faster contraction of the response. In our model, at the time of the peak of the response, cells stop to proliferate. Virus replication and dynamics could affect this process. Although LCMV Armstrong and clone-13 differ by only two amino acids (Matloubian et al., 1990, 1993), virus replication differs dramatically for chronic infection compared to acute infection. Between day 5 and 8 p.i., acute LCMV infection shows a decrease in serum viral load compared to chronic LCMV infection where virus load is increasing (Fig. 4.5, data by Wherry et al. (2003)). Ongoing expansion of $CD8^+$ T cells may cause immunopathology when the virus is not cleared. Therefore, the $CD8^+$ T cell proliferation might be stopped to reduce acute symptoms (Wodarz and Thomsen, 2005).

In the *Results* section, we assumed the expansion rates to be the same for an epitope-specific $CD8^+$ T cell response during acute and chronic LCMV infection. We also wanted to test two alternative hypotheses for the different dynamics during proliferation. First, we fitted the model to the data with a free expansion rate for $CD8^+$ T cell responses during chronic infection but a restricted T_{off} and A_0 for responses during acute and chronic infection. Second, $CD8^+$ T cells might start to proliferate earlier in one type of infection, i.e. the recruitment time could be different. As mentioned in *Materials and Methods*, in our model the recruitment time is at $t = 0$ and lumped together with the precursor frequency A_0. We can also introduce a $T_{\text{on}} \neq 0$ for later recruitment and a constant $\Delta T = T_{\text{off}} - T_{\text{on}}$ for the time-window of proliferation. Therefore we

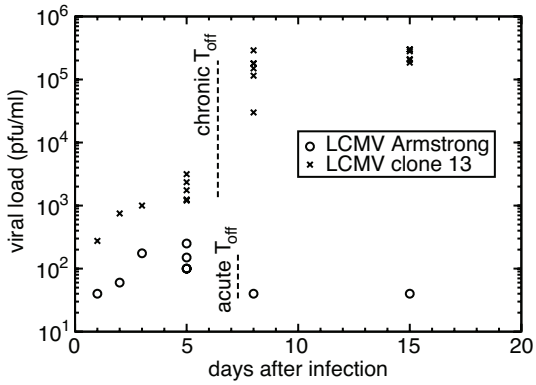

Figure 4.5 Serum viral load during acute and chronic LCMV infection as given in Wherry et al. (2003). The dashed lines represent the estimated time of the peak of the CD8$^+$ T cell responses, T_{off}, during chronic and acute infection, respectively. It can be seen that virus load increases between day 5 and 8 during chronic infection (shown as crosses) but decreases during acute infection (shown as circles).

fitted the model to the data with the same expansion rates and a single ΔT but a different T_{on} for the responses during acute and chronic infection. However, the quality of both fits proved to be worse than the one described in *Results* (based on mean squares, results not shown) and therefore we do not favor these alternative explanations. In Fig. 4.5 it can be seen that the serum viral load during the first five days is higher for chronic than acute infection. This is likely to be due to the higher infectious dose of clone-13. Indeed, there appears to be a constant log difference in serum viral load during the first five days, which suggests a similar replication rate of both virus strains during that time. The higher serum viral load for chronic infection could result in an earlier recruitment and/or a faster proliferation of the CD8$^+$ T cell responses. However, the fitting of the two alternative models described the chronic responses during proliferation with a later recruitment or a slower proliferation, which would disagree with the higher viral load. In combination with the lower quality of the fits of the alternative models, this analysis suggests that the earlier time of the peak during chronic infection is the most likely explanation. More measurements of CD8$^+$ T cell responses during the expansion phase (in between day 3 and 6 p.i.) would be helpful to check whether the proliferation rates for responses during acute and chronic infection are the same, and whether our hypothesis of an earlier peak is valid. The faster contraction rate after the peak derives from differences in the net death rate of activated cells δ_A. It was recently shown that the cytokine interleukin-10 (IL-10) is involved in the immune suppression induced by LCMV clone-13 infection (Ejrnaes et al., 2006; Brooks et al., 2006). Both the net death rate of activated cells and the time of the peak might be influenced by the levels of secreted IL-10. Another recent study by

Grayson et al. (2006) supports our estimates of the apoptosis rates δ_A. Their observation that Bim mutant (apoptosis gene knockout) mice exhibit a similar delay in the contraction of $CD8^+$ T cell responses to all epitopes during acute infection is in line with our finding that δ_A does not differ markedly between the different epitopes. Further, the immunodominance is altered during chronic viral infection in Bim mutant mice, with the loss of Bim preferentially affecting the deletion of $CD8^+$ T cells to epitope NP396. Our estimates for chronic infection show clearly that differences in δ_A between epitopes vary largely, and that the apoptosis rate is largest for NP396.

The fitting of the model to data by Miller et al. (2005) allowed us to give a reinterpretation of the effect of thymectomy on $CD8^+$ T cell responses during chronic LCMV infection. The only parameter that varied between SThx and Thx mice was the initial number of cells, A_0. Hence, we can account for the differences in the responses between SThx and Thx mice simply by differences in the number of naive T cells. This hypothesis is supported by findings that naive T cell numbers in thymectomized young mice are reduced by about 50% (I. den Barber, manuscript in preparation). To test our prediction, one could also perform experiments infecting Thx mice with LCMV Armstrong to see whether cell numbers around the peak of the $CD8^+$ T cell response are lower compared to SThx mice. An alternative explanation for the difference in the $CD8^+$ T cell responses is the lack of continued thymic output of naive T cells in Thx mice. It has indeed been shown that there is continuous recruitment of naive T cells during persistent polyoma virus infection (Vezys et al., 2006). Our model can also allow for the lower cell numbers in Thx mice by a difference in the net death rate of activated cells δ_A (results not shown). A decrease in a net death rate can be interpreted as missing recruitment of naive cells into the activated T cell pool of Thx mice.

Because the analyzed data are derived by infecting mice of the same strain with LCMV it is interesting to compare the different studies. We show that the data sets from different laboratories are kinetically and quantitatively different. Comparing the T cell measurements of a recent study from Grayson et al. (2006) by digitizing their published data also shows large differences to the data sets we used for our analysis (results not shown). Upon introducing a scaling factor between laboratories to account for differences in the total number of cells, the data sets become more consistent. However, there are still kinetic differences. Indeed, several factors could influence the $CD8^+$ T cell responses in these experiments. For example, the environment where the mice are kept in laboratories might be different, and cause a distinct state of the mice immune systems. Especially SThx mice could have a more inflammatory environment due to surgery that might change the dynamics of $CD8^+$ T cell responses. Furthermore, the mouse age at the time of infection differs between the study of Wherry et al. (2003) and Miller et al. (2005), which might affect the number of $CD8^+$ T cells in the spleen. Even within a laboratory, data fluctuations are expected due to the intrinsic stochasticity of the immune response, the so-called process noise (Milutinovic and De Boer, 2007). Alternatively, the estimated kinetic differences

could derive from the number of measurements over time. Again, several measurements around the peak of the response (i.e. between day 5 and 15 p.i.) appear to be important to precisely model the contraction phase of the response. However, some kinetic differences remain that seem to suggest different biological rates in different laboratories, e.g. different apoptosis rates (Table 4.1 and 4.2). Nevertheless, we would like to highlight the importance for multiple measurements around the peak in order to provide a better understanding of CD8$^+$ T cell dynamics.

Our analysis proved to be useful in discriminating the dynamics between CD8$^+$ T cell responses during acute and chronic LCMV infection. However, it remains to be established whether our results can be generalized for other LCMV-specific CD8$^+$ T cell responses not studied here. Although the analysis was done for responses that are dominant during acute or chronic infection, several other epitope-specific responses are likely to be important in clearance or control of viral replication. Indeed, a recent study by Kotturi et al. (2007) identified 19 novel epitopes in LCMV that have not been investigated so far. Additional insight into the dynamics of CD8$^+$ T cell responses could be provided by knockout experiments of mice. The recent study by Grayson et al. (2006) looks promising to get a more detailed knowledge on the influence of apoptosis during the contraction phase of the response. Further analysis in this direction can shed more light on the nature of acute and chronic infections and their accompanying cellular immune responses.

ACKNOWLEDGMENTS

We would like to thank the authors of Wherry et al. (2003) and Miller et al. (2005) for kindly providing us the data and E. John Wherry for giving helpful comments on an earlier version of this paper. We also thank José Borghans for carefully reading the manuscript. C.L.A. and R.J.D.B. gratefully acknowledge financial support by NWO grant 016.048.603. V.V.G. is supported by a Marie Curie Incoming International Fellowship (FP6).

Dynamics of immune escape during HIV/SIV infection

5

C.L. Althaus and R.J. De Boer
Theoretical Biology, Utrecht University
Padualaan 8, 3584 CH Utrecht, The Netherlands.

PLoS Comput Biol. **4(7)**: e1000103 (2008 Jul)

ABSTRACT

Several studies have shown that cytotoxic T lymphocytes (CTL) play an important role in controlling HIV/SIV infection. Notably, the observation of escape mutants suggests a selective pressure induced by the CTL response. However, it remains difficult to assess the definite role of the cellular immune response. We devise a computational model of HIV/SIV infection having a broad cellular immune response targeting different viral epitopes. The CTL clones are stimulated by viral antigen and interact with the virus population through cytotoxic killing of infected cells. Consequently, the virus population reacts through the acquisition of CTL escape mutations. Our model provides realistic virus dynamics and describes several experimental observations. We postulate that inter-clonal competition and immunodominance may be critical factors determining the sequential emergence of escapes. We show that even though the total killing induced by the CTL response can be high, escape rates against a single CTL clone are often slow and difficult to estimate from infrequent sequence measurements. Finally, our simulations show that a higher degree of immunodominance leads to more frequent escape with a reduced control of viral replication but a substantially impaired replicative capacity of the virus. This result suggests two strategies for vaccine design: Vaccines inducing a broad CTL response should decrease the viral load whereas vaccines stimulating a narrow but dominant CTL response are likely to induce escape but may dramatically reduce the replicative capacity of the virus.

5.1 INTRODUCTION

HIV infection in humans and SIV infection in non-human primates is not cleared by the host's immune system. However, there is partial control of virus replication that is mainly attributed to the cytotoxic T lymphocyte (CTL) response (Kaslow et al., 1996; Schmitz et al., 1999). Particularly the evolution of immune escape mutations posing severe fitness costs (Friedrich et al., 2004; Barouch et al., 2005; Kent et al., 2005; Peut and Kent, 2006; Crawford et al., 2007; Frater et al., 2007; Li et al., 2007), suggests that there is a strong selective pressure induced by the CTL response (Phillips et al., 1991; Goulder and Watkins, 2004).

It is a challenge to acquire longitudinal data on CTL escape since the virus diversity within a host has to be followed over a long phase of chronic infection. Additionally, little data is available during the early phase of infection, especially for HIV where the infection is difficult to diagnose during the first weeks. Asquith et al. (2006) analyzed several data sets of immune escape in HIV, and concluded that killing by the CTL response is inefficient in infected humans. More recent studies described more rapid immune escape of SIV, and estimated more efficient killing in non-human primates (Asquith and McLean, 2007; Loh et al., 2007; Mandl et al., 2007). Quantifying the process of CTL escape and estimating rates remains problematic since the underlying process of viral replication might be taken into account (Ganusov and De Boer, 2006). Furthermore, by analyzing escape at single epitopes it is difficult to assess the strength of the total response of different CTL clones recognizing different epitopes. Due to those difficulties it remains a challenge to devise a realistic model of HIV/SIV dynamics and the subsequent CTL escape.

The interaction of viral replication, mutation and selection by different CTL responses appears to be complex. Studies have observed CTL escape very early but also years after primary infection (Goulder et al., 1997; Allen et al., 2000; Cao et al., 2003). Also, it has been shown that the number of epitope-specific CTL responses varies over time (Altfeld et al., 2001; Draenert et al., 2006; Karlsson et al., 2007). Additionally, there is much controversy in the field of HIV evolution as to whether stochastic effects play a role in viral evolution within a host (Kouyos et al., 2006). For example, it has been suggested that the waiting time for compensatory mutations prolongs the emergence of escape variants (Kelleher et al., 2001). To better understand these processes, we present a computational model of HIV/SIV infection taking into account the dynamics of a broad cellular immune response targeting different viral epitopes. The simulations allow us to follow the dynamics in detail, and quantify several critical properties to compare them to data.

5.2 MODEL

We develop a computational model of HIV/SIV virus dynamics including a cellular immune response consisting of several CTL clones (Fig. 6.1). We have n different CTL clones recognizing n different epitopes derived from viral pro-

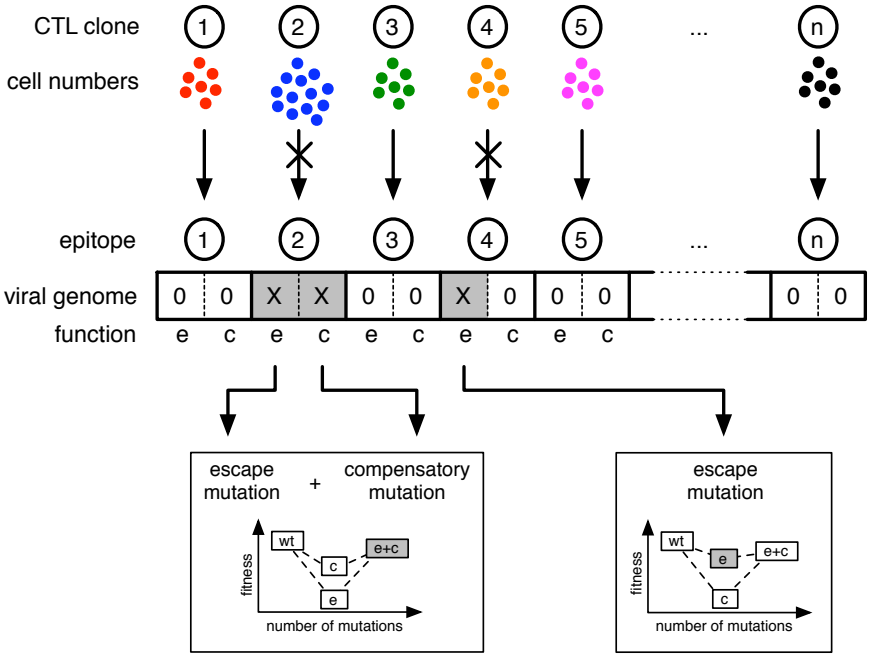

Figure 5.1 A scheme of the computational model of HIV/SIV infection. A number of n CTL clones can recognize n different epitopes and kill the cells infected with virus expressing those epitopes. The virus population can evade recognition from specific CTL clones by acquiring escape mutations (shown as e). Since escape mutations can be associated with a fitness cost in viral replication or infectivity, the virus additionally acquires compensatory mutations (shown as c) that can partially restore the viral fitness.

teins. On the viral genome we allow two mutations to occur per epitope. One mutation confers escape from recognition by the specific CTL clone. Since escape mutations may be associated with a fitness cost in viral replication or infectivity, a second mutation can at least partially compensate for the fitness loss.

We translate those interactions into a set of ordinary differential equations (ODEs) and add stochastic events for viral mutation. Classically, the processes of infecting target cells or the killing of infected cells by CTLs have been described with simple mass-action terms (Nowak and May, 2000; Perelson, 2002). For instance, a previous study already described antigenic escape from CTL clones during HIV-1 infection with a simple mathematical model (Nowak et al., 1995). Recently, we developed terms describing a density-dependent infection that results in a better description of the dynamics of acute infection (i.e. less oscillatory) of the viral load and the immune response (De Boer, 2007). More-

over, the interaction of infected cells with effector CTLs, both for proliferation of effector cells and the killing of infected cells, were assumed to saturate according to Michaelis-Menten kinetics. Here, we integrate those interaction terms to devise a new virus dynamics model consisting of several CTL clones that is described by the following differential equations:

$$\frac{dT}{dt} = \lambda - \delta_T T - \frac{\beta T \sum_{i=1}^{m} V_i f_i}{h_\beta + T + \sum_{i=1}^{m} I_i}, \tag{5.1}$$

$$\frac{dI_i}{dt} = \frac{\beta T V_i f_i}{h_\beta + T + \sum_{j=1}^{m} I_j} - \delta_I I_i - k I_i \sum_{j=1}^{n} \frac{E_j \alpha_{ij}}{h_k + \sum_{l=1}^{m} I_l \alpha_{lj} + \sum_{l=1}^{n} E_l \alpha_{il}}, \tag{5.2}$$

$$\frac{dV_i}{dt} = p I_i - \delta_V V_i, \tag{5.3}$$

$$\frac{dE_i}{dt} = \sigma + g E_i \sum_{j=1}^{m} \frac{I_j \alpha_{ji}}{h_{g_i} + \sum_{l=1}^{n} E_l \alpha_{jl} + \sum_{l=1}^{m} I_l \alpha_{li}} - \delta_E E_i. \tag{5.4}$$

Non-infected $CD4^+$ target cells T are produced at a rate of λ cells per day, die at a rate δ_T and can become infected by virus particles of type V_i with fitness f_i at a maximal rate of β per day. Target cell availability for virus particles is density dependent, as the infection rate per virus particle is saturating over the total number of $CD4^+$ cells (non-infected and infected). After infection of a target cell, reverse transcription occurs during which the virus can mutate with a probability of μ per position (for further details see *Methods*). Having two positions to mutate per n epitopes, the number of different viral variants, m, is maximally 2^{2n}. Infected cells I_i die at a rate of δ_I per day, and are cleared by those CTL clones that can recognize an epitope on its surface. The matrix α_{ij} defines the topology with which the CTL clone E_j recognizes epitopes presented on the surface of the infected cell of type i, and contains either 1 (recognition) or 0 (no recognition). Following Michaelis-Menten kinetics, the CTL clones compete with each other for clearance of infected cells (Fig. 5.2). When $\sum_{l=1}^{m} I_l \alpha_{lj} + \sum_{l=1}^{n} E_l \alpha_{il} \gg h_k$, an infected cell is killed at a maximal rate of k per day. With increasing h_k, we approach mass-action kinetics for the killing, i.e. when $\sum_{l=1}^{m} I_l \alpha_{lj} + \sum_{l=1}^{n} E_l \alpha_{il} \ll h_k$ cells are killed at a per capita rate of $\frac{k}{h_k} \sum_{j=1}^{n} E_j \alpha_{ij}$ per day. Since the dynamics of virus particles V_i is much faster than that of the cell populations (Ramratnam et al., 1999), we assume a quasi-steady-state for the virus particles and set $V_i = p I_i / \delta_V$ (De Boer and Perelson, 1998). 'Naive' CTLs E_i are produced at a rate of σ cells per day. If they recognize antigen produced by I_j (i.e. $\alpha_{ji} = 1$) they proliferate at a maximal rate g per day and die at a rate δ_E. Upon infection, virus replicates rapidly and typically $\sum_{l=1}^{m} I_l \alpha_{lj} \gg \sum_{l=1}^{n} E_l \alpha_{jl}$. Therefore, CTL effector cells are produced at a half-maximal rate when $\sum_{l=1}^{m} I_l \alpha_{li} = h_{g_i}$. To account for different avidities for the different CTL clones E_i we draw h_{g_i} from a uniform distribution. Once the total number of CTL effector cells is high, $\sum_{l=1}^{n} E_l \alpha_{jl}$ becomes important and we get inter-clonal competition between the CTL effector cells. An overview of the

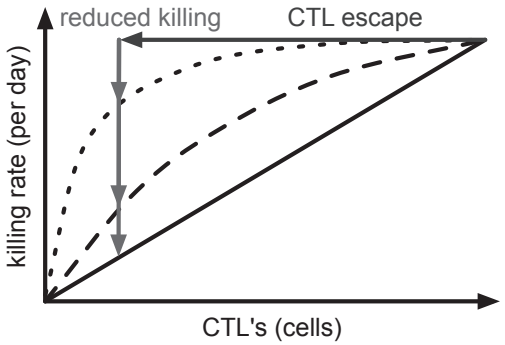

Figure 5.2 Killing rate of an infected cell as a function of the number of CTLs. For killing following mass-action dynamics, the killing rate is linearly increasing with increasing number of CTLs (straight line, $h_k = 10^{12}$). However, if CTL clones compete with each other to kill infected cells, a saturation effect occurs according to Michaelis-Menten kinetics (dashed ($h_k = 10^9$) and dotted ($h_k = 10^8$) line). After a virus escapes recognition from a single CTL clone (horizontal arrow), the killing of infected cells is reduced differently depending on these functions (vertical arrows).

parameters is given in Table 7.1. For a more detailed description of the model see chapter 5.5: *Methods*.

5.3 RESULTS

5.3.1 *Sequential escape from several CTL clones*

The most surprising phenomenon of CTL escape in HIV/SIV is the time scale at which it occurs. Selection of escape variants has been found to happen very early after acute infection, but also late after years (Goulder et al., 1997; Allen et al., 2000; Cao et al., 2003). Additionally, it has been shown that escape can occur sequentially (Geels et al., 2003). Although it has been suggested that compensatory mutations delay the appearance of escape variants, it is still unclear why escape variants would occur so late when the CTL clones recognizing the epitope have been present since acute infection.

Our model describes the virus dynamics of an HIV/SIV infection and the subsequent immune escape in a very realistic manner (Fig. 6.2). Many escapes occur widely spaced out in time and we observe that their appearance is determined by the dynamics of the different CTL clones. Starting with the same CTL clone repertoire, Fig. 6.2A represents a simulation where killing of infected cells approaches mass-action dynamics ($h_k = 10^{12}$). Fig. 6.2B shows a simulation where killing follows Michaelis-Menten kinetics and CTL clones compete for killing of infected cells ($h_k = 10^9$). In both simulations, the total number of infected cells peaks a few weeks after infection and reaches a set-point level of

Table 5.1 Parameters used for simulations of HIV/SIV infection.

Parameter	Value	Explanation and reference
$\beta \frac{p}{\delta_V} - \delta_I$	1.5 d^{-1}	Initial viral growth rate of 1.5 d^{-1} (Mattapallil et al., 2005).
g	1.0 d^{-1}	Maximal CTL proliferation rate (Davenport et al., 2004)
λ	2×10^7 cells d^{-1}	Source of $CD4^+$ target cells, tuned to obtain an infected cell count between 10^7 and 10^8 during the chronic phase (Haase et al., 1996).
$\frac{\sigma}{\delta_E}$	10^3 cells	Maintains a small number of 10^3 'naive' cells per CTL clone in absence of infection.
δ_T	0.01 d^{-1}	Natural death rate of $CD4^+$ target cells T.
δ_I	0.1 d^{-1}	Virus-induced death rate of infected cells (includes δ_T).
δ_E	0.01 d^{-1}	Death rate of cytotoxic T lymphocytes (Ogg et al., 1999; Casazza et al., 2001).
h_{g_i}	$[1.0, 5 \times 10^8]$ cells	Uniform distribution of avidities for the CTL clones. Generates a few dominant (low h_{g_i}) and many sub-dominant (high h_{g_i}) CTL clones (see Fig. 5.6).
k	$0.9(1 + \frac{h_k + I^*}{E^*})$ d^{-1}	Assumes a maximal death rate of infected cells of 1.0 d^{-1} (Bonhoeffer et al., 2003) with CTLs accounting for 90% of infected cell death at the steady-state.
h_k	$10^8 - 10^{12}$ cells	Allows killing of infected cells to follow Michaelis-Menten kinetics (small h_k) or to approach mass-action dynamics (large h_k).
μ	3×10^{-5}	HIV-1 mutation rate per nucleotide (Mansky and Temin, 1995).
n	20	Approximate number of epitopes that are recognized by the CTL responses (Yu et al., 2002; Draenert et al., 2006).

around 10^7 to 10^8 cells (black line in top panels) Haase et al. (1996). The colored lines represent the amount of virus infected cells containing an escape mutation at a specific epitope. Due to the large actual population size of infected cells and the high mutation rate, all single escape and compensatory mutants are produced rapidly during the acute phase of the infection and are maintained in a mutation-selection balance. Some escape variants are being selected early, and replace the wild-type variant at this epitope (e.g. blue line). However, many escapes occur late, despite their early presence in the virus population.

The dynamics of the CTL clones E_i are depicted in the bottom panels. Upon infection, the clones become stimulated depending on the parameter h_{g_i} defining their avidity, which generates a single or a few dominant CTL clones and many sub-dominant clones. Escape preferentially occurs from dominant clones that more efficiently kill infected cells. However, due to a severe fitness cost for the escape mutation, there is no escape from the most dominant CTL clone in this particular simulation run. When an escape variant replaces the wild-type variant, the CTL clone looses antigenic stimulation and declines. Because of inter-specific competition between CTL clones, previously sub-dominant clones can increase in size, increasing the selection pressure for the epitopes they recognize.

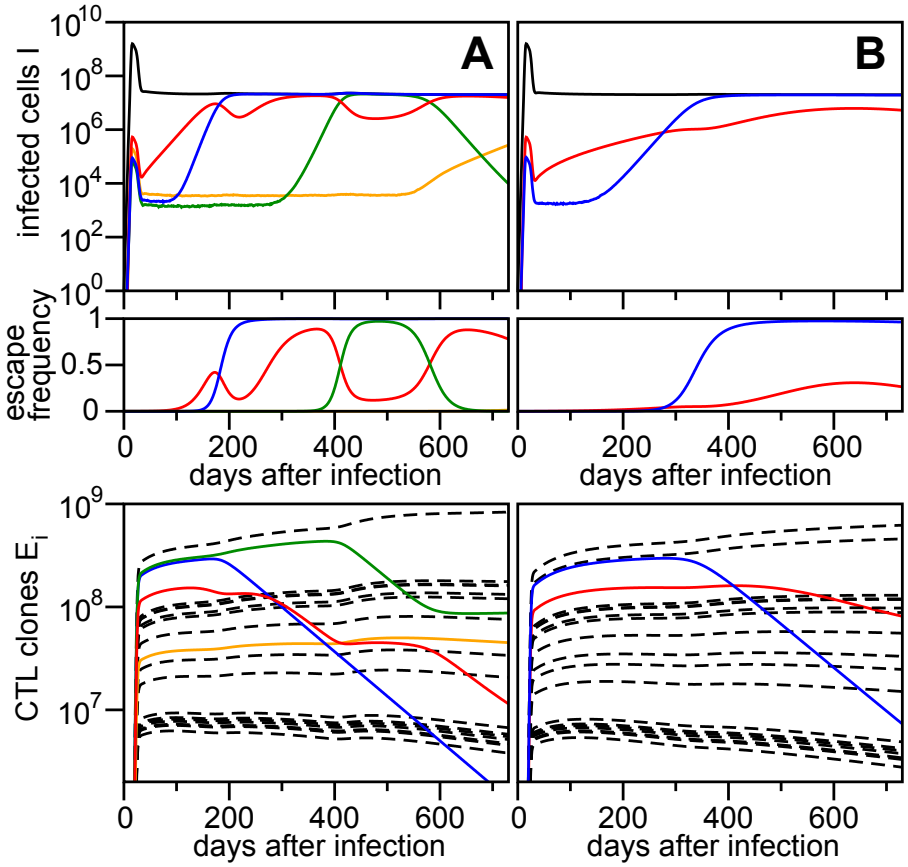

Figure 5.3 Immune escape during the first two years after infection. In the top panels, the total number of infected cells (black line) is shown together with the emerging escape mutants (colored lines). Escape variants expressed as a frequency of the total viral population are given in the middle panels. These variants can fluctuate in frequency (e.g. red line) and, after dominating the viral population, revert back to wild-type (e.g. green line). In the bottom panels, a number of CTL clones proliferate upon infection (full and dashed lines) but can slowly disappear after the virus population escapes recognition (full colored lines). Starting with the same CTL repertoire, more escapes occur when killing of infected cells approaches mass-action dynamics ($h_k = 10^{12}$, shown in A) compared to Michaelis-Menten kinetics ($h_k = 10^9$, shown in B).

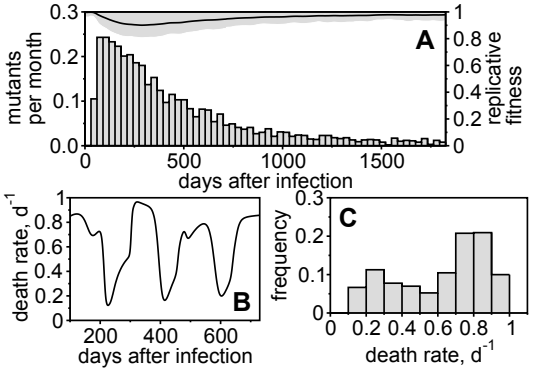

Figure 5.4 Distribution of immune escape over the course of infection. (A) Viral escapes over time given as an expected number of escapes per month (average of 1000 simulations). It can be seen that most escapes occur during the first year after infection (acute phase) and fewer afterwords (chronic phase). The straight line shows the replicative fitness of the viral population as an average over all simulation runs (standard deviation is given by the gray area). The time of escape is measured when an escape variant breaches a frequency of 50% of the total viral population for the first time. (B) Time-plot of average infected-cell death rates during the chronic phase of infection. The graph shows one simulation representing a single patient. (C) Histogram of the death rates that are bound between 0.1 d^{-1} and 1.0 d^{-1}. For (B) and (C), $\max(h_{g_i}) = 5 \times 10^9$. For all figures, $h_k = 10^{12}$, i.e. killing follows mass-action dynamics.

It has been suggested that many escapes occur early, i.e. during the decline phase in viral load after the peak of infection and that they potentially prevent clearance of HIV/SIV. However, in our simulations immune escape does not occur before the set-point level is reached around two to three months after infection (Fig. 5.4A). This is because the CTL clones only become effective during the decline phase of virus after the peak of infection (Davenport et al., 2004; De Boer, 2007). Due to a transient $CD4^+$ target cell depletion (Phillips, 1996; Li et al., 2005; Mattapallil et al., 2005), there is not enough viral replication for escape variants to increase in frequency during this phase. Therefore, escape variants become selected only after the set-point is approached. Nevertheless, many escapes occur during the first months after set-point levels have been attained. After about two years, the virus population stabilizes as the 'easy' escapes have been done, the replicative capacity is partially restored and only few escapes are expected to appear later during infection. However, it is important to note that Fig. 5.4A shows only the first appearance of escape variants. Some of those variants will start to fluctuate in frequency or revert back to wild-type and possibly re-emerge at a later time point. This has implications for the analysis of longitudinal data. If an escape is found to happen late it does not necessarily mean that it had not been selected earlier during infection

Infected-cell death rates from different patients have been found to be close to a normal distribution with a mean of 0.45 d^{-1} (Bonhoeffer et al., 2003). We show that variation of the average infected-cell death rate is also expected to occur within a patient due to the transient decrease of the death rate during an immune escape from CTL mediated killing (Fig. 5.4B). However, the death rate does not necessarily decrease over time, i.e. the half-life of infected cells is not expected to increase with disease progression.

5.3.2 *Rates of escape*

Escape variants not only appear at different times during infection but also with different rates. The rate at which an escape variant replaces the wild-type, the so-called escape rate, is determined by the balance between the evaded rate of killing and the fitness cost of the escape mutation (Fernandez et al., 2005; Asquith et al., 2006). Furthermore, the heterogeneity of the wild-type and the escape variant population at all other epitopes can lead to a different selection induced by other CTL clones. In general, we can define the escape rate as the 'escape variant growth rate - wild-type growth rate'. A recent study quantified this process and concluded on the basis of slow escape rates and minimal fitness costs that killing of HIV-1-infected cells is inefficient in humans (Asquith et al., 2006). Unfortunately, the available data sets do not allow us to follow the process of escape in detail. In contrast, our model provides a unique tool to follow the dynamics and analyze rates of escape and link those to rates of killing.

Fig. 5.5A shows the distribution of escape and the corresponding rates that occur in 1000 simulation runs over five years of infection. The histograms of killing and escape rates are shown in Fig. 5.5B and 5.5C, respectively. Although the total killing by all CTL clones is high (0.9 d^{-1}, see Table 7.1), most individual killing rates are below 0.4 d^{-1}, and most escape rates are below 0.2 d^{-1}. The lower rates of escape are due to the fitness cost of escape mutations that cannot totally be restored by compensatory mutations. Interestingly, the rates of escape are not distributed equally over the time of infection (Fig. 5.5A). We therefore calculate the mean of killing and escape rates per year after infection (Fig. 5.5D). It can be seen that escape rates decrease late during infection and reach relatively low values. The corresponding killing rates decrease after the first year of infection and dramatically increase late during infection. This result shows a) that the selection strength of CTL clones can increase after there has been escape from other clones and b) that escape against efficient CTL clones can be associated with a dramatic cost in viral fitness that slows down the selection of the escape variant.

In Fig. 5.5A-D we assumed mass-action kinetics for the interaction of CTLs to kill infected cells, i.e., we set $h_k = 10^{12}$. However, when CTL effector cells form a complex with infected cells before delivering their lethal hit, the killing should follow Michaelis-Menten kinetics (De Boer, 2007; Regoes et al., 2007). We analyzed the influence of a saturating killing term using several lower values of

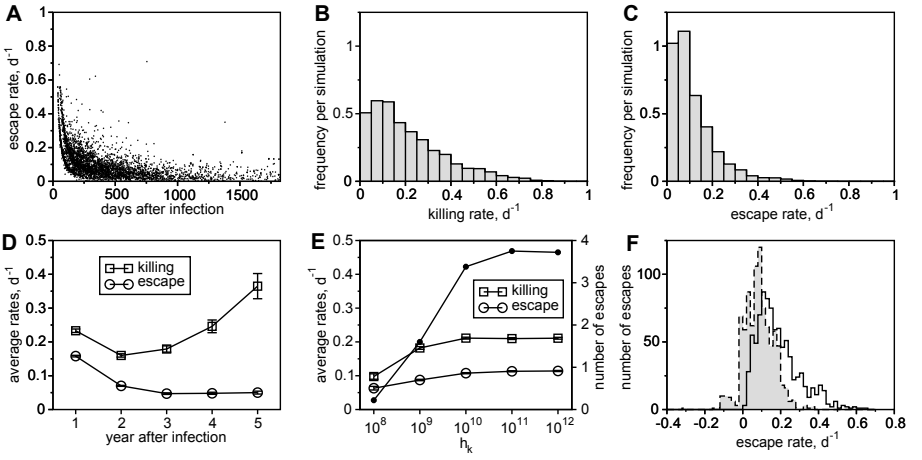

Figure 5.5 Rates of killing and escape. (A) The emergence of escape and the corresponding rates over a time course of 5 years of infection. (B) Given those escapes, the distribution of killing rates given as an average frequency per simulation run. (C) The distribution of escape rates given as an average frequency per simulation run. (D) Average killing and escape rates per year after infection. (E) The number of escapes during 5 years of infection (filled circles) and the average rate of killing and escape as a function of h_k (open symbols). (F) Estimated rates of escape by artificial virus sampling. The two histograms show the distribution of the estimated (gray bars) and the true escape rates (black line). Mean of the estimated rates is 0.09 ± 0.08 d^{-1} and the mean of the true rates is 0.19 ± 0.11 d^{-1}. All graphs represent data from 1000 simulation runs. The rates are measured when the frequency of the escape variant is 50%. Means are given with standard errors since standard deviations are usually very large. $h_k = 10^{12}$ if not otherwise indicated.

h_k (Fig. 5.5E). Although the maximal total killing is constant (see Table 7.1), we can see that killing and escape rates decrease if the model approaches Michaelis-Menten kinetics. Moreover, escape occurs relatively frequent for high values of h_k (mass-action) but rarely for low values of h_k (saturation) (black dots).

To estimate rates of escape from *in vivo* data one has to obtain ratios of escape variants to the wild-type. However, a problem arises when escapes are too rapid to be followed by the relatively long sampling intervals (Asquith and McLean, 2007). This shortcoming can lead to an underestimation of the rate of escape. To analyze this effect we measure the frequency of an escape variant at four time points (100, 150, 200 and 250 days after infection) and estimate the escape rate as described in Asquith et al. (2006) (see also chapter 5.5: *Methods*). Fig. 5.5F shows the distribution of the estimated escape rates (gray bars) and the true escape rates (black line). Even though the sampling intervals were relatively short (50 days) it can be clearly seen that the estimated rates are generally lower, with a mean of about 50% of the true rates.

Our analysis shows several properties of the process of escape. Even though the total killing induced by all CTL clones is high, escape rates are expected to be slow. First, escape rates slow down due to the acquired fitness cost in viral replication, especially during later phases of infection. Secondly, if killing of infected cells follows Michaelis-Menten kinetics, the rates of escape are decreased. In addition, estimating rates of escape from ratios of escape variants and wild-type virus is likely to lead to an underestimation of the true rate. These findings highlight that slow escape rates do not necessarily infer low killing rates.

5.3.3 *Immunodominance and viral evolution*

CTL responses during HIV infection generally consist of several CTL clones recognizing many different epitopes. The size of those CTL clones can differ substantially resulting in dominant and sub-dominant responses (Yu et al., 2002; Draenert et al., 2006). In our model, the relative size of a CTL clone depends on how well it can recognize viral antigen, and is defined by h_{g_i}. By changing $\max(h_{g_i})$ we can change the sizes of the CTL clones relative to each other. For high $\max(h_{g_i})$ we get strong immunodominance with a single or few dominant clones and many sub-dominant clones, whereas low values of $\max(h_{g_i})$ result in CTL clones that are very similar in size (Fig. 5.6A). Note, that the total killing induced by the sum of all CTL clones remains constant (0.9 d^{-1}) and is independent of $\max(h_{g_i})$.

To investigate the effect of immunodominance we run simulations for different values of $\max(h_{g_i})$. Strong immunodominance, where single CTL clones can induce a strong selection pressure on the viral population, leads to more frequent escape (Fig. 5.6B). Concurrently, viral replication is controlled less efficiently and the number of infected cells increases with increasing immunodominance (Fig. 5.6C). However, viral escape can be associated with a fitness cost. Even though the number of infected cells increases, the replicative capacity of the viral population is reduced substantially (Fig. 5.6D).

5.4 DISCUSSION

The interaction of the HIV quasispecies with the CTL response appears to be complex which makes the analysis of experimental data difficult. Mathematical and computational models have been helpful to investigate how different processes influence each other. For example, a previous model described how shifting immunodominance and antigenic oscillations can occur during HIV infection (Nowak et al., 1995). Now, with a model incorporating multiple CTL responses together with escape and compensatory mutations, we show that the dynamics of the CTL clones are sufficient to explain the sequential and late occurrence of escape variants. Upon loss of antigenic stimulation, CTL clones disappear slowly (Ogg et al., 1999; Casazza et al., 2001). Concomitantly, other CTL clones can increase in size and induce more efficient killing that leads to further escape that is sequentially distributed over many years after infec-

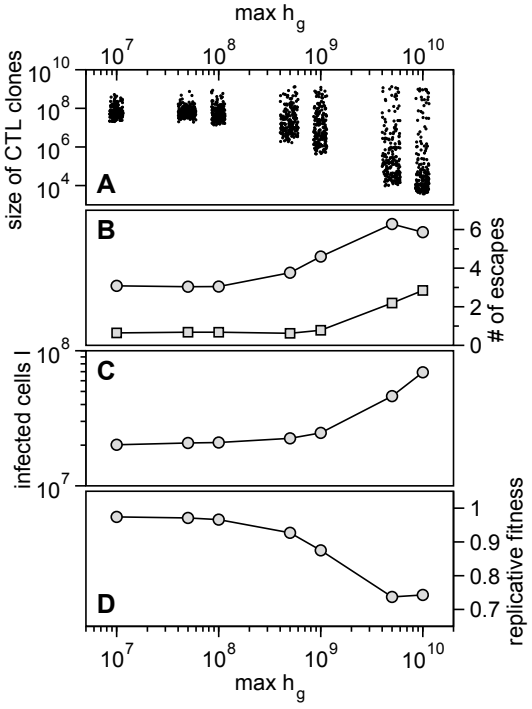

Figure 5.6 Influence of immunodominance on viral evolution. (A) The distribution of CTL clones plotted as a function of max(h_{g_i}). Lower values of max(h_{g_i}) yield a broad repertoire of CTL clones that are similar in size whereas for higher max(h_{g_i}) the degree of immunodominance increases. The dots represent the size of CTL clones for 10 simulations at 50 days after infection. Noise is added on the horizontal axis for better visibility. (B) Escape is more frequent for a higher degree of immunodominance. The numbers of escape variants that have occurred within 5 years of infection are shown as circles. As many escapes start to oscillate or revert back to wild-type, the number of escapes that are above 50% in frequency at 5 years after infection is shown as squares. (C) Infected cell numbers increase with increasing immunodominance. (D) The replicative fitness of the virus decreases with increasing immunodominance. Numbers are given after 5 years of infection and represent averages from 1000 simulation runs.

tion. Interestingly, the outgrowth of escape variants does not occur earlier even though they are always present in the viral population. It has been suggested that a small effective population size of HIV-infected cells is responsible for the late production and selection of escape variants (Liu et al., 2006). However, a recent study argues that stochastic effects play a minor role for the appearance of deleterious and beneficial mutations in HIV (Kouyos et al., 2006). Also, our simulations show that viral evolution is fairly deterministic. The model allows us to simulate two identical 'patients' that are infected with the same virus and have the same CTL repertoire. In that case, the stochastic generation of the viral variants results in a slow increase in variation over years (results not shown). For example, the emergence of a certain escape variant is predictable during the first years after infection but becomes more variable later on. This is in line with a recent study where concordant evolution of HIV has been observed in mono-zygotic twins early during infection but more variation has been shown at later stages of the infection (Draenert et al., 2006).

Another explanation for the late appearance of escape variants that has been put forward is the waiting time for compensatory mutations (Kelleher et al., 2001). Our simulations show that single compensatory mutations are expected to be present in the viral quasispecies and therefore should not slow down the emergence of escape. However, if more compensatory mutations are needed to restore the fitness loss of an escape variant they can delay their occurrence (results not shown). Due to epistasis however, the fitness interactions of several mutations are highly complex and therefore simulation results depend mainly on a presumed fitness landscape. Therefore, we propose a way to test the two hypotheses for the late appearance of escape variants. First, if the delay was due to the waiting time for compensatory mutations, late escapes would be associated with more compensatory mutations than early escapes. If on the other hand, the dynamics of CTL clones mainly determines the late appearance, CTL clones where escape has been detected late should have increased in size relative to the other CTL clones in the period before. Both of these hypotheses can be tested by analyzing longitudinal data of HIV/SIV infections.

Our simulations proved to be useful to analyze the process of escape. We conclude that, although killing can be very efficient, escape rates are expected to be low. The association with a fitness cost and the way how CTL clones interact with infected cells critically influence the rates of escape. Hence, it appears to be important to study those interactions to derive realistic killing terms (Regoes et al., 2007). Furthermore, we have shown that estimating rates of escape is difficult from infrequent sequence measurements. We propose that sequence intervals should be shortened to follow the outgrowth of the variants. Additionally, there might be other reasons that slow down the selection of escape variants. For example, our model does not take into account multiple infected cells. As the fraction of multiple infected cells is large (Jung et al., 2002), escape variants are likely to appear in cells that are also infected with wild-type virus. As long as wild-type epitopes are presented on the cells surface, the escape variant does not gain any growth advantage compared to the wild-type. As a

consequence, the selection of escape variants is expected to slow down.

Immunodominance affects the viral evolution within a host. A higher degree of immunodominance leads to more frequent escape with a reduced control of viral replication but a substantially impaired replicative capacity of the virus. This is interesting as vaccines generally aim to induce a broad CTL response where escape is unlikely to occur. However, a dramatic reduction of the replicative capacity of the virus due to escape could indeed slow down disease progression and/or reduce transmission (Altfeld and Allen, 2006). Based on these results we identify two strategies for vaccine design: Vaccines inducing a broad CTL response should decrease the viral load whereas vaccines stimulating a narrow but dominant CTL response are likely to induce escape and consequently reduce the replicative capacity of the virus.

The balance between the CTL response and the viral population acquiring escape mutations appears to be a dynamical process over a long period of infection. We have shown that it is important to analyze the kinetics of this process and also the time scale (acute and chronic phase) at which it occurs. More longitudinal data of HIV infections will help to further investigate this process and future research is likely to go into this direction.

5.5 METHODS

5.5.1 *Stochastic events*

The set of ordinary differential equations (ODEs) is extended with stochastic events for viral mutation (similar as in Nowak et al. (1991)). Initially at day 0, infection occurs with the wild-type. Therefore the number of viral variants, $m(0)$, is 1. In the following, the ODEs are integrated using the routine odeint from Numerical Recipes (Press et al., 1992). Every time step $\Delta t = 1$ day, we approximate the number of cells that have been infected with virus of type i during the last time step according to

$$\Delta I_i(t) = \frac{\beta T(t) V_i(t) f_i}{h_\beta + T(t) + \sum_{j=1}^{m} I_j(t)} \Delta t. \tag{5.5}$$

After infection, reverse transcription of the viral RNA occurs during which every position can mutate with the probability μ. For the cells being newly infected with virus of type i, we calculate the integer number x_{ij} of cells where the virus mutated into another type j. This is done by drawing from the binomial distribution $x_{ij} = B(\Delta I_i, \mu)$ for each of the two positions (escape and compensatory) over a total of n epitopes. Then, the infected cell populations are updated accordingly (i.e. $I_i = I_i - x_{ij}$ and $I_j = I_j + x_{ij}$). Whenever a previously not existing viral variant j is generated, $m(t) = m(t - \Delta t) + 1$, and the set of ODEs is expanded. We also take into account the actual population size of virus infected cells (Kouyos et al., 2006). If the number of infected cells of a certain variant falls below 1, the variant is deleted. Note, that in order for the

simulations to be computationally efficient, we only generate the viral variants stochastically but do not include possible fluctuations at small population sizes. However, this hybrid stochastic-deterministic approach is sufficient to keep the variants in a mutation-selection balance. Running the model using the Gillespie algorithm (Gillespie, 1977), we observed that whenever the different viral variants become selected, their growth approximates the deterministic description from the ODEs. A program of the model was written in C and simulations were run under Linux. The source code can be obtained freely on request from the authors.

5.5.2 *Viral fitness*

Escape mutations in HIV and SIV are likely to confer a fitness cost in viral replication or infectivity (Friedrich et al., 2004; Barouch et al., 2005; Kent et al., 2005; Peut and Kent, 2006; Crawford et al., 2007; Frater et al., 2007; Li et al., 2007). A recent study by Parera et al. (2007) showed that fitness effects caused by random single mutations are approximately uniformly distributed. Therefore, we draw the fitness of a virus containing a single mutation relative to the wild-type virus from a uniform distribution between 0.0 and 1.0. However, the combined effect of an escape mutation together with a compensatory mutation in a single epitope confers a higher fitness that is drawn uniformly between wild-type fitness ($f_{wt} = 1.0$) and the higher fitness of the two single variants.

5.5.3 *Estimating rates of escape*

The outgrowth of an escape variant and the subsequent replacement of the wild-type can be considered as a competitive growth between two populations:

$$\frac{dw}{dt} = aw - bw - cw, \tag{5.6}$$

$$\frac{de}{dt} = a'e - be, \tag{5.7}$$

where w is the wild-type and e is the escape variant. Cells infected with wild-type virus replicate at a net rate a and are killed by all CTL clones recognizing epitopes other than the escape epitope at rate b. The CTL clone recognizing the escape epitope kills wild-type cells at rate c. Cells infected with the escape variant replicate at a net rate a' and are only killed by the CTL clones recognizing epitopes other than the escape epitope. For $c > 0$, the escape variant gains a growth advantage as long as the fitness cost of the escape, $d = a - a'$, is not higher (i.e. $d < c$). As shown in Asquith et al. (2006) this model can be fitted to longitudinal data of escape. This is done using the routine lmfit (http://sourceforge.net/projects/lmfit) based on the Levenberg-Marquardt algorithm to solve nonlinear least-squares problems. However, the fitting is likely to underestimate the true rates of escape as it is illustrated in Fig. 5.7.

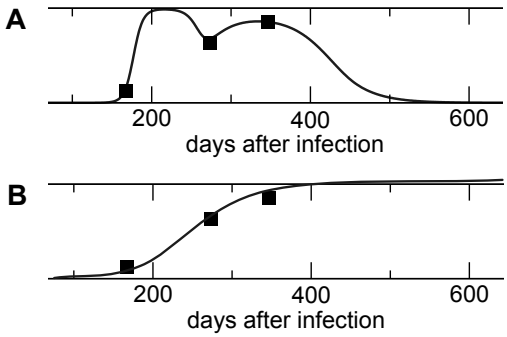

Figure 5.7 Estimating rates of escape. (A) Escape variants often only transiently replace the wild-type variant and oscillate thereafter. Sequence measurements are taken at arbitrary time points (squares). (B) When a model is fitted to those data points the initial escape rate is likely to be underestimated.

5.5.4 *Killing terms*

We assume Michaelis-Menten kinetics for the killing of infected cells by CTL effector cells:

$$kI_i \sum_{j=1}^{n} \frac{E_j \alpha_{ij}}{h_k + \sum_{l=1}^{m} I_l \alpha_{lj} + \sum_{l=1}^{n} E_l \alpha_{il}}. \tag{5.8}$$

This term takes into account the effector/target cell ratio of the cellular interaction: the total killing is proportional to infected cells at high effector cell densities and proportional to effector cells at high infected cell densities De Boer (2007). However, we also analyzed the outcome of other killing terms following different kinetics:

$$kI_i \sum_{j=1}^{n} E_j \alpha_{ij}. \tag{5.9}$$

Here, infected cells are killed by effector cells following simple mass-action kinetics. We mentioned that by increasing h_k in Equation (5.8) we approach mass-action kinetics and the results are discussed.

$$kI_i \frac{\sum_{j=1}^{n} E_j \alpha_{ij}}{h_k + \sum_{j=1}^{n} E_j \alpha_{ij}}. \tag{5.10}$$

Single saturation over CTL effector cells E is similar to the double-saturating term used in equation (5.8): once the set-point is reached, $\sum_{l=1}^{n} E_l \alpha_{il} \gg \sum_{l=1}^{m} I_l \alpha_{lj}$, and equation (5.8) approaches equation (5.10).

$$kI_i \sum_{j=1}^{n} \frac{E_j \alpha_{ij}}{h_k + \sum_{l=1}^{m} I_l \alpha_{lj}} \tag{5.11}$$

Taking into account that CTL effector cells need some time to interact with infected cells before delivering their lethal hit, a saturation effect occurs as given in equation (5.11) (see also De Boer (2007)). We define $k = \frac{0.9(h_k+I^*)}{E^*}$, to have infected cells being killed at a maximal rate of 0.9 d^{-1} during the chronic phase of infection. I^* and E^* are the numbers of infected cells and CTL effector cells, respectively, in the steady-state in absence of escape. During the acute phase, we observe three types of dynamics: 1) For $h_k \lessapprox 5 \times 10^7$, the infection is always cleared since an infected cell can be killed at a rate of $k\frac{E}{I}$ per day that can be enormous. 2) For $5 \times 10^7 \lessapprox h_k \lessapprox 7 \times 10^7$, a very rapid escape during acute infection can prevent clearance of the infection. 3) For $h_k \gtrapprox 7 \times 10^7$, we approach mass-action kinetics since $h_k \gg I$ and the term becomes $\frac{k}{h_k}IE$.

ACKNOWLEDGMENTS

We would like to thank Vitaly Ganusov for extensive discussions. Christian L. Althaus and Rob J. De Boer gratefully acknowledge financial support by the Netherlands Organisation for Scientific Research (VICI grant 016.048.603).

Intracellular delays and multiple infection of cells impede immune evasion in HIV

6

C.L. Althaus and R.J. De Boer
Theoretical Biology, Utrecht University
Padualaan 8, 3584 CH Utrecht, The Netherlands.

manuscript in preparation

ABSTRACT

Due to its high mutation rate, HIV is capable to escape recognition and killing from cytotoxic T lymphocytes (CTL). The rate at which escape variants appear can give insights into the selective pressure imposed by single CTL clones. Here, we investigate the effects of specific properties of the HIV life cycle on the dynamics of immune escape. First, a large fraction of cells in HIV-infected patients has been found to carry multiple copies of proviruses. If a cell harboring an escape variant is also infected with wild-type virus, the selective advantage of the escape variant should be diminished. To investigate how this process affects the emergence of immune escape, we develop a mathematical model of HIV dynamics with multiple infections of cells. With increasing frequency of multiple infected cells, the appearance of escape variants slows down. Interestingly, multiple infected cells can prevent the outgrowth of the escape virus if the variant is associated with a fitness cost that would otherwise allow the variant to become selected in the absence of multiple infected cells. Second, we study the effect of the intracellular eclipse phase on the rate of immune escape. Intracellular delays critically affect the replacement rates of viral variants and we can show again that escape rates are expected to be slower than previously anticipated. All together, our study illustrates that slow escape rates do not necessarily imply inefficient CTL-mediated killing of infected cells, but are at least partly a result of specific properties of the HIV replication life cycle.

6.1 INTRODUCTION

Cytotoxic T lymphocytes (CTLs) are attributed to induce a strong selection pressure on HIV replication through killing of virus-infected cells (Phillips et al., 1991; Goulder and Watkins, 2004; Kawashima et al., 2009). Due to the high mutation rate of HIV, the virus can acquire immune escape mutations and frequently evades recognition from the CTLs. Analyzing longitudinal data on the evolution of immune escape variants can give insights into the selective pressure that is induced by the CTLs. That is, the rate at which an escape variant replaces the wild-type virus reflects the difference in the growth rate of the two variants. Since the escape variant is considered to have evaded the killing induced by a specific CTL clone, the 'escape rate' has been related to the rate at which the infected cells were killed by specific CTLs. Asquith et al. (2006) have analyzed a large data set of longitudinal data on immune escape and generally found slow escape rates which suggested that CTL-mediated killing of infected cells is inefficient. However, interpreting data of immune escape is challenging and critically depends on the underlying assumptions of how immune escape variants replace the wild-type virus (Ganusov and De Boer, 2006; Althaus and De Boer, 2008).

Here, we investigate the effects of specific properties of the HIV replication life cycle on the dynamics of immune escape. It has been found by Jung et al. (2002) that a large fraction of HIV-infected cells in the spleen harbor more than one provirus. This observation has led to a series of models to study the influence of multiple infected cells during HIV infection. Mathematical and population genetic models have given important insights into the evolution of drug-resistant variants (Bretscher et al., 2004; Fraser, 2005; Althaus and Bonhoeffer, 2005). Dixit and Perelson (2004, 2005) have analyzed the process of multiple infection and how it affects the viral dynamics within a host. A more recent study investigated how multiple infected cells affect the evolution of the replicative fitness of HIV (Wodarz and Levy, 2007). An intriguing aspect of multiple infected cells has already been noted in the study by Jung et al. (2002), namely that *"mutation in an epitope that is encoded by one provirus would still leave the cell vulnerable to recognition of the same epitope encoded by the other proviruses"*. Unfortunately, there is no study to date that quantitatively investigates the impact of multiple infected cells on the evolution of immune escape variants. To this end, we devise a new mathematical model of HIV dynamics with multiple infected cells in order to study the appearance of CTL escape variants. Additionally, we investigate how the intracellular eclipse phase, i.e., the delay of an infected cell before it starts to produce new viral particles, affects the dynamics of immune escape in HIV. In both cases, we find that the rate of immune escape is expected to slow down due to the specific properties of the HIV replication life cycle. This suggests that although the rate of CTL-mediated killing can be high, the rate of immune escape is expected to be slower than previously anticipated by basic virus dynamics models.

Our findings have important implications on the quantitative aspects of CTL-mediated killing of HIV-infected cells. We illustrate that slow escape rates do not necessarily imply inefficient killing of infected cells, but are at least partly a result of certain properties of the viral life cycle. Hence, our study takes away evidence suggesting that CTLs are not important in the control of HIV infection, and emphasizes the importance of quantifying the dynamics of immune escape in HIV.

6.2 MODEL

6.2.1 *Multiple infections of cells*

We devise a mathematical model of HIV dynamics that is based on standard models of within-host virus dynamics (Nowak and May, 2000; Perelson, 2002). To account for multiple infections of cells, single infected cells can get infected by a second viral particle to become a double infected cell (Fig. 6.1):

$$\frac{dT}{dt} = \lambda - \beta V_w T - \beta' V_e T - \delta_T T, \tag{6.1}$$

$$\frac{dS_w}{dt} = \beta V_w T - r V_w S_w - r' V_e S_w - (\delta + k) S_w, \tag{6.2}$$

$$\frac{dS_e}{dt} = \beta' V_e T - r' V_e S_e - r V_w S_e - \delta S_e, \tag{6.3}$$

$$\frac{dD_{ww}}{dt} = r V_w S_w - (\delta + k) D_{ww}, \tag{6.4}$$

$$\frac{dD_{we}}{dt} = r V_w S_e + r' V_e S_w - (\delta + k) D_{we}, \tag{6.5}$$

$$\frac{dD_{ee}}{dt} = r' V_e S_e - \delta D_{ee}, \tag{6.6}$$

$$\frac{dV_w}{dt} = p(S_w + D_{ww} + D_{we}/2) - \delta_V V_w, \tag{6.7}$$

$$\frac{dV_e}{dt} = p(S_e + D_{ee} + D_{we}/2) - \delta_V V_e. \tag{6.8}$$

Non-infected $CD4^+$ target cells T are produced at a rate of λ cells per day and die with rate δ_T. They can become infected with either the wild-type virus, V_w, at rate β or the escape variant, V_e, at rate β'. We define $\beta' = \beta(1-c)$ to account for a potential fitness cost of the escape variant. After a cell has been infected with a single virus (S_w and S_e), it can become double infected with wild-type or escape virus at rate r or r', respectively. Again, we set $r' = r(1-c)$ to account for a potential fitness cost of the escape variant. The resulting double infected cells are either infected with the same virus (D_{ww} and D_{ee}) or infected with the wild-type and the escape variant (D_{we}). To account for different frequencies of multiple infected cells, we will vary the secondary infection rate r. We define f as the fraction of multiple infected cells in the absence of an escape variant when

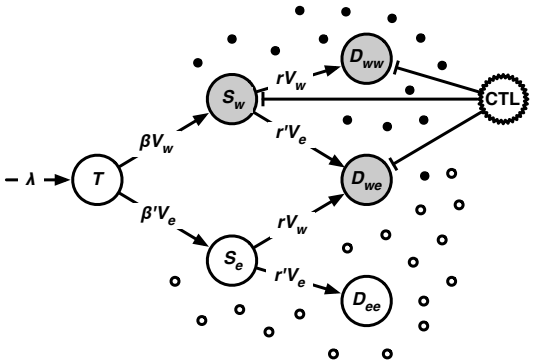

Figure 6.1 Illustration of multiple infections of cells with HIV. Uninfected target cells, T, can either become infected with wild-type virus (V_w) or the escape variant (V_e). A secondary infection of a single infected cell with another virus results in a double infected cell. The single and double infected cells, S and D with their corresponding indices, respectively, produce wild-type (black dots) and escape variant virus (open circles). CTL-mediated killing only targets the cells that produce wild-type virus (gray cells). Death rates of cells and virus production and clearance rates are not shown.

the infection has approached the chronic steady-state, i.e., $f = D_{ww}/(S_w + D_{ww})$. The secondary infection rate r can then be expressed as a function of f in the interval of $[0, 1)$, i.e., any desired fraction of multiple infected cells can be obtained setting r as:

$$r = \frac{f\beta\delta_V(\delta + k)^2}{(f-1)(\delta_T\delta_V(\delta + k) - p\beta\lambda)}. \tag{6.9}$$

Wild-type and escape virus is produced by their corresponding cells with rate p per day and cleared at rate δ_V per day. The production of cells that are doubly infected with both variants is divided into one-half for each. Cells that produce wild-type virus will additionally be killed by a specific CTL clone at a rate k per day. We also include mutation in our model but for better clarity it is not shown in the equations. Shortly, mutation happens upon infection and is included in all infection terms. For example, if a target cell, T, becomes infected with wild-type virus V_w, a small fraction mutates into an escape variant ($\mu\beta V_w T$) whereas the majority remains wild-type ($(1-\mu)\beta V_w T$). The parameters for the model are given in Table 7.1.

6.2.2 *Intracellular delay*

Additionally, we devise a model of virus dynamics to study the effects of an intracellular delay on the rate of immune escape. As the escape variant competes with the wild-type virus on the same resource, i.e., infecting the $CD4^+$ target cells, they replace each other at a rate that is given by the difference between

Table 6.1 Parameter values for the HIV dynamics model with multiple infections.

Parameter	Value	Explanation and reference
λ	3×10^7 cells d^{-1}	Tuned to obtain a total number of 10^7 – 10^8 infected cells (Haase et al., 1996; Kouyos et al., 2006).
δ_T	0.1 d^{-1}	Natural death rate of $CD4^+$ target cells T.
β	1×10^{-10} d^{-1}	Infection rate per virus particle. Results in an initial viral growth rate of 1.5 d^{-1} (Mattapallil et al., 2005).
$\delta + k$	1.0 d^{-1}	Maximal death rate of virus-producing cells (see Chapter 3 and Dixit and Perelson (2004)).
p	2300 d^{-1}	Virus production rate.
δ_V	23 d^{-1}	Clearance rate of viral particles (Ramratnam et al., 1999).
μ	3×10^{-5}	HIV-1 mutation rate per nucleotide (Mansky and Temin, 1995).

their corresponding net growth rates. In order to derive an analytical solution of the 'escape rate', we simplify the description of HIV dynamics into cells that are infected with either the wild-type virus or the escape variant:

$$\frac{dI_w}{dt} = bP_w - \gamma I_w - \delta_I I_w - k_I I_w, \tag{6.10}$$

$$\frac{dP_w}{dt} = \gamma I_w - \delta_P P_w - k_P P_w, \tag{6.11}$$

$$\frac{dI_e}{dt} = bP_e - \gamma I_e - \delta_I I_e, \tag{6.12}$$

$$\frac{dP_e}{dt} = \gamma I_e - \delta_P P_e. \tag{6.13}$$

Infected cells, I_w and I_e, move through an intracellular eclipse phase with rate γ per day to become virus-producing cells, P_w and P_e. In the model, the production of new infected cells is not density-dependent as we exclude an equation for target cells like the one given in Eq. 6.1. New infected cells are 'produced' at a per capita rate b proportional to the number of virus-producing cells. The infected cells during the eclipse phase are subject to a death rate δ_I, and the cells infected with wild-type virus are additionally killed by CTLs at a rate k_I. Virus-producing cells die with rate δ_P, and if they produce wild-type virus are also killed at rate k_P.

6.3 RESULTS

6.3.1 *HIV dynamics with multiple infections of cells*

To study the impact of multiple infected cells on the dynamics of immune escape in HIV, we follow the evolution of escape variants during the time course of an infection. We assume that the host is initially infected with wild-type virus only ($V_w(0) = 1$). In a model without multiple infection of cells, the escape

variant is generated through mutation and replaces the wild-type virus for the given parameters around 100 days after infection (Fig. 6.2A). The rate at which the escape variant replaces the wild-type, i.e., the escape rate, is determined by the loss in CTL-mediated killing, k, and the fitness cost, c (Asquith et al., 2006). Allowing half of the infected cells to be co-infected with a second virus ($f = 0.5$) results in a disadvantage for the escape variant and the rate of escape slows down (Fig. 6.2B). The time until the frequency of the escape variant is high enough to be detected by a conventional assay (5%–10%) is being delayed substantially. Further increasing the fraction of multiple infected cells ($f = 0.75$) results in a threshold, where the escape variant does not become selected anymore (Fig. 6.2C). Since the escape variant carries a fitness cost and frequently infects cells that are also infected with the wild-type virus, the advantage of evading CTL-mediated killing is diminished, which prevents the outgrowth of the variant. Through continuous mutation, the escape variant can only be held in a mutation-selection balance (Althaus and De Boer, 2008).

For these natural parameters, we find three different behaviors. If cells are not multiple infected, the escape variant replaces the wild-type rapidly because the loss in CTL-mediated killing, k, outweighs the negative effect of the fitness cost c. Increasing the fraction of multiple infected cells delays the appearance of escape variants and slows down the rate of escape. Above a critical fraction of multiple infected cells, the escape variant cannot become selected anymore, because the escape variant most often infects cells that are also infected with wild-type virus and the advantage of escaping CTL-mediated killing diminishes.

6.3.2 *Emergence of immune escape*

In the previous section, we found that multiple infected cells can delay and slow down the emergence of immune escape in HIV. To investigate the dynamics of escape over a wider parameter regime, we calculate the time until an escape variant replaces the wild-type virus, i.e., the time when the escape variant breaches a frequency of 50% of the total viral population (Fig. 6.3A). Given a certain killing rate k, the contour lines indicate that the time of appearance of the immune escape variant is being prolonged with an increasing frequency of multiple infected cells. The same trend happens for the escape rate, that we define as the rate at which the two variants replace each other at equal frequency ($V_e = V_w$) (Fig. 6.3B). Above, we have already illustrated that further increasing the fraction of multiple infected cells can result in a threshold above which some escape variants cannot become selected anymore (Fig. 6.2C). To investigate this behavior in more detail, we study the appearance of immune escape for a given killing rate, k, as a function of the fraction of multiple infected cells, f, and the fitness cost, c. Given a low fitness cost, the threshold above which the escape variant does not become selected only occurs for high frequencies of multiple infected cells (Fig. 6.3C, white area). However, if the effect of the fitness cost is stronger but still smaller than the advantage entailed by the immune escape,

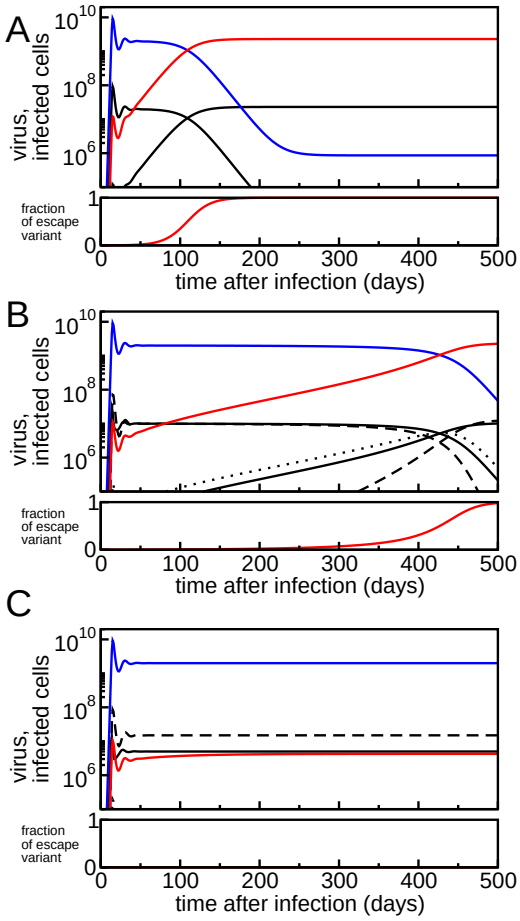

Figure 6.2 Selection of immune escape variants during HIV infection. (A) If cells are not multiple infected ($f = 0.0$), the escape variant (red line) rapidly replaces the wild-type virus (blue line). (B) If half of the infected cells carry more than one provirus ($f = 0.5$), the emergence of the immune escape variant is being delayed. (C) At higher multiplicities of infection ($f = 0.75$), some escape variants cannot become selected anymore because they suffer from an initial growth advantage. Single infected cells are shown as full lines, double infected cells are given as dashed (if they carry wild-type or escape virus only) or dotted lines (if they carry wild-type and escape virus). At the bottom of each panel, the escape variant is expressed as a frequency of the total viral population. In all simulations: $\delta = 0.9$ d^{-1}, $k = 0.1$ d^{-1} and $c = 0.03$.

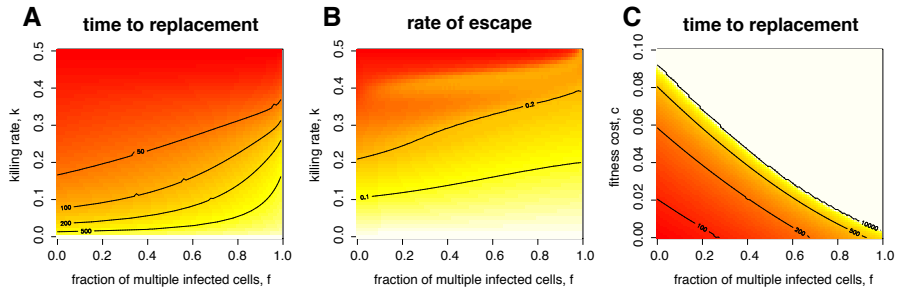

Figure 6.3 Timing and rate of immune escape during HIV infection. (A) Increasing the fraction of multiple infected cells increases the time until the escape variant replaces the wild-type variant ($V_e > V_w$) for any killing rate k. (B) A higher multiplicity of infection slows down of the escape rate, i.e., the replacement rate of the two variants when $V_e = V_w$. (C) Multiple infection of cells results in a threshold that prevents an escape variant, given a certain fitness cost, to replace the wild-type virus. In (A) and (B), we assume no fitness cost. In (C) we set $k = 0.1$ d^{-1}, i.e, $c < k$. Contour lines indicate the time to replacement in days or the rate of escape per day.

even low fractions of multiple infected cells can prevent the escape variant to replace the wild-type virus.

This phenomenon resembles a process of frequency dependent selection that is known in ecology as the Allee effect (Allee, 1949). In a selection process, where the fitness of an individual is correlated with its population size or frequency, invasion or outgrowth of a population variant can be prevented. In our case, multiple infected cells contain different virus variants proportional to their frequency in the population. The escape virus can only fully exploit its selective advantage if it is not co-infected or co-infects a cell that is already infected with an escape variant. However, at low frequencies of the variant, it happens rarely that two escape variants infect the same cell to benefit together from the loss in CTL-mediated killing. Rather, cells that harbor the escape variant tend to be co-infected with the wild-type virus and the selective advantage is diminished. This phenomenon suggests that the initial frequency of the escape variant determines whether it can outgrow the wild-type virus or not. If the escape variant were present at a higher frequency, e.g., when a patient is infected with a virus strain that already contains the escape mutation, double infected cells would often harbor two escape variants, and outgrowth of the variant would become possible.

6.3.3 *Intracellular delay and the rate of escape*

The escape rate can be expressed as the difference in the net growth rate between an escape variant and the wild-type virus it replaces. Let us consider a simple case where a population of wild-type virus competes with a population

of an escape variant that is not killed by a specific CTL clone at a rate k. It can be shown, assuming no fitness cost of the escape variant, that the escape rate equals the killing rate k (Asquith et al., 2006). However, more detailed models of HIV dynamics that include an intracellular delay before an infected cell starts to produce viral particles critically affect the viral generation time and therefore the growth rate of the virus (see Chapter 2 and 3).

Given the model in section 6.2.2, we define R as the ratio of the escape variant over the wild-type variant. Since we do not explicitly consider the virus populations, we simply take the ratio of the virus-producing cells, i.e., $R = P_e/P_w$. The rate ρ at which the ratio of the two variants is changing during the replacement corresponds to the escape rate, i.e., the difference in the net growth rate of the two variants:

$$\frac{dR}{dt} = \rho R. \tag{6.14}$$

In our two-stage model, it is not straightforward to express the time-derivative of the ratio as a function of R alone. Hence, we make the following assumptions. First, we assume that during replacement of the two variants, the ratio of the infected cells over the virus producing cells, I_w/P_w and I_e/P_e, is approaching a quasi steady-state (De Boer, 2007). This allows us to set the derivatives of these ratios to zero ($d(I_w/P_w)/dt = 0$ and $d(I_e/P_e)/dt = 0$). Second, we assume the wild-type population has approached equilibrium ($dI_w/dt = 0$ and $dP_w/dt = 0$) and consider the invasions of the escape mutant, which allows us to express the 'infection rate' b as a function of the other parameters:

$$b = \frac{(\delta_I + k_I + \gamma)(\delta_P + k_P)}{\gamma}. \tag{6.15}$$

Now, the system of equations can be solved and it can be shown that if an escape variant invades the wild-type population, it will replace the wild-type with an escape rate that is given by

$$\rho = \frac{1}{2}\left(\sqrt{(\delta_I + \delta_P + \gamma)^2 + 4(k_I\delta_P + k_P(\delta_I + k_I + \gamma))} - \gamma - \delta_I - \delta_P \right). \tag{6.16}$$

The intracellular delay has been found to last for about 24 hours (Dixit and Perelson, 2004) but we can show that in the limit where γ goes to infinity and the delay disappears, the expression simplifies to $\rho = k$. We also validated the analytical solution with numerical simulations of a virus dynamics model that includes an intracellular delay and $CD4^+$ target cells to account for a density-dependent infection rate (results not shown).

We illustrate the effect of an intracellular delay on the escape rate with three different examples (Fig. 6.4). Splitting the HIV-infected cells into an 'early' stage during the intracellular eclipse phase and a 'late' stage of virus production, allows us to vary the death rates and the killing rates. Different CTL-clones have indeed been found to induce killing of infected cells early or late during the viral life cycle (van Baalen et al., 2002). Generally, it is believed that once

viral proteins are expressed, the infected cells can be recognized and killed by CTLs. If viral protein expression is linked to the release of viral particles, the infected cells during the intracellular delay would not be prone to CTL-mediated killing, and we call this case 'late' killing ($k_I = 0$). On the other hand, HIV-infected cells have been found to be recognized and killed by CTLs very early after infection of a cell (Sacha et al., 2007a). In addition, HIV can down-regulate MHC-I molecules which could prevent the 'late' stage from being a target for killing (e.g., $k_P = 0$). We attempt to make a fair comparison between the two stages by restricting the total death rate at each stage to reflect the death rate of infected cells that is observed during antiretroviral drug treatment ($\delta_I + k_I = 1.0$ d^{-1} and $\delta_P + k_P = 1.0$ d^{-1}, see Chapter 3).

We find that if CTL-mediated killing is only induced during one stage of an infected cell, i.e., during the intracellular delay or the phase of virus production, the escape rate is expected to be lower than the killing rate k_I or k_P (Fig. 6.4, dashed and dotted line). Only in the case when killing occurs during both stages of an infected cell ($k_I = k_P > 0$), the escape rate is equal to the killing rate ($x = k$, solid line). The different relation between the killing rate and the escape rate can be explained by the different impact of CTL-mediated killing on the lifespan of an infected cell. If killing occurs during both stages of an infected cell, the killing rate directly affects the whole lifespan. In the case when killing only targets infected cells during the intracellular delay or the stage of virus production, the impact of CTL-mediated killing on the total lifespan of an infected cell is smaller. Since the average lifespan of an infected cell can directly correspond to the viral generation time (see Chapter 3), the different killing regimes will be reflected in the net growth rate of the virus and are eventually reflected in the rate of escape.

6.4 DISCUSSION

In this chapter we investigated how specific properties of the viral life cycle affect the dynamics of immune escape in HIV. A previous study suggested that multiple infection of cells can result in a disadvantage for the escape variant to grow and replace the wild-type virus (Jung et al., 2002). Since a cell that is infected with an escape variant can be co-infected with the wild type, the cell will still be subject to CTL-mediated killing by clones that recognize epitopes from the wild-type virus. We study this process in a mathematical model and find that with increasing frequency of multiple infected cells, the appearance of escape variants is being delayed and slowed down. Interestingly, multiple infected cells can prevent the escape variant to replace the wild-type virus if the variant is associated with a fitness cost that would otherwise allow the variant to become selected in the absence of multiple infected cells. It is important to note, that our findings are based on the assumption that a secondary infection of a cell occurs at random and does not depend on the virus that infected the cell first. Where this assumption might be valid for a well-mixed system such as the peripheral blood, the situation in the lymphoid tissue is likely to be different.

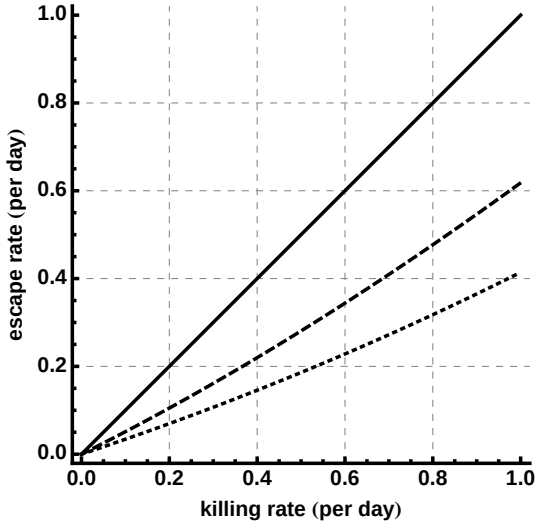

Figure 6.4 Escape rate as a function of the killing rate. If CTL-mediated killing occurs during the intracellular eclipse phase and the phase of virus production ($k_I = k_P$), the escape rate directly corresponds to the killing rate (solid line). The intracellular delay decreases the rate of escape if killing only occurs during the stage of virus production ($k_I = 0$, dashed line). CTL-mediated killing might also occur during the intracellular eclipse phase only ($k_P = 0$). This results in an escape rate that is lower than the killing rate (dotted line). In all three cases, we set $\gamma = 1.0$ per day and assume that the maximal death during both stages is 1.0 per day, i.e., $\delta_I + k_I = 1.0$ d^{-1} and $\delta_P + k_P = 1.0$ d^{-1}.

Studies have shown that HIV can exhibit a spatially distributed meta-population dynamics within an infected host, which suggests a non-random distribution of the viral quasispecies (Delassus et al., 1992; Frost et al., 2001; Funk et al., 2005). Specifically, cells in close proximity could infect each other through cell-to-cell transmission (Sato et al., 1992; Dixit and Perelson, 2004). If that were the case, the proviruses in multiple infected cells would most often derive from the same cell and therefore be of the same type. As long as escape variants are often co-infected with the same escape variant, the intrinsic disadvantage of multiple infections does not occur. However, the study by Jung et al. (2002) showed that the numerous proviruses in multiple infected cells are diverse, suggesting that they possibly encode for wild-type and escaped epitopes. Lastly, the frequency of multiple infected cells is also a matter of debate and a recent analysis of HIV-infected cells in blood plasma showed that most infected cells carry only a single provirus (poster by Sarah Palmer et al., HIV Dynamics & Evolution, 2008).

The intracellular delay, i.e., the stage of an infected cell before viral particles are produced, can critically affect the virus dynamics (see Chapter 2 and 3). In a second model in this chapter, we study the effect of such a delay on the

rate of immune escape. We again find that the escape rates can be lower than previously anticipated, depending on which stages of an infected cell are subject to CTL-mediated killing. The notion that killing of infected cells can depend on the stage of the HIV life cycle highlights an important aspect of the impact of CTLs on the viral replication. We further investigate the impact of 'early' and 'late' killing on the *in vivo* dynamics of HIV in Chapter 7 of this thesis.

Both of our models suggest that the late appearance of escape variants and the slow replacement of the wild-type virus do not necessarily indicate inefficient CTL-mediated killing of HIV-infected cells. The characteristic dynamics might at least partly be a result of specific properties of the HIV life cycle, challenging the view that the rate of immune escape directly reflects the rate at which infected cells are killed by CTLs. Although escape rates are usually found to be slow, our conjecture is that CTLs could play an important role in controlling viral infections such as HIV and induce a strong selection pressure on the viral population.

ACKNOWLEDGMENTS

Christian L. Althaus and Rob J. De Boer are supported by the Netherlands Organisation for Scientific Research (VICI grant 016.048.603).

CTL killing mediated early during the intracellular eclipse phase explains large variations in HIV set-point levels

7

C.L. Althaus and R.J. De Boer
Theoretical Biology, Utrecht University
Padualaan 8, 3584 CH Utrecht, The Netherlands.

manuscript submitted

ABSTRACT

Patients infected with HIV exhibit orders of magnitude differences in their set-point levels of the plasma viral load. This difference in the control of virus replication has been attributed to varying efficacies of the patients immune responses to induce cytotoxic T lymphocyte (CTL)-mediated killing of infected cells. Recent studies have shown that HIV-infected cells present viral epitopes and are also recognized by CTLs during the viral eclipse phase, i.e., during the intracellular delay before the infected cell starts to produce new viral particles. Here, we use a mathematical model to investigate the possible impact of early killing of HIV-infected cells on the viral replication. We suggest that the majority of CTL-mediated killing could occur during the viral eclipse phase, whereas the killing of virus-producing cells could be substantially lower due to MHC-I-down-regulation. This allows us to explain the large variations in viral set-point levels without affecting the typical decay rate of virus load after drug treatment. Further, 'early killing' also accounts for the effects of $CD8^+$ T cell depletion experiments. The model provides a formal explanation why CTL responses directed against epitopes that are presented early after infection are most efficient in reducing the viral load. The time-window for responses against viral genes that are expressed late might be too short to reduce the viral load substantially.

7.1 INTRODUCTION

Infection with HIV typically leads to a vast replication of the virus during the acute phase of the infection which is followed by a chronic phase where the viral load approaches a quasi-steady-state, known as the viral set-point. It has been shown that the viral load levels can vary over orders of magnitude between patients (Piatak et al., 1993; Muller et al., 2001; Kiepiela et al., 2007) and the set-point level has been recognized to be an important predictor for disease progression (Mellors et al., 1996). The difference in the control of HIV replication between patients has been attributed to varying efficacies of the patient's immune responses to induce cytotoxic T lymphocyte (CTL)-mediated killing of infected cells (Kaslow et al., 1996; Schmitz et al., 1999; Kim et al., 2008). However, it is remarkable that the virus load declines at very similar rates in different patients when they are treated with antiretroviral drugs (Ho et al., 1995; Wei et al., 1995). The viral load decay during antiretroviral therapy is typically related to the loss of HIV-infected cells and occurs at a rate between 0.5 and 1.5 per day (Bonhoeffer et al., 2003). Therefore, it is puzzling how CTL-mediated killing of infected cells can account for the large differences in the viral set-point when the infected cells apparently experience approximately the same clearance rate.

Klenerman et al. (1996) have presented a mathematical model to show that CTLs can markedly reduce the virus load by limiting virus production with small effects on the half-life of infected cells. Assuming that the rate at which an infected cell becomes a target for CTLs is slow (e.g. 0.4 d^{-1}), it will be this transition rate rather than the death rate of the cells that is reflected in the viral load decline. Others have adopted this model in combination with experiments to highlight the impact of epitope expression kinetics on the recognition of HIV-infected cells by CTLs (van Baalen et al., 2002; Gruters et al., 2002). Recently however, Sacha et al. (2007a,b) have shown that HIV-infected cells become a target for CTLs as soon as 2 to 6 hours after infection. This shows that the transition rate at which cells turn into a target for CTLs is very fast (4 to 12 d^{-1}), and is much higher than the typical decline rate of viral load after drug treatment. This observation highlights two important features. First, that infected cells become a target for CTL-mediated killing very early, and secondly, that infected cells can be killed during the viral eclipse phase, i.e., during the intracellular delay before the infected cell starts to produce new viral particles.

HIV evolved a mechanism to partially evade killing by CTLs through down-regulation of MHC-I molecules in infected cells (Collins et al., 1998; Scheppler et al., 1989; Swigut et al., 2004). Down-regulation is induced by the protein Nef (Schwartz et al., 1996) and starts as early as 12 h post-infection (Sacha et al., 2007b). The intracellular eclipse phase lasts around 24 hours (Dixit et al., 2004). Hence, CTL-mediated killing of infected cells during the eclipse phase can be more efficient because MHC-I is not yet down-regulated. CTLs recognizing epitopes that are presented early, such as epitopes derived from the viral protein Gag, might then mediate efficient cytotoxic killing soon after the cell has been

infected. In contrast, virus-producing cells can partly evade killing by CTLs which, together with the virus-induced death rate and killing by natural killer (NK) cells, might lead to the typical death rate of infected cells (0.5 - 1.5 d^{-1}) that is observed after the start of drug therapy.

We devise a mathematical model of HIV dynamics to investigate the impact of early CTL-mediated killing of infected cells during the viral eclipse phase. Our model can account for large variations in viral set-point levels without affecting the typical decay rate of virus load after drug treatment, and is fully consistent with the unexpected effects of $CD8^+$ depletion experiments during antiretroviral therapy (presentation by Nichole Klatt et al., Conference on Retroviruses and Opportunistic Infections, 2008). Finally, we provide a formal explanation why CTL responses directed against epitopes derived from the viral protein Gag are most efficient in reducing the viral load (Borghans et al., 2007; Kiepiela et al., 2007). On the other hand, the time-window for responses against viral genes that are expressed late during the eclipse phase might be too short to reduce the viral load substantially.

7.2 MODEL

For the mathematical analysis on the influence of clearing HIV-infected cells early or late during their viral life cycle, we devise a model of HIV dynamics that is based on standard models of within-host virus dynamics (Nowak and May, 2000; Perelson, 2002). In addition, we include an early stage of infected cells, that accounts for the eclipse phase during which cells do not produce virus yet (Klenerman et al., 1996; De Boer, 2007):

$$\begin{aligned} \frac{dT}{dt} &= \lambda - \beta TV - \delta_T T, \\ \frac{dI}{dt} &= \beta TV - \gamma I - \delta_I I, \\ \frac{dP}{dt} &= \gamma I - \delta_P P, \\ \frac{dV}{dt} &= pP - \delta_V V. \end{aligned} \tag{7.1}$$

Here, non-infected $CD4^+$ target cells T are produced at a rate of λ cells per day, die at a rate δ_T and can become infected by virus particles V at a rate β per day. An infected cell I can either move through the viral eclipse phase with rate γ per day to become a virus-producing cell P, or die at a rate δ_I per day. Virus-producing cells P will die with the death rate δ_P. Viral particles V are produced at a rate p per day and are cleared at a rate δ_V. All parameters used for the analysis of the virus dynamics are given in Table 7.1 in the *Appendix*. In the main text, we will vary the death rate of infected cells, δ_I, to account for early CTL-mediated killing during the viral eclipse phase. The effects of non-

cytotoxic mechanisms that can be mediated by $CD8^+$ T cells are discussed in the *Appendix*.

7.3 RESULTS

7.3.1 *Early vs. late killing of HIV-infected cells*

Our model considers two types of cells infected with HIV. Infected cells during the viral eclipse phase, I, do not produce virus yet, whereas cells that pass the eclipse phase (caused by an intra-cellular delay of virion production) become productively infected cells, P, and release new viral particles (Fig. 7.1, top). Both populations experience cell death that can at least partly be due to CTL-mediated killing.

First, we analyze which parameter regimes prove to be realistic to describe the known characteristics of HIV dynamics. Fig. 7.2 shows the influence of the death rates of infected cells, δ_I, and virus-producing cells, δ_P, on the reduction of the viral set-point (contour lines) and the predicted exponential slope of the virus decline during drug treatment (area between dashed lines). It illustrates that the death rates of infected cells and virus-producing cells are restricted by the viral load decay slope which is bound between 0.5 d^{-1} and 1.5 d^{-1}. One possibility to reduce the viral load significantly is that δ_P is high with δ_I being low (depicted by region B in Fig. 7.2). This regime has been previously described by Klenerman et al. (1996) and it requires that the decline slope after drug treatment is not reflecting the death rate of virus-producing cells but the slowest rate at which cells move through the eclipse phase (γ in the model from Eq. 7.1).

In contrast to those assumptions, recent studies have shown that infected cells can also be recognized and killed by CTLs during the viral eclipse phase (Sacha et al., 2007a,b). Additionally, HIV evolved a mechanism to partially evade killing by CTLs through down-regulation of MHC-I molecules in infected cells (Collins et al., 1998; Scheppler et al., 1989; Swigut et al., 2004). Fig. 7.1 illustrates the density of MHC-I molecules and the epitope presentation on the surface of an HIV-infected cell as given in Sacha et al. (2007a,b). MHC-I density is high during the viral eclipse phase and the infected cells, I, can be recognized and killed by CTLs efficiently. Around 12 hours after infection of a cell, the viral protein Nef starts to down-regulate MHC-I molecules that might lead to a more moderate killing rate of virus-producing cells P. This regime is depicted by region A in Fig. 7.2 and in the following we hypothesize that CTL-mediated killing is high during the viral eclipse phase whereas virus-producing cells experience a moderate and constant death rate, δ_P.

7.3.2 *Set-point viral load*

In the previous section we found that if the death rate of infected cells during the viral eclipse phase is high, and the death rate of virus-producing cells is

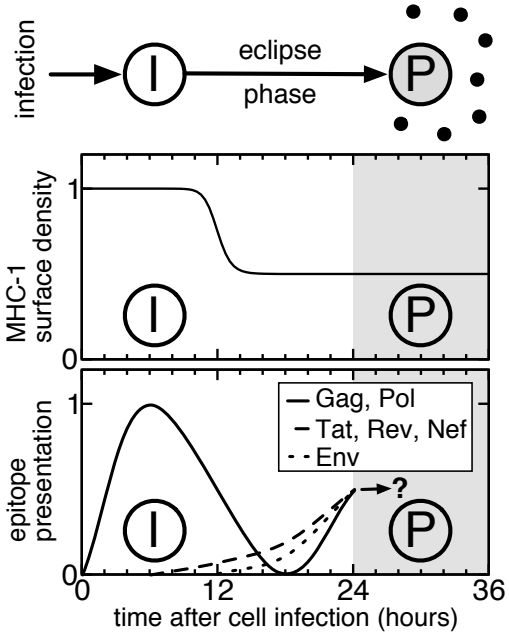

Figure 7.1 MHC-I density and epitope presentation on the surface of an HIV-infected cell. On top, an infected cell, I, is shown that passes through the eclipse phase to become a virus-producing cell, P. In the middle panel, the relative MHC-I density is shown as being down-regulated around 12 h after infection. The bottom panel depicts the early surface presentation of epitopes during the first 24 hours after infection. Gag and Pol epitopes show a peak shortly after infection since they are derived from the infecting virus particles. Later, *de novo* synthesis of viral proteins takes place, generating the early proteins Tat, Rev and Nef and the late proteins Env, Gag and Pol. The viral eclipse phase is denoted by the white area. After the eclipse phase, virus-producing cells, P, are likely to experience a moderate death rate due to the MHC-I-down-regulation (gray area). The illustrations are based on kinetic data from Sacha et al. (2007a,b).

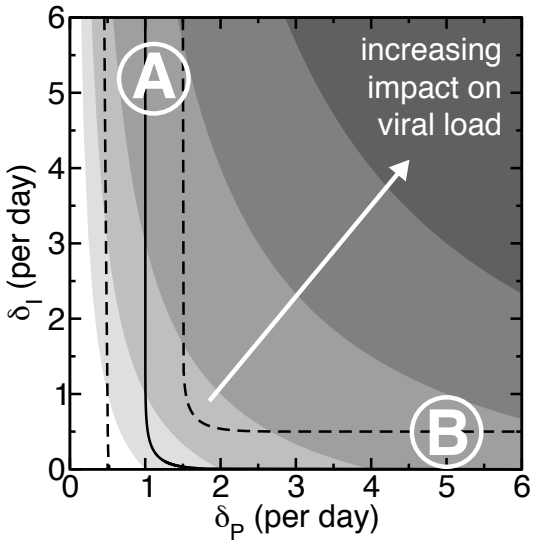

Figure 7.2 Influence of early and late death rates of HIV-infected cells on the viral load and the slope of the virus decline after drug treatment. During the viral eclipse phase, infected cells, I, experience a death rate of δ_I per day whereas virus-producing cells, P, die at a rate δ_P. The contour lines depict the impact of cell death on reducing the viral load (see *Appendix*). The area where the virus decline slope is between 0.5 d^{-1} and 1.5 d^{-1} is given by the dashed lines. Region A: Infected cells experience a higher death rate during the eclipse phase than later when they start to produce new viral particles. Hence, the slope of the virus decline after drug treatment is determined by δ_P. Region B: As the death rate of infected cells during the eclipse phase is low, the decline slope after drug treatment is determined by the rate at which cells move through the eclipse phase ($\gamma = 1.0\ d^{-1}$). The exponential slope of the virus decline is calculated at 5 days after the start of treatment. For the mathematical derivation we refer to the *Appendix*.

moderate to reflect the rate of the virus decline after drug treatment (as given by region A from Fig. 7.2), our model can describe the characteristic dynamics of HIV. Now, we are interested in how CTL-mediated killing can suppress viral replication and reduce the set-point viral load if CTLs act with different efficacies during the viral eclipse phase.

To analyze the effect of early CTL-mediated killing of HIV-infected cells, we extend Eq. 7.1, and describe the death rate of infected cells as $\delta_I = \delta_T + \kappa$, which sums the natural death rate of $CD4^+$ cells, δ_T, with a function of CTL-mediated killing, κ. Additionally, we keep the death rate of virus-producing cells, δ_P, small and constant and argue that it will be a combination of natural death, virus induced cytotoxicity, moderate CTL-mediated killing and killing by NK cells as a consequence of MHC-I down-regulation. For our analysis, we consider two types of CTL-mediated killing for the infected cells during the

eclipse phase. 1) Cells are cleared at a total rate k per day (i.e., $\kappa = k$) by the CTL response. 2) We account for CTL effector cells E that proliferate according to a function ρ and die at a rate δ_E per day. These CTLs kill infected cells, I, according to a specific function κ. For the detailed mathematical description of the CTL proliferation ρ and the CTL-mediated killing κ, we refer to the *Appendix*.

When CTL-mediated killing is induced at a total rate k per day, the set-point viral load is reduced (Fig. 7.3A). Increasing the rate of killing above a threshold of $k \approx 5$ d^{-1} will clear the infection. The basic reproductive ratio (R_0) (Heffernan et al., 2005) indeed falls below 1 at the same critical value of k (Fig. 7.3C). A more interesting relation between the CTL response and the viral load is derived when we account for CTL effector cells, E, that kill infected cells, I, according to the function κ per day. Here, we can change the saturation parameter h_k (see *Appendix*) in order to account for different efficacies of CTL-mediated killing. Decreasing h_k will increase the total killing and shift the activity of CTL responses towards 'early' epitopes. This allows us to have a single parameter of immune responsiveness that can account for orders of magnitude differences in viral load set-point levels (Fig. 7.3B). The corresponding R_0 now approaches 1 when h_k is reduced, i.e., the efficacy of CTL-mediated killing is increased (Fig. 7.3D).

To summarize, we can show that if CTL-mediated killing happens before the infected cell starts to produce new viral particles, the viral load can be suppressed effectively by the CTL response even to levels below the limit of detection, independent of the predicted downslope of the viral load during drug treatment. Interestingly, the infected cells can be cleared by the CTL response during the eclipse phase at a rate of up to 5 per day, a value that cannot be determined from viral load decay data and therefore has previously not been anticipated (Asquith et al., 2006).

7.3.3 *Reproducing experimental observations of HIV dynamics*

Viral load decay after drug treatment

A striking observation in HIV-infected patients is the small variation in the exponential decay of the viral load after the administration of antiretroviral drugs (Bonhoeffer et al., 2003). If CTLs were responsible for killing virus-producing cells, they cannot account for large differences in the suppression of viral replication and small difference in the rate of the viral load decay together. In contrast, when CTLs kill infected cells before they produce virus, the viral load can be suppressed to any set-point level whereas the exponential decay after drug treatment is unaffected since the death rate of virus-producing cells can be kept low (see Fig. 7.2). This characteristic behavior is depicted by the solid lines in Fig. 7.4A, where the set-point viral load can vary over orders of magnitude but, upon start of therapy, decreases with the same rate δ_P. To illustrate that CTL-mediated killing is not responsible for the death of virus-producing cells and the typical decay slope after drug treatment, we perform an *in silico* experi-

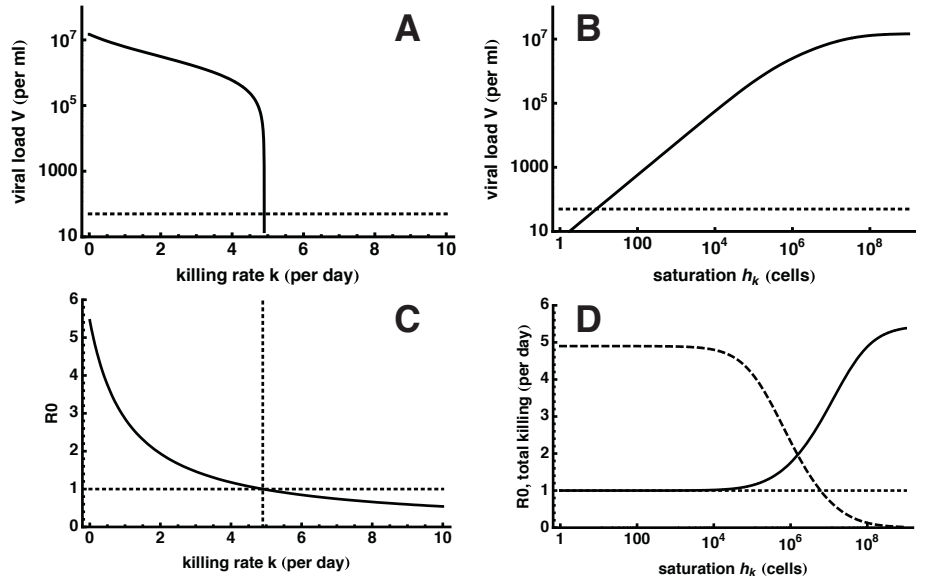

Figure 7.3 Set-point viral load and the basic reproductive ratio, R_0, as a function of CTL-mediated killing. The left panels depict the behavior when killing is induced with a total rate k per day. The viral load decreases sharply for $k \approx 5$ d^{-1} (A) since R_0 falls below one, and the infection is cleared (C). If CTL effector cells form a complex with the infected cell before delivering their lethal hit, we assume a maximal killing rate ($k_{\max} = 50$ d^{-1}) and change the Michaelis-Menten constant h_k instead. This way, we can account for orders of magnitude differences in the viral load (B) since R_0 is slowly approaching one (solid line, D). The total killing (dashed line, D) induced by all CTL effector cells is approaching the same critical value around 5 d^{-1} although $k_{\max} = 50$ d^{-1}. In panel (A) and (B), the dotted line represents the usual detection limit for HIV-1. The dotted line in panel (C) and (D) depicts the R_0 of 1 below which the infection cannot sustain itself anymore.

ment where CD8$^+$ depletion takes place at the same time when drug treatment is started. Technically speaking, we set the infection rate β to zero and the number of CTL effector cells to low levels at the onset of treatment. Not surprisingly, we obtain the same exponential decay of the viral load that is given by the death rate of the virus-producing cells δ_P, as observed without removing the CTL (dashed lines in Fig. 7.4A). Interestingly, the shoulder phase after the start of treatment, that is typically assumed to be caused by the intra-cellular delay, becomes longer when CD8$^+$ depletion is performed. This is due to the fact that a larger fraction of the cells in the eclipse phase at the start of treatment will move into the state of virus-producing cells when CTLs are removed.

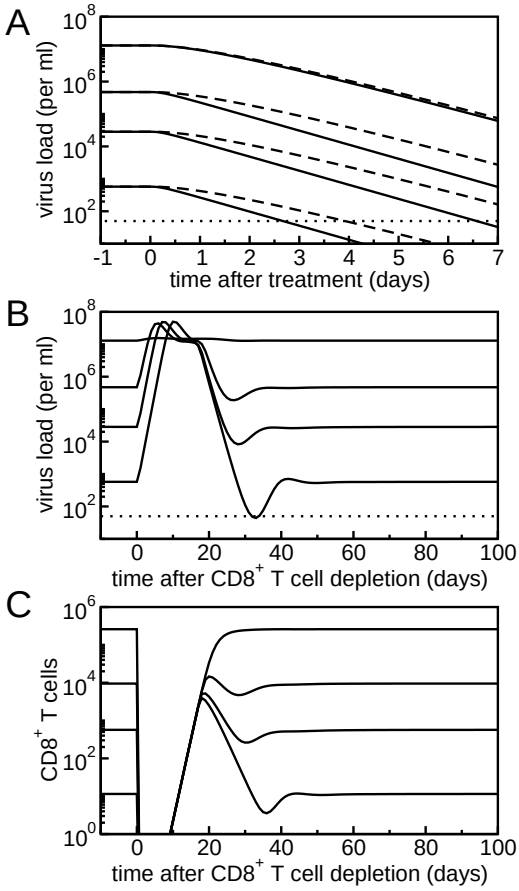

Figure 7.4 Reproducing experimental observations of HIV dynamics. A) After drug treatment, the viral load declines proportionally to the number of virus-producing cells (straight lines). Since the death rate of these cells, δ_P, is constant, we observe the same slope for the exponential decay of viral load although different patients have varying efficacies of their CTL response. Hence, the dynamics is not affected by the killing efficacy h_k which determines the set-point level of viral load before treatment. If CTLs were depleted at the start of drug treatment, the same phenomenon would be observed. The virus load declines exponentially with the death rate of virus-producing cells that is unaffected by CTL-mediated killing (dashed lines). B) In $CD8^+$ depletion experiments, the viral load increases over orders of magnitude, peaks around two weeks after depletion, reduces again, and stabilizes afterwards at the previous set-point level. C) The CTLs are depleted and start to proliferate thereafter. Black lines denote different hypothetical patients with varying efficacies of their CTL response. Lines from top to bottom: $h_k = 10^8$, $h_k = 10^5$, $h_k = 5 \times 10^3$ and $h_k = 10^2$. After $CD8^+$ depletion, the concentration of CTL effector cells is set to $E = 10^{-4}$. The dotted lines represent the usual detection limit for HIV-1.

$CD8^+$ depletion experiments

Strong evidence that CTLs are responsible in suppressing the viral load during chronic HIV infection comes from the marked increase in the viral load after $CD8^+$ T cell depletion. Monkeys infected with simian immunodeficiency virus (SIV) show a rapid and transient increase in their viral load over orders of magnitude upon depleting their $CD8^+$ T cells (Schmitz et al., 1999; Jin et al., 1999; Friedrich et al., 2007). This observation was difficult to explain with a mechanism where CTLs suppress HIV replication by killing virus-producing cells since the death rate of these cells does not vary over a broad range. A mathematical model in Jin et al. (1999) illustrated that if $CD8^+$ T cell depletion affects the death rate of virus-producing cells, it cannot account for the rapid increase as observed in the experiments. They also investigated how the absence of non-cytotoxic mechanisms such as increasing virus production or increasing infection rates could result in the observed dynamics but concluded that the model fails to accurately describe the experiments. Later, it was suggested that an 'early cytotoxic' immune response could eliminate infected cells before they produce viral particles and therefore serve as an explanation for anti-$CD8^+$ T cell treatment (Muller et al., 2001). Similarly, with our new model we can account for a strong suppression of virus replication because infected cells can be effectively killed during the eclipse phase. Upon $CD8^+$ T cell depletion, the amount of cells becoming virus-producing cells will increase rapidly leading to a transient increase in the viral load (Fig. 7.4B). Afterwards, the viral load reaches the previous set-point since the $CD8^+$ T cells start to proliferate again (Fig. 7.4C). Thus, the effects of $CD8^+$ T cell depletion do not rule out cytotoxic control of viral replication, if this control occurs early in the life cycle of an infected cell.

7.4 DISCUSSION

This paper investigates how early CTL-mediated killing of HIV-infected cells during the viral eclipse phase, i.e., during the intracellular delay before the infected cell starts to produce new viral particles, affects the virus dynamics. Until recently, it was believed that infected cells have to express viral proteins first, in order to present epitopes derived from these proteins that are then recognized by CTL responses. New studies have shown that HIV-infected cells can be recognized by specific CTL responses during the viral eclipse phase, i.e., before they start to express viral proteins, since epitopes can also be derived from the proteins that enter the cell with a viral particle (Sacha et al., 2007a,b). In order to analyze the effects of early killing of HIV-infected cells, we devised a new mathematical model and investigated its properties on the virus dynamics.

An open problem of HIV dynamics is that CTL-mediated killing seems to be important in controlling the viral replication, whereas the death rate of virus-producing cells, as observed during drug treatment experiments, seems to exhibit little variation between patients. This discrepancy has caused problems in

describing the HIV dynamics, since CTL-mediated killing of virus-producing cells cannot account for the large variations in viral load levels. One solution was given by a theoretical study that illustrated how small variations in different parameters can account for wide variations in the viral load set-point instead (Muller et al., 2001). Another study approached the problem from a different angle. Klenerman et al. (1996) derived a model where HIV-infected cells become a target for CTL-mediated killing at a relatively slow rate. Then, the rate of virus decline after drug therapy does not reflect the cell death rate, but is given by the slow transition of cells becoming a target for the CTLs. In disagreement with this hypothesis, the recent studies by Sacha et al. (2007a,b) have shown that infected cells become a target for CTL lysis very early after infection. Here, we argue that CTL-mediated killing of virus-producing cells is reduced due to MHC-I-down-regulation. Before the down-regulation, the infected cells during the viral eclipse phase possibly experience very efficient CTL-mediated killing. These assumptions allow us to explain the large variations in the set-point viral load with a single parameter, i.e., the efficacy of the CTLs to induce 'early' responses, illustrating that the CTL response can solely account for the suppression of the viral replication.

A remarkable experimental observation in SIV-infected monkeys is the transient increase in virus load over several orders of magnitude upon depleting $CD8^+$ T cells (Schmitz et al., 1999; Jin et al., 1999; Friedrich et al., 2007). With our model, we can reproduce this observation and have the opportunity to perform an *in silico* experiment. To illustrate that in our model, the exponential decline of the virus load after drug treatment is not affected by the CTL response, we simulate CTL depletion at the start of drug therapy. As it has been shown recently (presentation by Nichole Klatt et al., Conference on Retroviruses and Opportunistic Infections, 2008), the slope of the exponential decline is unaffected (dashed lines in Fig. 7.4A), with the exception of a somewhat longer shoulder phase during the first day after the start of treatment. This predicted shoulder could in principle be tested *in vivo*. However, the required sampling frequency of viral load decay data in addition with the measurement noise makes it unlikely to observe such differences during the shoulder phase when $CD8^+$ T cells are depleted. Another experiment to test whether CTL-mediated killing acts during the viral eclipse phase would be to follow the dynamics of different cell populations after drug treatment. The virus-producing cells are expected to decline with the same rate as the viral load. In contrast, we hypothesize that infected cells during the early stage before MHC-I-down-regulation experience strong CTL-mediated killing, and therefore should decay with a faster rate than the viral load. Finally, the hypothesis that the death rate of virus-producing cells is largely unaffected by the CTL response is not only supported by the finding that the death rates of those cells show little variation between HIV-infected patients, but also by recent experiments with SIV-infected sooty mangabeys and African green monkeys. Upon antiretroviral drug treatment, these non-human primates which are natural hosts of SIV show similar decay kinetics of the viral load compared to HIV-infected humans, although they have little immune

activation and likely trigger weak CTL responses (Gordon et al., 2008; Pandrea et al., 2008).

The intriguing finding of the studies from Sacha et al. (2007a,b) is that they provide an explanation why CTL responses targeting epitopes from the protein Gag are more efficient in controlling the viral replication than CTL responses targeting epitopes from other viral proteins (Borghans et al., 2007; Kiepiela et al., 2007). Since Gag epitopes are presented on the infected cells surface soon after infection, the CTLs have a sufficient time-window to recognize infected cells before MHC-I is down-regulated. Although Pol epitopes are presented early as well, responses targeting those epitopes seem to be less efficient in controlling the viral replication. It has been argued that the number of proteins in a virion which enters the cell leads to a different concentration of protein-derived epitopes on the cell surface. While Gag proteins are highly abundant with a copy number of $\sim$5000 per virion (Briggs et al., 2004), Pol proteins are present at lower copy numbers. Further, structural constraints in the protein Gag make it more difficult for the virus to accumulate epitope escape mutations in order to evade the CTL responses (Borghans et al., 2007).

Nevertheless, the new studies by Sacha et al. (2007a,b) are in conflict with previous findings on the impact of epitope expression kinetics on the efficacy of CTL responses (Lichterfeld et al., 2005). It has been argued that since Gag is a 'late' protein that is expressed at the end of the viral eclipse phase, CTL responses against 'early' proteins such as Rev should be more effective in the control of the viral replication. Indeed, it was shown with recombinant viruses that RT- and Gag-specific CTL responses become much more effective in the control of virus replication if the epitopes are expressed as part of an early protein, such as Rev or Nef (van Baalen et al., 2002; Ali et al., 2004). In contrast with those findings, if the epitopes derived from the proteins Gag and Pol were presented early after infection as suggested by Sacha et al. (2007a,b), the efficacy of those CTL responses should not strictly correlate with the *de novo* protein expression kinetics. One possible explanation for this apparent discrepancy comes from the observation that not all epitopes from a specific protein become presented with the same kinetics, i.e., epitopes derived from the same viral protein experience differential antigen presentation kinetics (Sacha et al., 2008). Indeed, the studies by van Baalen et al. (2002) and Ali et al. (2004) used other epitopes than the studies by Sacha et al. (2007a,b) that might explain the different results of their experiments. The antigen presentation kinetics of epitopes could be influenced by different cleavage efficacies of the peptides by the proteasome. Early after infection of a cell, the peptides are likely to be cleaved by the constitutive proteasome only. Later, when *de novo* proteins have been expressed, peptides are additionally cleaved by the immunoproteasome. However, analysis of the cleavage scores obtained by the epitope predictor NetChop (Kesmir et al., 2002; Nielsen et al., 2005) did not result in a clearly distinct cleavage pattern between the epitopes that have been investigated in the references above (results not shown). In addition, the studies also used different assays to investigate the impact of the CTL response. In Sacha et al. (2007a,b), the

elimination of p27 positive cells was followed during a single infection cycle of SIVmac239 whereas the earlier studies measured the amount of p24 antigen that is suppressed by adding CTLs over several rounds of infection with HIV-1 (van Baalen et al., 2002; Ali et al., 2004). It would be interesting to see how the results of the longitudinal assay are affected by using CTLs that are specific for an 'early' epitope that has been established by the single-round assay.

Lastly, it needs to be investigated how efficient an HIV-infected cell can escape recognition by CTLs through down-regulation of MHC-I. While the viral protein Nef can down-modulate HLA-A and HLA-B, the surface presentation of HLA-C seems to be not affected. It has been speculated that this might be a strategy of the virus to escape the most efficient CTL responses, which have been found to be directed against epitopes presented on HLA-A and HLA-B, whereas the lack of down-regulation of HLA-C might prevent the cell from NK-directed killing (Cohen et al., 1999). The small variation in the death rates of virus-producing cells from patients having vastly different viral loads indeed challenges the view that CTL-mediated killing is effective during the productive stage of the cell. Therefore, we highlight that CTL-mediated killing could be most efficient during the viral eclipse phase and provide a formal model describing this process.

7.5 APPENDIX

7.5.1 *Influence of cell death on virus production*

To investigate the influence of cell death on virus production, we can calculate the average duration of a cell producing viral particles. Increasing the death rate of infected cells, δ_I, will reduce the fraction of cells that become virus-producing cells. The lifespan of virus-producing cells ($1/\delta_P$) determines the amount of virus that is produced by a single cell. From Eq. 7.1, the average duration at which an infected cell will produce viral particles can be given by

$$d = \frac{\gamma}{\gamma + \delta_I} \frac{1}{\delta_P}, \tag{7.2}$$

which suggests that changing δ_P has a larger effect on virus production than changing δ_I.

7.5.2 *Viral load decay slopes*

After the administration of antiretroviral drugs, the viral load declines exponentially during the first week and is typically related to the loss of virus-producing cells. Since the turnover of the virus is a fast process (Ramratnam et al., 1999), we can set V into a quasi-steady-state with the virus-producing cells P (De Boer and Perelson, 1998). After the start of treatment, we assume that the infection

rate β becomes 0 and the virus will decline as follows:

$$V(t) = \frac{V_0((\delta_I + \gamma)e^{-\delta_P t} - \delta_P e^{-(\delta_I+\gamma)t})}{\delta_I + \gamma - \delta_P}. \tag{7.3}$$

For any value of δ_I, δ_P and γ, this allows us to calculate the exponential slope of the virus load decline at a specific time t after drug treatment.

7.5.3 *CTL-mediated killing of infected cells*

From the general scheme where an unbound CTL effector cell, E_u, binds a target cell, I, to form a complex, C, that after a time delivers cytotoxic killing and releases the effector cell, i.e., $E_u + I \underset{k_u}{\overset{k_b}{\rightleftharpoons}} C \xrightarrow{k} E_u$, one can make the total quasi-steady-state assumption (tQSSA), $dC/dt = 0$, to obtain the following:

$$\kappa = kC = \frac{k_{\max} IE}{h_k + I + E}, \tag{7.4}$$

where $k_{\max} = k$ is now the maximal killing rate and $h_k = (k_u + k)/k_b$ is a generalized Michaelis-Menten constant (Borghans et al., 1996; De Boer, 2007; Althaus and De Boer, 2008).

7.5.4 *Proliferation of CTL effector cells*

CTL effector cells are stimulated by cells presenting viral antigen on their surface. Similar as for the killing of an infected cell, we can derive a general scheme where an unbound CTL effector cell, E_u, binds an antigen-presenting cell, I, to form a complex, C, that after a time dissociates and causes the CTL effector cell to divide, i.e., $E_u + I \underset{g_u}{\overset{g_b}{\rightleftharpoons}} C \xrightarrow{g} 2E_u + I$. Making the total quasi-steady-state assumption (tQSSA), $dC/dt = 0$, one obtains the following:

$$\rho = gC = \frac{g_{\max} IE}{h_g + I + E}, \tag{7.5}$$

where $g_{\max} = g$ is now the maximal proliferation rate and $h_g = (g_u + g)/g_b$ is a generalized Michaelis-Menten constant (Borghans et al., 1996; De Boer, 2007; Althaus and De Boer, 2008).

7.5.5 *Non-cytotoxic mechanisms of CD8$^+$ T cells*

CD8$^+$ T cells can also mediate non-cytotoxic effects on HIV-infected cells (Yang and Walker, 1997). Mathematically, this can be described by a process function f that will affect certain stages of the viral life cycle. Similar as in Muller et al. (2001), we define

$$f = \frac{1}{1 + \epsilon E}, \tag{7.6}$$

Table 7.1 List of parameter values for the HIV dynamics model.

Parameter	Value	Explanation and reference
λ	2×10^5 cells d^{-1}	Tuned to obtain a maximal viral load around 10^7 per ml in the absence of a CTL response.
δ_T	0.1 d^{-1}	Natural death rate of $CD4^+$ target cells T.
β	3×10^{-8} d^{-1}	Infection rate per virus particle. Results in a maximal viral growth rate of 1.5 d^{-1} (Mattapallil et al., 2005).
γ	1.0 d^{-1}	Viral eclipse phase of 24 hours (Dixit et al., 2004).
δ_I	0.1 d^{-1}	Natural death rate of infected cells I.
δ_P	1.0 d^{-1}	Death rate of virus-producing cells (Dixit et al., 2004).
p	2300 d^{-1}	Virus production rate.
δ_V	23 d^{-1}	Clearance rate of viral particles (Ramratnam et al., 1999).
g	1.5 d^{-1}	Maximal CTL proliferation rate of 1.0 d^{-1} (Davenport et al., 2004).
h_g	0 cells	CTLs are stimulated to proliferate rapidly.
δ_E	0.5 d^{-1}	Death rate of CTL effector cells.

where $CD8^+$ T cells E act as non-cytotoxic effector cells with efficacy ϵ. If $CD8^+$ T cells reduce the number of new infections, the process function f will reduce the infection rate β, i.e., the total amount of new infections in Eq. 7.1 becomes $\beta f T V$. Non-cytotoxic mechanisms can also render newly infected cells non-infectious. This will affect the rate at which cells move through the eclipse phase, and the transition rate γ is affected by the process function, i.e., is given by γf. The infected cells that do not become virus-producing cells will instead render into target cells again with rate $\gamma(1 - f)$.

The effects of a model with non-cytotoxic effects of $CD8^+$ T cells on the virus dynamics are the same as shown in the main text, except that the parameter region B in Fig. 7.2 is also a valid explanation for the invariant decline slope of the virus load during drug treatment experiments. Since infected cells are not cleared anymore by CTL effector cells, the death rate of infected cells δ_I, can be moderate and smaller than the rate at which cells move through the eclipse phase. Hence, the decay rate of viral load after drug treatment could in principle reflect the rate at which cells move through the eclipse phase, γ, as it has been suggested by Klenerman et al. (1996).

ACKNOWLEDGMENTS

We would like to thank Jonah Sacha and Monique Nijhuis for constructive comments on the manuscript. CLA and RJDB gratefully acknowledge financial support by the Netherlands Organisation for Scientific Research (VICI grant 016.048.603).

Discussion and Outlook

8

This thesis addresses a series of quantitative aspects of virus dynamics and the impact of the cellular immune response on viral replication. To summarize the results from the different chapters, we first critically evaluate the turnover of HIV-1 *in vivo*. Second, we discuss some differences between acute and chronic viral infections and bring together our findings on different aspects of CTL control during HIV infection. Third, since the CTL response leads to frequent escape in HIV, we quantify the process of immune escape and discuss its implications on CTL-mediated killing of infected cells. In the last section, we attempt to describe quantitative aspects of virus replication and the cellular immune response in a broader sense and speculate about the nature of viral infections in different host species.

8.1 ESTIMATING THE TURNOVER OF HIV-1

Due to the slow disease progression in HIV-infected patients, it was long believed that not much virus replication is happening during this transient period. Similar to other chronic viral infections, such as the ones caused by viruses from the herpes family, HIV-1 was considered to exhibit a slow turnover or even viral latency before the onset of AIDS. In 1995, two independent studies measured the change in the plasma virus concentration after antiretroviral drugs were given to HIV-infected patients (Ho et al., 1995; Wei et al., 1995). The observation that the virus load in infected patients dropped rapidly illustrated that virus-infected cells are subject to a rapid turnover *in vivo*.

More detailed measurements of the decrease in plasma concentrations of HIV-1 indicated a shoulder phase during the first day after treatment (Perelson et al., 1996). Initially explained by the decay of viral particles that had been released already at the start of therapy, the shoulder phase was later conjectured to reflect the intracellular delay of infected cells before they start to produce new virus particles. Various 'shapes' of the intracellular delay have been studied extensively with mathematical models that either assumed the delay to be discrete or to underlie a certain distribution (Herz et al., 1996; Mittler et al., 1998). For example, a gamma-distributed delay is expected if an infected cell has to go through a cascade of processes with each of them happening at the same rate. In Chapter 2 we have investigated the intracellular trans-activation circuit of HIV that eventually renders an infected cell into a virus-producing cell. Stochastic simulations have shown that the delay caused by the intracellular transactivation resembles a log-normal distribution. Such a distribution is indeed expected when stochastic noise propagates through a circuit that is constituted of processes that happen at different rates. Our more realistic de-

scription of the intracellular delay strongly suggests that infected cells do not move through the delay at a constant rate. After the initial shoulder phase, it is therefore unlikely to find intracellular delays to be reflected in the exponential decay slope during drug treatment experiments (see Chapter 7).

Instead, the rapid exponential decline of plasma virus after drug treatment is generally associated with the loss of virus-producing cells through cell death. Our findings from Chapter 2 indicate that the decline slope may also partly be determined by other factors. It is likely that virus-producing cells not only disappear through cell death but also through reversion into latently infected cells. Similarly, reactivation of latently infected cells into virus-producing cells may affect the decay slope. Nevertheless, our analysis from Chapter 2 suggests that the influence of these processes on the decay dynamics are minor, emphasizing that the exponential loss of infected cells largely reflects their death rate.

We extend the notion that properties of the HIV life cycle depend on the age of an infected cell in Chapter 3. Namely, we test the hypotheses that the death rate of infected cells and the rate at which cells produce viral particles depend on the age of the cell. By re-analyzing experimental data of plasma virus load decay during drug therapy in patients infected with HIV-1, we can exclude the possibility of increasing infected cell death rates with the age of an infected cell. However, viral production rates that increase with the age of an infected cell are perfectly consistent with the data. Interestingly, these assumptions can result in higher estimates of the infected cell death rate than previously anticipated. If this were the case, the lifespan of infected cells will be reduced accordingly, but the estimates for the viral generation time, i.e., the time between the onset of two consecutive productive phases of infected cells, will not be affected. Hence, we disentangle the death rate of infected cells from the viral turnover and postulate that, as long as it is unclear whether viral production rates increase with the age of an infected cell, we cannot clearly identify the infected cell lifespan. In contrast, the viral generation time of HIV-1 *in vivo* can be reliably determined from the viral decay dynamics during drug treatment.

Since mutation happens largely once during the viral life cycle, the viral generation time is an important indicator for the evolutionary potential of the HIV-1 quasispecies within an infected patient. On the other hand, the intracellular delay and the lifespan of infected cells will affect, but are also influenced by, the ability of CTL responses to recognize and eliminate infected cells. We will elaborate more on that in the next section.

8.2 CTL-MEDIATED CONTROL OF CHRONIC INFECTIONS

One of the fundamental questions of infectious diseases is what determines a virus to be only acute or to cause a chronic state of infection. LCMV is an excellent model virus and is therefore frequently used to study the dynamics of T cell responses after infection in mice. Different strains of this virus can lead to distinct courses of infection. The Armstrong strain of LCMV causes acute infection where the virus is cleared shortly after infection, whereas clone-13

causes a persistent infection (Wherry et al., 2003). Although the outcome of LCMV infection in mice at least partly depends on the administered infectious dose, the virus strains distribute differently in host tissues. Importantly, both virus strains show very similar growth rates during acute infection. However, after mice have been infected with clone-13, the virus load cannot be contained during the expansion phase of the $CD8^+$ T cell response. We have argued in Chapter 4 that the proliferation of $CD8^+$ T cells might interrupt to prevent immunopathology. Subsequently, the T cells differentiate into an effector/memory type and, in a balance with ongoing viral replication, 'control' the infection.

In the case of the chronic infection of HIV, it has been similarly argued that the virus replicates too rapidly during the acute phase of infection to be eliminated by the $CD8^+$ T cell response. For efficient killing of infected cells to happen, the effector/target ratio, i.e., the ratio of CTLs over the virus-infected cells, must be high enough. Apparently, this is only achieved after the initial peak in the viral load when virus replication slows down due to innate immune responses or target cell limitation (De Boer, 2007). This scenario can also explain why vaccines based on $CD8^+$ T cells fail to protect from HIV infection but provide control resulting in lower set-point levels of the virus load (Davenport et al., 2004). In this thesis, we have investigated several aspects of CTL-mediated control of HIV infection that we discuss in the following.

Different clones of T cells can recognize different epitope-MHC complexes on virus-infected cells, leading to a broad $CD8^+$ T cell response. By fitting a mathematical model to previously published data of LCMV infection in mice, we could estimate the kinetics at which different $CD8^+$ T cell clones proliferate during the expansion phase and contract into an effector/memory phase thereafter (see Chapter 4). Because the naive T cell numbers of different clones can vary, the $CD8^+$ T cells exhibit a unique immunodominance pattern at the peak of the response that can alter during the contraction phase. A similar phenomenon is found during HIV infection, where a large number of CTL clones can recognize different viral epitopes (Yu et al., 2002; Draenert et al., 2006). In Chapter 5, we have adopted this notion and devised a computational model including several CTL clones that recognize different viral epitopes. We have investigated how the viral quasispecies deals with the selection pressure that is induced through killing of infected cells by many different CTL clones. A broad CTL response targeting epitopes with similar avidity, i.e., a response consisting of clones that are similar in size, results in the most optimal control of HIV infection.

Unfortunately, the model only allows for small variations in the resulting number of infected cells, or the viral set-point level, as a result of CTL-mediated killing. This is in strong contrast to observations in HIV-infected patients who exhibit orders of magnitude differences in their set-point levels of the plasma viral load. If these differences were due to varying efficacies of the CTL response to induce killing of infected cells, our model from Chapter 5 fails to accurately describe the impact of the cellular immune response on viral replication. We explicitly considered the total killing that is induced by all CTL clones to account

for the majority of infected cell death. However, we were restricting the maximal rate at which infected cells die to be 1.0 per day, i.e., to reflect the death rate of infected cells that were estimated during drug treatment experiments (see Chapter 3). Due to this limitation at which virus-producing cells can be subject to CTL-mediated killing, the cellular immune response cannot account for large differences of the viral load set-point in such a model. This puzzling discrepancy has challenged the interpretation of mathematical models of virus dynamics (Klenerman et al., 1996; Jin et al., 1999; Muller et al., 2001) and has even led to controversy in the field as to whether CTLs are important in the control of HIV replication.

Recent experimental data suggest that HIV-infected cells could be recognized and eliminated very early after infection of a cell (Sacha et al., 2007a,b). Namely, the intracellular eclipse phase, caused by the delay that we discussed in Section 8.1, could be a target for efficient CTL-mediated killing. If virus-infected cells were eliminated before they start to produce new viral particles, the rapid killing of these cells would not be reflected in the virus load decay during drug treatment. In order to analyze the process of 'early' killing in Chapter 7, we devised a new mathematical model that can account for large variations in viral set-point levels and is fully consistent with the unexpected effects of $CD8^+$ depletion experiments during antiretroviral therapy. Hence, we postulate that although eradication of HIV cannot be realized during the acute phase of infection, efficient control of HIV replication can be achieved if virus-infected cells are recognized and eliminated early after they were infected with a viral particle, i.e., during the intracellular eclipse phase.

8.3 QUANTIFYING IMMUNE ESCAPE IN HIV

The rate at which immune escape variants appear and replace the wild-type variant has been conjectured to be an indicator of the selection pressure that is induced by the CTL response. Specifically, the 'escape rate' has been suggested to at least partly reflect the 'killing rate' at which single CTL clone eliminate virus-infected cells. Quantifying the dynamics of immune escape is useful in order to assess the impact of CTL-mediated killing on viral replication. Previous studies have fitted basic virus dynamics models to longitudinal data of immune escape to estimate the rate of escape (Asquith et al., 2006; Mandl et al., 2007). Interestingly, escape rates for HIV are generally found to be slow, which led to the conclusion that the killing induced by the CTL clones is inefficient. Further, it has long been speculated why immune escape variants often appear late during infection, although antigen-specific CTL clones can be detected long before the escape variant replaces the wild-type virus (Goulder et al., 1997).

In Chapter 5 and 6 we elucidate two seperate mechanisms that can explain the late appearance of escape variants. First, we investigated the dynamics of immune escape in the context of a broad CTL response. Upon loss of antigenic stimulation, CTL clones disappear and other clones slowly increase in size to induce more efficient killing. This alteration of the size of CTL clones relative

to each other leads to a sequential occurrence of immune escape with some variants appearing only years after primary infection. Second, since a cell that is infected with an escape variant can be co-infected with the wild type, the infected cell will still be subject to CTL-mediated killing by the specific clone. The selective advantage due to the loss in killing is therefore diminished and the appearance of the escape variant is being delayed.

In addition, we have found several factors that could influence the rate of escape during HIV infection. First, fitness costs that are associated with the escape mutations are expected to slow down the rate of immune escape. Our simulations in Chapter 5 indicate that on average this can easily decrease the escape rate by 50% or more. Second, due to the reduction in the selective advantage of escape variants in multiple infected cells, the rate at which the escape variant replaces the wild-type variant is also expected to decrease (see Chapter 6). Third, intracellular delays critically affect the growth rate and viral generation time. As shown in Chapter 6, these properties of the HIV life cycle need to be taken into account if one wants to infer killing rates from escape rates. Lastly, we illustrated in Chapter 5 that fitting longitudinal data of immune escape can result in an underestimation of the 'true' rate of escape by about 50% on average.

Even if all of these factors have only a moderate influence on the rate of immune escape, the combination of them could result in large differences between the observed escape rate and the killing rate *in vivo*. For example, if escape rates are found to be 0.01 per day (Asquith et al., 2006), it could well be that this reflects the immune escape from a CTL clone that is eliminating infected cells at a rate that is about 10-fold higher, i.e., 0.1 per day. Since there is generally a broad cellular immune response against HIV, CTL-mediated killing through different clones could therefore easily account for most of the infected cell death, especially if killing happens during the intracellular eclipse phase, as discussed in Section 8.2.

8.4 OF MICE AND MEN: SOME GENERAL PRINCIPLES

Most chapters of this thesis deal with quantitative aspects of HIV infection in humans. In addition, we investigated the kinetics of $CD8^+$ T cell responses upon LCMV infection in mice in Chapter 4. Since we are interested in quantitative aspects of viral replication and the cellular immune response, it is worthwhile to speculate about some general principles of virus and immune system dynamics and how they apply to different host species.

Discrepancies between experimental findings of the mice and human immune system have been described and illustrate that using mice as preclinical models for the study of human diseases can be challenging (Mestas and Hughes, 2004). Besides these differences that could be a result of separate evolution, there are apparent quantitative differences between the mice and human immune system. Due to differences in body size, the number of lymphocytes or the size of the circulatory system differs dramatically between different ani-

mals. The relationship between biological properties or structures and the size of an animal, i.e., the allometry, is a well-known field of study in biology. Many quantitative properties such as the lifespan of an animal, the metabolic rate or the number of certain cell types have indeed been found to depend on body size (Kleiber, 1932; Peters, 1983; Schmidt-Nielsen, 1984; Calder, 1996; West et al., 1997; Savage et al., 2007). It is therefore only natural to argue that the dynamics of viruses and the cellular immune response should depend on the size of the host.

Allometric scaling between host species could indeed influence quantitative aspects of within-host disease dynamics. In this regard, it is important to note that HIV research is often based on experimental findings from the macaque model. Despite being a non-natural host, rhesus macaques can be infected with SIV, the simian counterpart of HIV. Infected animals are found to progress to the immunodeficiency syndrome as observed in humans, but at a faster rate. Similarly, the viral replication dynamics within a host has been found to be slightly more rapid in macaques than in humans (Little et al., 1999; Brandin et al., 2006). In this light, it is interesting to compare the dynamics of immune escape in HIV-infected humans and SIV-infected macaques. The observation that escape rates in macaques appear to be faster compared to humans suggests more efficient CTL-mediated killing of infected cells in rhesus macaques (Asquith and McLean, 2007). However, in Chapter 6 we have illustrated that the rate of immune escape strongly depends on the viral turnover itself. In other words, more rapid immune escape in SIV-infected macaques does not necessarily imply more efficient killing but could be a result of the faster replication rate of SIV in the macaque species. If the viral production and turnover is linked to the metabolic rate of an infected cell, biological constraints in a specific host species could account for the observed differences. Allometric theory predicts that the total metabolic rate of an organism scales approximately as $M^{3/4}$, with M being the body mass (Kleiber, 1932; West et al., 1997). Assuming invariant size and volume of cells between host species, the metabolic rate of a single infected cell scales as $M^{-1/4}$. With a 10-fold difference in body mass between humans ($\sim$70 kg) and macaques ($\sim$7 kg), allometric scaling predicts a roughly 2-fold difference in the metabolic rate of a single cell between the two species. Where this factor can account for the reported differences in the mean of the escape rates (Asquith et al., 2006; Asquith and McLean, 2007), the differences in the viral turnover rates between humans and macaques seem to be less pronounced. An allometric relationship for the time to disease progression has been found recently for a small set of pathogens in different host species (Cable et al., 2007). However, the wide variation in disease progression of HIV-infected humans, ranging from years to decades, makes it difficult to compare it to the more rapid disease progression of 1 to 2 years in SIV-infected macaques. Although host genetic factors have been found to be strongly associated with disease progression, it is tempting to speculate whether allometric scaling between humans and macaques could at least partly account for the differences that we observe.

Similarly, it can also be argued that quantitative processes of the cellular immune response are affected by allometric scaling. In the case of T cell responses, some general principles on how the number of naive T cells scales with body size have been derived (Wiegel and Perelson, 2004). Lymphocyte trafficking, i.e., the circulation of T cells through blood, tissues and the lymphatic system in order to recognize antigen and eliminate virus-infected cells, has also been suggested to underlie general scaling laws (Perelson and Wiegel, 2009). In addition, the proliferation rate of $CD8^+$ T cell responses during the acute phase of an infection could be linked to the metabolic rate of the host. Unfortunately, only little data is available on the kinetics of T cell responses upon viral infection in different host species. However, the rapid expansion of $CD8^+$ T cells in mice after infection with LCMV at a rate of about 2.0 - 3.0 per day (De Boer et al., 2001, 2003), compared to the slower expansion rate of specific T cell responses upon SIV-infection in rhesus macaques of about 1.0 per day (Davenport et al., 2004), shows a 2- to 3-fold difference in the proliferation rates of T cell responses. Here, allometric theory predicts a roughly 4-fold difference between the metabolic rates of a single cell in mice ($\sim$20 g) compared to macaques ($\sim$7 kg). Taken together, there are indications that T cell responses develop slower upon viral infections in larger animals but it remains unclear whether this influences the ability of the cellular immune responses to eradicate viruses during the acute phase of an infection, especially if virus replication also underlies allometric scaling principles. More data is needed on the kinetics of virus replication and the dynamics of T cell responses in different host species to shed more light on the question whether the nature of viral infections is affected by the size of their host.

Bibliography

Ali, A., Lubong, R., Ng, H., Brooks, D. G., Zack, J. A., and Yang, O. O. (2004). Impacts of epitope expression kinetics and class I downregulation on the antiviral activity of human immunodeficiency virus type 1-specific cytotoxic T lymphocytes. *J Virol*, 78(2):561–567. (Cited on pages 106 and 107.)

Alizon, S. and van Baalen, M. (2008). Acute or chronic? Within-host models with immune dynamics, infection outcome, and parasite evolution. *Am Nat*, 172(6):E244–56. (Cited on page 6.)

Allee, W. C. (1949). *Principles of Animal Ecology*. Saunders Co., Philadelphia. (Cited on page 90.)

Allen, T., O'Connor, D., Jing, P., Dzuris, J., Mothe, B., Vogel, T., Dunphy, E., Liebl, M., Emerson, C., Wilson, N., Kunstman, K., Wang, X., Allison, D., Hughes, A., Desrosiers, R., Altman, J., Wolinsky, S., Sette, A., and Watkins, D. (2000). Tat-specific cytotoxic T lymphocytes select for SIV escape variants during resolution of primary viraemia. *Nature*, 407(6802):386–90. (Cited on pages 66 and 69.)

Altfeld, M. and Allen, T. (2006). Hitting HIV where it hurts: an alternative approach to HIV vaccine design. *Trends Immunol*, 27(11):504–10. (Cited on pages 4 and 78.)

Altfeld, M., Rosenberg, E., Shankarappa, R., Mukherjee, J., Hecht, F., Eldridge, R., Addo, M., Poon, S., Phillips, M., Robbins, G., Sax, P., Boswell, S., Kahn, J., Brander, C., Goulder, P., Levy, J., Mullins, J., and Walker, B. (2001). Cellular immune responses and viral diversity in individuals treated during acute and early HIV-1 infection. *J Exp Med*, 193(2):169–80. (Cited on page 66.)

Althaus, C. L. and Bonhoeffer, S. (2005). Stochastic interplay between mutation and recombination during the acquisition of drug resistance mutations in human immunodeficiency virus type 1. *J Virol*, 79(21):13572–13578. (Cited on pages 6 and 84.)

Althaus, C. L. and De Boer, R. J. (2008). Dynamics of immune escape during HIV/SIV infection. *PLoS Comput Biol*, 4(7):e1000103. (Cited on pages 84, 88, and 108.)

Anderson, R. M. and May, R. M. (1991). *Infectious Diseases of Humans: Dynamics and Control*. Oxford University Press, Oxford. (Cited on page 5.)

Antia, R., Bergstrom, C., Pilyugin, S., Kaech, S., and Ahmed, R. (2003). Models of CD8+ responses: 1. What is the antigen-independent proliferation program. *J Theor Biol*, 221(4):585–98. (Cited on pages 6, 50, and 51.)

Antia, R., Ganusov, V., and Ahmed, R. (2005). The role of models in understanding CD8+ T-cell memory. *Nat Rev Immunol*, 5(2):101–11. (Cited on pages 50 and 51.)

Armitage, P. and Berry, G. (1994). *Statistical Methods in Medical Research, 2nd edition*. Blackwell, Oxford. (Cited on page 52.)

Asquith, B., Edwards, C., Lipsitch, M., and McLean, A. (2006). Inefficient cytotoxic T lymphocyte-mediated killing of HIV-1-infected cells in vivo. *PLoS Biol*, 4(4):e90. (Cited on pages 6, 66, 73, 74, 79, 84, 88, 91, 101, 114, 115, and 116.)

Asquith, B. and McLean, A. (2007). In vivo CD8+ T cell control of immunodeficiency virus infection in humans and macaques. *Proc Natl Acad Sci U S A*, 104(15):6365–70. (Cited on pages 66, 74, and 116.)

Badovinac, V. P., Porter, B. B., and Harty, J. T. (2002). Programmed contraction of CD8+ T cells after infection. *Nat. Immunol.*, 3:619–626. (Cited on page 51.)

Barber, D., Wherry, E., Masopust, D., Zhu, B., Allison, J., Sharpe, A., Freeman, G., and Ahmed, R. (2006). Restoring function in exhausted CD8 T cells during chronic viral infection. *Nature*, 439(7077):682–7. (Cited on page 50.)

Barouch, D., Powers, J., Truitt, D., Kishko, M., Arthur, J., Peyerl, F., Kuroda, M., Gorgone, D., Lifton, M., Lord, C., Hirsch, V., Montefiori, D., Carville, A., Mansfield, K., Kunstman, K., Wolinsky, S., and Letvin, N. (2005). Dynamic immune responses maintain cytotoxic T lymphocyte epitope mutations in transmitted simian immunodeficiency virus variants. *Nat Immunol*, 6(3):247–52. (Cited on pages 66 and 79.)

Barre-Sinoussi, F., Chermann, J. C., Rey, F., Nugeyre, M. T., Chamaret, S., Gruest, J., Dauguet, C., Axler-Blin, C., Vezinet-Brun, F., Rouzioux, C., Rozenbaum, W., and Montagnier, L. (1983). Isolation of a T-lymphotropic retrovirus from a patient at risk for acquired immune deficiency syndrome (AIDS). *Science*, 220(4599):868–871. (Cited on page 5.)

Bell, G. I., Perelson, A. S., and Pimbley, G. H. (1978). *Theoretical Immunology*. Immunology series ; 8. M. Dekker, New York. (Cited on page 6.)

Beltman, J. B., Maree, A. F. M., Lynch, J. N., Miller, M. J., and de Boer, R. J. (2007). Lymph node topology dictates T cell migration behavior. *J Exp Med*, 204(4):771–780. (Cited on page 6.)

Blattman, J., Antia, R., Sourdive, D., Wang, X., Kaech, S., Murali-Krishna, K., Altman, J., and Ahmed, R. (2002). Estimating the precursor frequency of naive antigen-specific CD8 T cells. *J Exp Med*, 195(5):657–64. (Cited on page 52.)

Bocharov, G. (1998). Modelling the dynamics of LCMV infection in mice: conventional and exhaustive CTL responses. *J Theor Biol*, 192(3):283–308. (Cited on pages 6 and 50.)

Bonhoeffer, S., Chappey, C., Parkin, N. T., Whitcomb, J. M., and Petropoulos, C. J. (2004). Evidence for positive epistasis in HIV-1. *Science*, 306(5701):1547–1550. (Cited on page 6.)

Bonhoeffer, S., Funk, G., Gunthard, H., Fischer, M., and Muller, V. (2003). Glancing behind virus load variation in HIV-1 infection. *Trends Microbiol*, 11(11):499–504. (Cited on pages 70, 73, 96, and 101.)

Bonhoeffer, S., May, R. M., Shaw, G. M., and Nowak, M. A. (1997). Virus dynamics and drug therapy. *Proc Natl Acad Sci U S A*, 94(13):6971–6976. (Cited on page 6.)

Borghans, J. A., de Boer, R. J., and Segel, L. A. (1996). Extending the quasi-steady state approximation by changing variables. *Bull Math Biol*, 58(1):43–63. (Cited on page 108.)

Borghans, J. A. M., Molgaard, A., de Boer, R. J., and Kesmir, C. (2007). HLA alleles associated with slow progression to AIDS truly prefer to present HIV-1 p24. *PLoS ONE*, 2(9):e920. (Cited on pages 97 and 106.)

Brandin, E., Thorstensson, R., Bonhoeffer, S., and Albert, J. (2006). Rapid viral decay in simian immunodeficiency virus-infected macaques receiving quadruple antiretroviral therapy. *J Virol*, 80(19):9861–9864. (Cited on page 116.)

Bretscher, M. T., Althaus, C. L., Muller, V., and Bonhoeffer, S. (2004). Recombination in HIV and the evolution of drug resistance: for better or for worse? *Bioessays*, 26(2):180–188. (Cited on pages 6 and 84.)

Briggs, J. A. G., Simon, M. N., Gross, I., Krausslich, H.-G., Fuller, S. D., Vogt, V. M., and Johnson, M. C. (2004). The stoichiometry of Gag protein in HIV-1. *Nat Struct Mol Biol*, 11(7):672–675. (Cited on page 106.)

Brooks, D., Trifilo, M., Edelmann, K., Teyton, L., McGavern, D., and Oldstone, M. (2006). Interleukin-10 determines viral clearance or persistence in vivo. *Nat Med*, 12(11):1301–1309. (Cited on page 62.)

Brooks, D. G., Hamer, D. H., Arlen, P. A., Gao, L., Bristol, G., Kitchen, C. M. R., Berger, E. A., and Zack, J. A. (2003). Molecular characterization, reactivation, and depletion of latent HIV. *Immunity*, 19(3):413–423. (Cited on page 21.)

Bucy, R. P. (1999). Immune clearance of HIV type 1 replication-active cells: a model of two patterns of steady state HIV infection. *AIDS Res Hum Retroviruses*, 15(3):223–227. (Cited on page 22.)

Burnett, J. C., Miller-Jensen, K., Shah, P. S., Arkin, A. P., and Schaffer, D. V. (2009). Control of stochastic gene expression by host factors at the HIV promoter. *PLoS Pathog*, 5(1):e1000260. (Cited on pages 7 and 22.)

Cable, J. M., Enquist, B. J., and Moses, M. E. (2007). The allometry of host-pathogen interactions. *PLoS ONE*, 2(11):e1130. (Cited on page 116.)

Calder, W. A. (1996). *Size, Function, and Life History*. Dover Publications, Mineola, N.Y. (Cited on page 116.)

Cao, J., McNevin, J., Malhotra, U., and McElrath, M. (2003). Evolution of CD8+ T cell immunity and viral escape following acute HIV-1 infection. *J Immunol*, 171(7):3837–46. (Cited on pages 66 and 69.)

Casazza, J., Betts, M., Picker, L., and Koup, R. (2001). Decay kinetics of human immunodeficiency virus-specific CD8+ T cells in peripheral blood after initiation of highly active antiretroviral therapy. *J Virol*, 75(14):6508–16. (Cited on pages 70 and 75.)

Chun, T., Carruth, L., Finzi, D., Shen, X., DiGiuseppe, J., Taylor, H., Hermankova, M., Chadwick, K., Margolick, J., Quinn, T., Kuo, Y., Brookmeyer, R., Zeiger, M., Barditch-Crovo, P., and Siliciano, R. (1997). Quantification of latent tissue reservoirs and total body viral load in HIV-1 infection. *Nature*, 387(6629):183–8. (Cited on pages 12, 15, and 20.)

Chun, T., Justement, J., Moir, S., Hallahan, C., Maenza, J., Mullins, J., Collier, A., Corey, L., and Fauci, A. (2007). Decay of the HIV reservoir in patients receiving antiretroviral therapy for extended periods: implications for eradication of virus. *J Infect Dis*, 195(12):1762–4. (Cited on page 18.)

Cohen, G. B., Gandhi, R. T., Davis, D. M., Mandelboim, O., Chen, B. K., Strominger, J. L., and Baltimore, D. (1999). The selective downregulation of class I major histocompatibility complex proteins by HIV-1 protects HIV-infected cells from NK cells. *Immunity*, 10(6):661–671. (Cited on page 107.)

Collins, K., Chen, B., Kalams, S., Walker, B., and Baltimore, D. (1998). HIV-1 Nef protein protects infected primary cells against killing by cytotoxic T lymphocytes. *Nature*, 391(6665):397–401. (Cited on pages 96 and 98.)

Crawford, H., Prado, J., Leslie, A., Hue, S., Honeyborne, I., Reddy, S., van der Stok, M., Mncube, Z., Brander, C., Rousseau, C., Mullins, J., Kaslow, R., Goepfert, P., Allen, S., Hunter, E., Mulenga, J., Kiepiela, P., Walker, B., and Goulder, P. (2007). Compensatory mutation partially restores fitness and delays reversion of escape mutation within the immunodominant HLA-B*5703-restricted Gag epitope in chronic human immunodeficiency virus type 1 infection. *J Virol*, 81(15):8346–51. (Cited on pages 66 and 79.)

Davenport, M., Ribeiro, R., and Perelson, A. (2004). Kinetics of virus-specific CD8+ T cells and the control of human immunodeficiency virus infection. *J Virol*, 78(18):10096–103. (Cited on pages 70, 72, 109, 113, and 117.)

De Boer, R. (2007). Understanding the failure of CD8+ T-cell vaccination against simian/human immunodeficiency virus. *J Virol*, 81(6):2838–48. (Cited on pages 6, 67, 72, 73, 80, 81, 91, 97, 108, and 113.)

De Boer, R., Homann, D., and Perelson, A. (2003). Different dynamics of CD4+ and CD8+ T cell responses during and after acute lymphocytic choriomeningitis virus infection. *J Immunol*, 171(8):3928–3935. (Cited on pages 6, 50, 53, 55, 56, 57, 59, 60, 61, and 117.)

De Boer, R., Oprea, M., Antia, R., Murali-Krishna, K., Ahmed, R., and Perelson, A. (2001). Recruitment times, proliferation, and apoptosis rates during the CD8(+) T-cell response to lymphocytic choriomeningitis virus. *J Virol*, 75(22):10663–10669. (Cited on pages 6, 50, 51, and 117.)

De Boer, R. and Perelson, A. (1998). Target cell limited and immune control models of HIV infection: a comparison. *J Theor Biol*, 190(3):201–14. (Cited on pages 6, 30, 68, and 107.)

De Boer, R. J. and Perelson, A. S. (1995). Towards a general function describing T cell proliferation. *J Theor Biol*, 175(4):567–576. (Cited on page 6.)

De Roos, A. M., Diekmann, O., and Metz, J. A. J. (1992). Studying the dynamics of structured population models: A versatile technique and its application to daphnia. *The American Naturalist*, 139(1):123–147. (Cited on page 25.)

Delassus, S., Cheynier, R., and Wain-Hobson, S. (1992). Nonhomogeneous distribution of human immunodeficiency virus type 1 proviruses in the spleen. *J Virol*, 66(9):5642–5645. (Cited on page 93.)

Diekmann, O. and Heesterbeek, J. A. P. (2000). *Mathematical Epidemiology of Infectious Diseases: Model Building, Analysis, and Interpretation*. John Wiley, Chichester. (Cited on page 5.)

Dixit, N. and Perelson, A. (2004). Multiplicity of human immunodeficiency virus infections in lymphoid tissue. *J Virol*, 78(16):8942–5. (Cited on pages 84, 87, 91, and 93.)

Dixit, N. M., Markowitz, M., Ho, D. D., and Perelson, A. S. (2004). Estimates of intracellular delay and average drug efficacy from viral load data of HIV-infected individuals under antiretroviral therapy. *Antivir Ther*, 9(2):237–246. (Cited on pages 28, 96, and 109.)

Dixit, N. M. and Perelson, A. S. (2005). HIV dynamics with multiple infections of target cells. *Proc Natl Acad Sci U S A*, 102(23):8198–8203. (Cited on page 84.)

Doherty, P. and Christensen, J. (2000). Accessing complexity: the dynamics of virus-specific T cell responses. *Annu Rev Immunol*, 18:561–592. (Cited on page 50.)

Dowling, M. R., Milutinovic, D., and Hodgkin, P. D. (2005). Modelling cell lifespan and proliferation: is likelihood to die or to divide independent of age? *J R Soc Interface*, 2(5):517–526. (Cited on page 28.)

Draenert, R., Allen, T., Liu, Y., Wrin, T., Chappey, C., Verrill, C., Sirera, G., Eldridge, R., Lahaie, M., Ruiz, L., Clotet, B., Petropoulos, C., Walker, B., and Martinez-Picado, J. (2006). Constraints on HIV-1 evolution and immunodominance revealed in monozygotic adult twins infected with the same virus. *J Exp Med*, 203(3):529–39. (Cited on pages 66, 70, 75, 77, and 113.)

Efron, B. and Tibshirani, R. (1986). Bootstrap methods for standard errors, confidence intervals, and other measures of statistical accuracy. *Stat. Sci.*, 1:54–77. (Cited on page 52.)

Eigen, M., Biebricher, C. K., Gebinoga, M., and Gardiner, W. C. (1991). The hypercycle. Coupling of RNA and protein biosynthesis in the infection cycle of an RNA bacteriophage. *Biochemistry*, 30(46):11005–11018. (Cited on page 12.)

Ejrnaes, M., Filippi, C., Martinic, M., Ling, E., Togher, L., Crotty, S., and von Herrath, M. (2006). Resolution of a chronic viral infection after interleukin-10 receptor blockade. *J Exp Med*, 203(11):2461–2472. (Cited on page 62.)

Elowitz, M. B., Levine, A. J., Siggia, E. D., and Swain, P. S. (2002). Stochastic gene expression in a single cell. *Science*, 297(5584):1183–1186. (Cited on page 12.)

Fernandez, C., Stratov, I., De Rose, R., Walsh, K., Dale, C., Smith, M., Agy, M., Hu, S., Krebs, K., Watkins, D., O'connor, D., Davenport, M., and Kent, S. (2005). Rapid viral escape at an immunodominant simian-human immunodeficiency virus cytotoxic T-lymphocyte epitope exacts a dramatic fitness cost. *J Virol*, 79(9):5721–31. (Cited on page 73.)

Finzi, D., Blankson, J., Siliciano, J., Margolick, J., Chadwick, K., Pierson, T., Smith, K., Lisziewicz, J., Lori, F., Flexner, C., Quinn, T., Chaisson, R., Rosenberg, E., Walker, B., Gange, S., Gallant, J., and Siliciano, R. (1999). Latent infection of CD4+ T cells provides a mechanism for lifelong persistence of HIV-1, even in patients on effective combination therapy. *Nat Med*, 5(5):512–7. (Cited on pages 13 and 20.)

Fraser, C. (2005). HIV recombination: what is the impact on antiretroviral therapy? *J R Soc Interface*, 2(5):489–503. (Cited on page 84.)

Frater, A., Brown, H., Oxenius, A., Gunthard, H., Hirschel, B., Robinson, N., Leslie, A., Payne, R., Crawford, H., Prendergast, A., Brander, C., Kiepiela, P., Walker, B., Goulder, P., McLean, A., and Phillips, R. (2007). Effective T-cell responses select human immunodeficiency virus mutants and slow disease progression. *J Virol*, 81(12):6742–51. (Cited on pages 66 and 79.)

Friedrich, T., Dodds, E., Yant, L., Vojnov, L., Rudersdorf, R., Cullen, C., Evans, D., Desrosiers, R., Mothe, B., Sidney, J., Sette, A., Kunstman, K., Wolinsky, S., Piatak, M., Lifson, J., Hughes, A., Wilson, N., O'Connor, D., and Watkins, D. (2004). Reversion of CTL escape-variant immunodeficiency viruses in vivo. *Nat Med*, 10(3):275–81. (Cited on pages 66 and 79.)

Friedrich, T., Valentine, L., Yant, L., Rakasz, E., Piaskowski, S., Furlott, J., Weisgrau, K., Burwitz, B., May, G., Leon, E., Soma, T., Napoe, G., Capuano, 3rd, S., Wilson, N., and Watkins, D. (2007). Subdominant CD8+ T-cell responses are involved in durable control of AIDS virus replication. *J Virol*, 81(7):3465–76. (Cited on pages 104 and 105.)

Frost, S. D., Dumaurier, M. J., Wain-Hobson, S., and Brown, A. J. (2001). Genetic drift and within-host metapopulation dynamics of HIV-1 infection. *Proc Natl Acad Sci U S A*, 98(12):6975–6980. (Cited on page 93.)

Funk, G. A., Jansen, V. A. A., Bonhoeffer, S., and Killingback, T. (2005). Spatial models of virus-immune dynamics. *J Theor Biol*, 233(2):221–236. (Cited on page 93.)

Funk, G. A., Oxenius, A., Fischer, M., Opravil, M., Joos, B., Flepp, M., Weber, R., Gunthard, H. F., and Bonhoeffer, S. (2006). HIV replication elicits little cytopathic effects in vivo: analysis of surrogate markers for virus production, cytotoxic t cell response and infected cell death. *J Med Virol*, 78(9):1141–1146. (Cited on page 36.)

Ganusov, V. and De Boer, R. (2006). Estimating costs and benefits of CTL escape mutations in SIV/HIV infection. *PLoS Comput Biol*, 2(3):e24. (Cited on pages 66 and 84.)

Geels, M., Cornelissen, M., Schuitemaker, H., Anderson, K., Kwa, D., Maas, J., Dekker, J., Baan, E., Zorgdrager, F., van den Burg, R., van Beelen, M., Lukashov, V., Fu, T., Paxton, W., van der Hoek, L., Dubey, S., Shiver, J., and Goudsmit, J. (2003). Identification of sequential viral escape mutants associated with altered T-cell responses in a human immunodeficiency virus type 1-infected individual. *J Virol*, 77(23):12430–40. (Cited on page 69.)

Gilchrist, M. A., Coombs, D., and Perelson, A. S. (2004). Optimizing within-host viral fitness: infected cell lifespan and virion production rate. *J Theor Biol*, 229(2):281–288. (Cited on page 28.)

Gillespie, D. (1977). Exact stochastic simulation of coupled chemical reactions. *The Journal of Physical Chemistry*, 81(25):2340–2361. (Cited on pages 23 and 79.)

Goldsby, R. A., Kindt, T. J., Osborne, B. A., and Kuby, J. (2003). *Immunology*. W.H. Freeman, New York, 5th ed edition. (Cited on page 2.)

Gompertz, B. (1825). On the nature of the function expressive of the law of human mortality, and on a new mode of determining the value of life contingencies. *Philosophical Transactions Series I*, 115:513–583. (Cited on page 33.)

Gordon, S. N., Dunham, R. M., Engram, J. C., Estes, J., Wang, Z., Klatt, N. R., Paiardini, M., Pandrea, I. V., Apetrei, C., Sodora, D. L., Lee, H. Y., Haase, A. T., Miller, M. D., Kaur, A., Staprans, S. I., Perelson, A. S., Feinberg, M. B.,

and Silvestri, G. (2008). Short-lived infected cells support virus replication in sooty mangabeys naturally infected with simian immunodeficiency virus: implications for aids pathogenesis. *J Virol*, 82(7):3725–3735. (Cited on page 106.)

Goulder, P., Phillips, R., Colbert, R., McAdam, S., Ogg, G., Nowak, M., Giangrande, P., Luzzi, G., Morgan, B., Edwards, A., McMichael, A., and Rowland-Jones, S. (1997). Late escape from an immunodominant cytotoxic T-lymphocyte response associated with progression to AIDS. *Nat Med*, 3(2):212–7. (Cited on pages 66, 69, and 114.)

Goulder, P. and Watkins, D. (2004). HIV and SIV CTL escape: implications for vaccine design. *Nat Rev Immunol*, 4(8):630–40. (Cited on pages 66 and 84.)

Grayson, J., Weant, A., Holbrook, B., and Hildeman, D. (2006). Role of Bim in regulating CD8+ T-cell responses during chronic viral infection. *J Virol*, 80(17):8627–8638. (Cited on pages 63 and 64.)

Gruters, R., van Baalen, C., and Osterhaus, A. (2002). The advantage of early recognition of HIV-infected cells by cytotoxic T-lymphocytes. *Vaccine*, 20(15):2011–5. (Cited on page 96.)

Gunthard, H. F., Wong, J. K., Spina, C. A., Ignacio, C., Kwok, S., Christopherson, C., Hwang, J., Haubrich, R., Havlir, D., and Richman, D. D. (2000). Effect of influenza vaccination on viral replication and immune response in persons infected with human immunodeficiency virus receiving potent antiretroviral therapy. *J Infect Dis*, 181(2):522–531. (Cited on page 13.)

Haase, A., Henry, K., Zupancic, M., Sedgewick, G., Faust, R., Melroe, H., Cavert, W., Gebhard, K., Staskus, K., Zhang, Z., Dailey, P., Balfour, Jr, H., Erice, A., and Perelson, A. (1996). Quantitative image analysis of HIV-1 infection in lymphoid tissue. *Science*, 274(5289):985–9. (Cited on pages 70 and 87.)

Haase, A. T., Stowring, L., Harris, J. D., Traynor, B., Ventura, P., Peluso, R., and Brahic, M. (1982). Visna DNA synthesis and the tempo of infection in vitro. *Virology*, 119(2):399–410. (Cited on pages 28, 29, and 38.)

Han, Y., Wind-Rotolo, M., Yang, H., Siliciano, J., and Siliciano, R. (2007). Experimental approaches to the study of HIV-1 latency. *Nat Rev Microbiol*, 5(2):95–106. (Cited on pages 12 and 22.)

Haseltine, E., Rawlings, J., and Yin, J. (2005). Dynamics of viral infections: incorporating both the intracellular and extracellular levels. *Computers and Chemical Engineering*, 29(3):675–686. (Cited on pages 12 and 21.)

Haseltine, E. L., Yin, J., and Rawlings, J. B. (2008). Implications of decoupling the intracellular and extracellular levels in multi-level models of virus growth. *Biotechnol Bioeng*, 101(4):811–820. (Cited on pages 12 and 21.)

Heffernan, J. M., Smith, R. J., and Wahl, L. M. (2005). Perspectives on the basic reproductive ratio. *J R Soc Interface*, 2(4):281–293. (Cited on page 101.)

Herz, A. V., Bonhoeffer, S., Anderson, R. M., May, R. M., and Nowak, M. A. (1996). Viral dynamics in vivo: limitations on estimates of intracellular delay and virus decay. *Proc Natl Acad Sci U S A*, 93(14):7247–7251. (Cited on pages 28 and 111.)

Ho, D. D. and Huang, Y. (2002). The HIV-1 vaccine race. *Cell*, 110(2):135–138. (Cited on page 28.)

Ho, D. D., Neumann, A. U., Perelson, A. S., Chen, W., Leonard, J. M., and Markowitz, M. (1995). Rapid turnover of plasma virions and CD4 lymphocytes in HIV-1 infection. *Nature*, 373(6510):123–126. (Cited on pages 5, 28, 96, and 111.)

Holland, J., Spindler, K., Horodyski, F., Grabau, E., Nichol, S., and VandePol, S. (1982). Rapid evolution of RNA genomes. *Science*, 215(4540):1577–1585. (Cited on page 3.)

Homann, D., Teyton, L., and Oldstone, M. (2001). Differential regulation of antiviral T-cell immunity results in stable CD8+ but declining CD4+ T-cell memory. *Nat Med*, 7(8):913–919. (Cited on pages 53, 55, 57, and 59.)

Jeeninga, R. E., Westerhout, E. M., van Gerven, M. L., and Berkhout, B. (2008). HIV-1 latency in actively dividing human T cell lines. *Retrovirology*, 5:37. (Cited on page 22.)

Jin, X., Bauer, D. E., Tuttleton, S. E., Lewin, S., Gettie, A., Blanchard, J., Irwin, C. E., Safrit, J. T., Mittler, J., Weinberger, L., Kostrikis, L. G., Zhang, L., Perelson, A. S., and Ho, D. D. (1999). Dramatic rise in plasma viremia after CD8(+) T cell depletion in simian immunodeficiency virus-infected macaques. *J Exp Med*, 189(6):991–998. (Cited on pages 104, 105, and 114.)

Jordan, A., Defechereux, P., and Verdin, E. (2001). The site of HIV-1 integration in the human genome determines basal transcriptional activity and response to Tat transactivation. *EMBO J*, 20(7):1726–1738. (Cited on page 18.)

Jung, A., Maier, R., Vartanian, J., Bocharov, G., Jung, V., Fischer, U., Meese, E., Wain-Hobson, S., and Meyerhans, A. (2002). Multiply infected spleen cells in HIV patients. *Nature*, 418(6894):144. (Cited on pages 77, 84, 92, and 93.)

Kaech, S. M. and Ahmed, R. (2001). Memory CD8+ T cell differentiation: initial antigen encounter triggers a developmental program in naive cells. *Nat. Immunol.*, 2:415–422. (Cited on page 51.)

Karlsson, A., Iversen, A., Chapman, J., de Oliviera, T., Spotts, G., McMichael, A., Davenport, M., Hecht, F., and Nixon, D. (2007). Sequential broadening of CTL responses in early HIV-1 infection is associated with viral escape. *PLoS ONE*, 2:e225. (Cited on page 66.)

Karn, J. (1999). Tackling Tat. *J Mol Biol*, 293(2):235–254. (Cited on page 12.)

Kaslow, R., Carrington, M., Apple, R., Park, L., Munoz, A., Saah, A., Goedert, J., Winkler, C., O'Brien, S., Rinaldo, C., Detels, R., Blattner, W., Phair, J., Erlich, H., and Mann, D. (1996). Influence of combinations of human major histocompatibility complex genes on the course of HIV-1 infection. *Nat Med*, 2(4):405–11. (Cited on pages 66 and 96.)

Kawashima, Y., Pfafferott, K., Frater, J., Matthews, P., Payne, R., Addo, M., Gatanaga, H., Fujiwara, M., Hachiya, A., Koizumi, H., Kuse, N., Oka, S., Duda, A., Prendergast, A., Crawford, H., Leslie, A., Brumme, Z., Brumme, C., Allen, T., Brander, C., Kaslow, R., Tang, J., Hunter, E., Allen, S., Mulenga, J., Branch, S., Roach, T., John, M., Mallal, S., Ogwu, A., Shapiro, R., Prado, J., Fidler, S., Weber, J., Pybus, O., Klenerman, P., Ndung'u, T., Phillips, R., Heckerman, D., Harrigan, P., Walker, B., Takiguchi, M., and Goulder, P. (2009). Adaptation of HIV-1 to human leukocyte antigen class I. *Nature*. (Cited on page 84.)

Keeling, M. J. and Rohani, P. (2008). *Modeling Infectious Diseases in Humans and Animals*. Princeton University Press, Princeton. (Cited on page 5.)

Kelleher, A., Long, C., Holmes, E., Allen, R., Wilson, J., Conlon, C., Workman, C., Shaunak, S., Olson, K., Goulder, P., Brander, C., Ogg, G., Sullivan, J., Dyer, W., Jones, I., McMichael, A., Rowland-Jones, S., and Phillips, R. (2001). Clustered mutations in HIV-1 gag are consistently required for escape from HLA-B27-restricted cytotoxic T lymphocyte responses. *J Exp Med*, 193(3):375–86. (Cited on pages 66 and 77.)

Kent, S., Fernandez, C., Dale, C., and Davenport, M. (2005). Reversion of immune escape HIV variants upon transmission: insights into effective viral immunity. *Trends Microbiol*, 13(6):243–6. (Cited on pages 66 and 79.)

Kermack, W. O. and McKendrick, A. G. (1927). A contribution to the mathematical theory of epidemics. *Royal Society of London Proceedings Series A*, 115:700–721. (Cited on page 4.)

Kesmir, C. and De Boer, R. (2003). Clonal exhaustion as a result of immune deviation. *Bull Math Biol*, 65(3):359–74. (Cited on page 50.)

Kesmir, C., Nussbaum, A. K., Schild, H., Detours, V., and Brunak, S. (2002). Prediction of proteasome cleavage motifs by neural networks. *Protein Eng*, 15(4):287–296. (Cited on page 106.)

Kiepiela, P., Ngumbela, K., Thobakgale, C., Ramduth, D., Honeyborne, I., Moodley, E., Reddy, S., de Pierres, C., Mncube, Z., Mkhwanazi, N., Bishop, K., van der Stok, M., Nair, K., Khan, N., Crawford, H., Payne, R., Leslie, A., Prado, J., Prendergast, A., Frater, J., McCarthy, N., Brander, C., Learn, G., Nickle, D., Rousseau, C., Coovadia, H., Mullins, J., Heckerman, D., Walker, B., and Goulder, P. (2007). CD8+ T-cell responses to different HIV proteins

have discordant associations with viral load. *Nat Med*, 13(1):46–53. (Cited on pages 96, 97, and 106.)

Kim, E.-Y., Veazey, R. S., Zahn, R., McEvers, K. J., Baumeister, S. H. C., Foster, G. J., Rett, M. D., Newberg, M. H., Kuroda, M. J., Rieber, E. P., Piatak, M. J., Lifson, J. D., Letvin, N. L., Wolinsky, S. M., and Schmitz, J. E. (2008). Contribution of CD8+ T cells to containment of viral replication and emergence of mutations in Mamu-A*01-restricted epitopes in simian immunodeficiency virus-infected rhesus monkeys. *J Virol*, 82(11):5631–5635. (Cited on page 96.)

Kim, H. and Perelson, A. S. (2006). Viral and latent reservoir persistence in HIV-1-infected patients on therapy. *PLoS Comput Biol*, 2(10):e135. (Cited on pages 13 and 18.)

Kim, H. and Yin, J. (2005). Robust growth of human immunodeficiency virus type 1 (HIV-1). *Biophys J*, 89(4):2210–21. (Cited on pages 22 and 24.)

Kirschner, D. and Webb, G. F. (1996). A model for treatment strategy in the chemotherapy of aids. *Bull Math Biol*, 58(2):376–390. (Cited on pages 7, 12, and 28.)

Kleiber, M. (1932). Body size and metabolism. *Hilgardia*, 6:315–353. (Cited on page 116.)

Klenerman, P., Phillips, R., Rinaldo, C., Wahl, L., Ogg, G., May, R., McMichael, A., and Nowak, M. (1996). Cytotoxic T lymphocytes and viral turnover in HIV type 1 infection. *Proc Natl Acad Sci U S A*, 93(26):15323–8. (Cited on pages 96, 97, 98, 105, 109, and 114.)

Kohler, B. (2007). Mathematically modeling dynamics of t cell responses: Predictions concerning the generation of memory cells. *J Theor Biol*, 245(4):669–676. (Cited on pages 6 and 51.)

Kotturi, M. F., Peters, B., Buendia-Laysa, F. J., Sidney, J., Oseroff, C., Botten, J., Grey, H., Buchmeier, M. J., and Sette, A. (2007). The CD8+ T-cell response to lymphocytic choriomeningitis virus involves the l antigen: Uncovering new tricks for an old virus. *J Virol*, 81(10):4928–4940. (Cited on page 64.)

Kouyos, R., Althaus, C., and Bonhoeffer, S. (2006). Stochastic or deterministic: what is the effective population size of HIV-1? *Trends Microbiol*, 14(12):507–11. (Cited on pages 6, 66, 77, 78, and 87.)

Kulkosky, J., Culnan, D. M., Roman, J., Dornadula, G., Schnell, M., Boyd, M. R., and Pomerantz, R. J. (2001). Prostratin: activation of latent HIV-1 expression suggests a potential inductive adjuvant therapy for HAART. *Blood*, 98(10):3006–3015. (Cited on page 21.)

Lassen, K., Han, Y., Zhou, Y., Siliciano, J., and Siliciano, R. (2004a). The multifactorial nature of HIV-1 latency. *Trends Mol Med*, 10(11):525–31. (Cited on pages 12 and 22.)

Lassen, K. G., Bailey, J. R., and Siliciano, R. F. (2004b). Analysis of human immunodeficiency virus type 1 transcriptional elongation in resting CD4+ T cells in vivo. *J Virol*, 78(17):9105–9114. (Cited on pages 13 and 21.)

Lau, L., Jamieson, B., Somasundaram, T., and Ahmed, R. (1994). Cytotoxic T-cell memory without antigen. *Nature*, 369(6482):648–52. (Cited on page 50.)

Li, B., Gladden, A., Altfeld, M., Kaldor, J., Cooper, D., Kelleher, A., and Allen, T. (2007). Rapid reversion of sequence polymorphisms dominates early human immunodeficiency virus type 1 evolution. *J Virol*, 81(1):193–201. (Cited on pages 66 and 79.)

Li, Q., Duan, L., Estes, J., Ma, Z., Rourke, T., Wang, Y., Reilly, C., Carlis, J., Miller, C., and Haase, A. (2005). Peak SIV replication in resting memory CD4+ T cells depletes gut lamina propria CD4+ T cells. *Nature*, 434(7037):1148–52. (Cited on page 72.)

Li, X. D., Moore, B., and Cloyd, M. W. (1996). Gradual shutdown of virus production resulting in latency is the norm during the chronic phase of human immunodeficiency virus replication and differential rates and mechanisms of shutdown are determined by viral sequences. *Virology*, 225(1):196–212. (Cited on page 22.)

Lichterfeld, M., Yu, X. G., Le Gall, S., and Altfeld, M. (2005). Immunodominance of HIV-1-specific CD8(+) T-cell responses in acute HIV-1 infection: at the crossroads of viral and host genetics. *Trends Immunol*, 26(3):166–171. (Cited on page 106.)

Little, S. J., McLean, A. R., Spina, C. A., Richman, D. D., and Havlir, D. V. (1999). Viral dynamics of acute HIV-1 infection. *J Exp Med*, 190(6):841–850. (Cited on pages 42 and 116.)

Liu, Y., Mullins, J., and Mittler, J. (2006). Waiting times for the appearance of cytotoxic T-lymphocyte escape mutants in chronic HIV-1 infection. *Virology*, 347(1):140–6. (Cited on page 77.)

Lloyd, A. L. (2001). The dependence of viral parameter estimates on the assumed viral life cycle: limitations of studies of viral load data. *Proc Biol Sci*, 268(1469):847–854. (Cited on page 28.)

Loh, L., Batten, C., Petravic, J., Davenport, M., and Kent, S. (2007). In vivo fitness costs of different Gag CD8 T-cell escape mutant simian-human immunodeficiency viruses for macaques. *J Virol*, 81(10):5418–22. (Cited on page 66.)

Lotka, A. J. (1925). *Elements of Physical Biology*. Williams & Wilkins company, Baltimore. (Cited on page 4.)

Mandl, J. N., Regoes, R. R., Garber, D. A., and Feinberg, M. B. (2007). Estimating the effectiveness of simian immunodeficiency virus-specific CD8+ T cells from the dynamics of viral immune escape. *J Virol*, 81(21):11982–11991. (Cited on pages 66 and 114.)

Mansky, L. and Temin, H. (1995). Lower in vivo mutation rate of human immunodeficiency virus type 1 than that predicted from the fidelity of purified reverse transcriptase. *J Virol*, 69(8):5087–94. (Cited on pages 4, 70, and 87.)

Marquardt, D. W. (1963). Finite difference algorithm for curve fitting. *J. Soc. Ind. Appl. Math.*, 11:431–441. (Cited on page 52.)

Matloubian, M., Kolhekar, S., Somasundaram, T., and Ahmed, R. (1993). Molecular determinants of macrophage tropism and viral persistence: importance of single amino acid changes in the polymerase and glycoprotein of lymphocytic choriomeningitis virus. *J Virol*, 67(12):7340–7349. (Cited on pages 53 and 61.)

Matloubian, M., Somasundaram, T., Kolhekar, S., Selvakumar, R., and Ahmed, R. (1990). Genetic basis of viral persistence: single amino acid change in the viral glycoprotein affects ability of lymphocytic choriomeningitis virus to persist in adult mice. *J Exp Med*, 172(4):1043–1048. (Cited on pages 53 and 61.)

Mattapallil, J., Douek, D., Hill, B., Nishimura, Y., Martin, M., and Roederer, M. (2005). Massive infection and loss of memory CD4+ T cells in multiple tissues during acute SIV infection. *Nature*, 434(7037):1093–7. (Cited on pages 70, 72, 87, and 109.)

McAdams, H. H. and Arkin, A. (1997). Stochastic mechanisms in gene expression. *Proc Natl Acad Sci U S A*, 94(3):814–819. (Cited on page 12.)

McLean, A. R. and Kirkwood, T. B. (1990). A model of human immunodeficiency virus infection in T helper cell clones. *J Theor Biol*, 147(2):177–203. (Cited on page 5.)

Mellors, J. W., Rinaldo, C. R. J., Gupta, P., White, R. M., Todd, J. A., and Kingsley, L. A. (1996). Prognosis in HIV-1 infection predicted by the quantity of virus in plasma. *Science*, 272(5265):1167–1170. (Cited on page 96.)

Mercado, R., Vijh, S., Allen, S., Kerksiek, K., Pilip, I., and Pamer, E. (2000). Early programming of T cell populations responding to bacterial infection. *J Immunol*, 165(12):6833–6839. (Cited on page 51.)

Mestas, J. and Hughes, C. C. W. (2004). Of mice and not men: differences between mouse and human immunology. *J Immunol*, 172(5):2731–2738. (Cited on page 115.)

Miller, N., Bonczyk, J., Nakayama, Y., and Suresh, M. (2005). Role of thymic output in regulating CD8 T-cell homeostasis during acute and chronic viral infection. *J Virol*, 79(15):9419–9429. (Cited on pages 50, 51, 52, 56, 57, 58, 59, 63, and 64.)

Milutinovic, D. and De Boer, R. J. (2007). Process noise: An explanation for the fluctuations in the immune response during acute viral infection. *Biophys J*, 92(10):3358–3367. (Cited on page 63.)

Mittler, J. E., Sulzer, B., Neumann, A. U., and Perelson, A. S. (1998). Influence of delayed viral production on viral dynamics in HIV-1 infected patients. *Math Biosci*, 152(2):143–163. (Cited on page 111.)

Muller, V., Maree, A., and De Boer, R. (2001). Small variations in multiple parameters account for wide variations in HIV-1 set-points: a novel modelling approach. *Proc Biol Sci*, 268(1464):235–42. (Cited on pages 96, 104, 105, 108, and 114.)

Muller, V., Vigueras-Gomez, J., and Bonhoeffer, S. (2002). Decelerating decay of latently infected cells during prolonged therapy for human immunodeficiency virus type 1 infection. *J Virol*, 76(17):8963–5. (Cited on pages 13, 18, 21, and 25.)

Murali-Krishna, K., Altman, J., Suresh, M., Sourdive, D., Zajac, A., Miller, J., Slansky, J., and Ahmed, R. (1998). Counting antigen-specific CD8 T cells: a reevaluation of bystander activation during viral infection. *Immunity*, 8(2):177–187. (Cited on pages 50 and 59.)

Nelson, P., Gilchrist, M., Coombs, D., Hyman, J., and Perelson, A. (2004). An age-structured model of HIV infection that allows for variations in the production rate of viral particles and the death rate of productively infected cells. *Math. Biosci. Eng.*, 1(2):267–288. (Cited on pages 7, 12, 28, and 29.)

Nelson, P. W. and Perelson, A. S. (2002). Mathematical analysis of delay differential equation models of HIV-1 infection. *Math Biosci*, 179(1):73–94. (Cited on page 28.)

Nielsen, M., Lundegaard, C., Lund, O., and Kesmir, C. (2005). The role of the proteasome in generating cytotoxic t-cell epitopes: insights obtained from improved predictions of proteasomal cleavage. *Immunogenetics*, 57(1-2):33–41. (Cited on page 106.)

Nowak, M., Anderson, R., McLean, A., Wolfs, T., Goudsmit, J., and May, R. (1991). Antigenic diversity thresholds and the development of AIDS. *Science*, 254(5034):963–9. (Cited on page 78.)

Nowak, M., Lloyd, A., Vasquez, G., Wiltrout, T., Wahl, L., Bischofberger, N., Williams, J., Kinter, A., Fauci, A., Hirsch, V., and Lifson, J. (1997). Viral dynamics of primary viremia and antiretroviral therapy in simian immunodeficiency virus infection. *J Virol*, 71(10):7518–25. (Cited on page 42.)

Nowak, M. and May, R. (2000). *Virus Dynamics: Mathematical Principles of Immunology and Virology*. Oxford Univerity Press, Oxford. (Cited on pages 6, 12, 28, 67, 85, and 97.)

Nowak, M., May, R., Phillips, R., Rowland-Jones, S., Lalloo, D., McAdam, S., Klenerman, P., Koppe, B., Sigmund, K., Bangham, C., and et al. (1995). Antigenic oscillations and shifting immunodominance in HIV-1 infections. *Nature*, 375(6532):606–11. (Cited on pages 6, 67, and 75.)

Nowak, M. A., May, R. M., and Anderson, R. M. (1990). The evolutionary dynamics of HIV-1 quasispecies and the development of immunodeficiency disease. *AIDS*, 4(11):1095–1103. (Cited on page 5.)

Ogg, G., Jin, X., Bonhoeffer, S., Moss, P., Nowak, M., Monard, S., Segal, J., Cao, Y., Rowland-Jones, S., Hurley, A., Markowitz, M., Ho, D., McMichael, A., and Nixon, D. (1999). Decay kinetics of human immunodeficiency virus-specific effector cytotoxic T lymphocytes after combination antiretroviral therapy. *J Virol*, 73(1):797–800. (Cited on pages 70 and 75.)

Palmer, S., Maldarelli, F., Wiegand, A., Bernstein, B., Hanna, G. J., Brun, S. C., Kempf, D. J., Mellors, J. W., Coffin, J. M., and King, M. S. (2008). Low-level viremia persists for at least 7 years in patients on suppressive antiretroviral therapy. *Proc Natl Acad Sci U S A*, 105(10):3879–3884. (Cited on pages 12, 20, and 21.)

Pandrea, I., Ribeiro, R. M., Gautam, R., Gaufin, T., Pattison, M., Barnes, M., Monjure, C., Stoulig, C., Dufour, J., Cyprian, W., Silvestri, G., Miller, M. D., Perelson, A. S., and Apetrei, C. (2008). Simian immunodeficiency virus SIVagm dynamics in african green monkeys. *J Virol*, 82(7):3713–3724. (Cited on page 106.)

Parera, M., Fernandez, G., Clotet, B., and Martinez, M. (2007). HIV-1 protease catalytic efficiency effects caused by random single amino acid substitutions. *Mol Biol Evol*, 24(2):382–7. (Cited on page 79.)

Perelson, A. (2002). Modelling viral and immune system dynamics. *Nat Rev Immunol*, 2(1):28–36. (Cited on pages 12, 28, 67, 85, and 97.)

Perelson, A., Essunger, P., Cao, Y., Vesanen, M., Hurley, A., Saksela, K., Markowitz, M., and Ho, D. (1997). Decay characteristics of HIV-1-infected compartments during combination therapy. *Nature*, 387(6629):188–91. (Cited on pages 20 and 21.)

Perelson, A., Neumann, A., Markowitz, M., Leonard, J., and Ho, D. (1996). HIV-1 dynamics in vivo: virion clearance rate, infected cell life-span, and viral generation time. *Science*, 271(5255):1582–6. (Cited on pages 28, 29, 31, 34, 35, 36, 38, 44, 45, 46, 47, and 111.)

Perelson, A. S., Kirschner, D. E., and De Boer, R. (1993). Dynamics of HIV infection of CD4+ T cells. *Math Biosci*, 114(1):81–125. (Cited on page 5.)

Perelson, A. S. and Wiegel, F. W. (2009). Scaling aspects of lymphocyte trafficking. *J Theor Biol*, 257(1):9–16. (Cited on page 117.)

Peters, R. H. (1983). *The Ecological Implications of Body Size*. Cambridge University Press, Cambridge. (Cited on page 116.)

Peut, V. and Kent, S. (2006). Fitness constraints on immune escape from HIV: Implications of envelope as a target for both HIV-specific T cells and antibody. *Curr HIV Res*, 4(2):191–7. (Cited on pages 66 and 79.)

Phillips, A. (1996). Reduction of HIV concentration during acute infection: independence from a specific immune response. *Science*, 271(5248):497–9. (Cited on page 72.)

Phillips, R., Rowland-Jones, S., Nixon, D., Gotch, F., Edwards, J., Ogunlesi, A., Elvin, J., Rothbard, J., Bangham, C., Rizza, C., and et al. (1991). Human immunodeficiency virus genetic variation that can escape cytotoxic T cell recognition. *Nature*, 354(6353):453–9. (Cited on pages 4, 66, and 84.)

Piatak, Jr, M., Saag, M., Yang, L., Clark, S., Kappes, J., Luk, K., Hahn, B., Shaw, G., and Lifson, J. (1993). High levels of HIV-1 in plasma during all stages of infection determined by competitive PCR. *Science*, 259(5102):1749–54. (Cited on page 96.)

Pircher, H., Moskophidis, D., Rohrer, U., Burki, K., Hengartner, H., and Zinkernagel, R. M. (1990). Viral escape by selection of cytotoxic T cell-resistant virus variants in vivo. *Nature*, 346(6285):629–633. (Cited on page 4.)

Press, W. H., Teukolsky, S. A., Vetterling, W. T., and Flannery, B. P. (1992). *Numerical Recipes in C: The Art of Scientific Computing*. Cambridge University Press, New York, NY, USA. (Cited on page 78.)

R Development Core Team (2005). *R: A Language and Environment for Statistical Computing*. R Foundation for Statistical Computing, Vienna, Austria. ISBN 3-900051-07-0. (Cited on page 53.)

Ramratnam, B., Bonhoeffer, S., Binley, J., Hurley, A., Zhang, L., Mittler, J., Markowitz, M., Moore, J., Perelson, A., and Ho, D. (1999). Rapid production and clearance of HIV-1 and hepatitis C virus assessed by large volume plasma apheresis. *Lancet*, 354(9192):1782–5. (Cited on pages 28, 30, 31, 39, 68, 87, 107, and 109.)

Ramratnam, B., Mittler, J., Zhang, L., Boden, D., Hurley, A., Fang, F., Macken, C., Perelson, A., Markowitz, M., and Ho, D. (2000). The decay of the latent reservoir of replication-competent HIV-1 is inversely correlated with the extent of residual viral replication during prolonged anti-retroviral therapy. *Nat Med*, 6(1):82–5. (Cited on page 20.)

Reddy, B. and Yin, J. (1999). Quantitative intracellular kinetics of HIV type 1. *AIDS Res Hum Retroviruses*, 15(3):273–83. (Cited on pages 7, 12, 22, 24, and 37.)

Regoes, R., Yates, A., and Antia, R. (2007). Mathematical models of cytotoxic T-lymphocyte killing. *Immunol Cell Biol*, 85(4):274–9. (Cited on pages 37, 73, and 77.)

Regoes, R. R., Crotty, S., Antia, R., and Tanaka, M. M. (2005). Optimal replication of poliovirus within cells. *Am Nat*, 165(3):364–373. (Cited on page 12.)

Regoes, R. R., Wodarz, D., and Nowak, M. A. (1998). Virus dynamics: the effect of target cell limitation and immune responses on virus evolution. *J Theor Biol*, 191(4):451–462. (Cited on page 6.)

Reilly, C., Wietgrefe, S., Sedgewick, G., and Haase, A. (2007). Determination of simian immunodeficiency virus production by infected activated and resting cells. *AIDS*, 21(2):163–168. (Cited on pages 28, 29, and 38.)

Ribeiro, R. M. and Bonhoeffer, S. (1999). A stochastic model for primary HIV infection: optimal timing of therapy. *AIDS*, 13(3):351–357. (Cited on page 6.)

Rong, L., Feng, Z., and Perelson, A. S. (2007). Mathematical analysis of age-structured HIV-1 dynamics with combination antiretroviral therapy. *SIAM Journal on Applied Mathematics*, 67(3):731–756. (Cited on page 28.)

Sacha, J., Chung, C., Rakasz, E., Spencer, S., Jonas, A., Bean, A., Lee, W., Burwitz, B., Stephany, J., Loffredo, J., Allison, D., Adnan, S., Hoji, A., Wilson, N., Friedrich, T., Lifson, J., Yang, O., and Watkins, D. (2007a). Gag-specific CD8+ T lymphocytes recognize infected cells before AIDS-virus integration and viral protein expression. *J Immunol*, 178(5):2746–54. (Cited on pages 92, 96, 98, 99, 104, 105, 106, and 114.)

Sacha, J. B., Chung, C., Reed, J., Jonas, A. K., Bean, A. T., Spencer, S. P., Lee, W., Vojnov, L., Rudersdorf, R., Friedrich, T. C., Wilson, N. A., Lifson, J. D., and Watkins, D. I. (2007b). Pol-specific CD8+ T cells recognize simian immunodeficiency virus-infected cells prior to Nef-mediated major histocompatibility complex class I downregulation. *J Virol*, 81(21):11703–11712. (Cited on pages 96, 98, 99, 104, 105, 106, and 114.)

Sacha, J. B., Reynolds, M. R., Buechler, M. B., Chung, C., Jonas, A. K., Wallace, L. T., Weiler, A. M., Lee, W., Piaskowski, S. M., Soma, T., Friedrich, T. C., Wilson, N. A., and Watkins, D. I. (2008). Differential antigen presentation kinetics of CD8+ T-cell epitopes derived from the same viral protein. *J Virol*, 82(18):9293–9298. (Cited on page 106.)

Sahaf, B., Atkuri, K., Heydari, K., Malipatlolla, M., Rappaport, J., Regulier, E., Herzenberg, L. A., and Herzenberg, L. A. (2008). Culturing of human peripheral blood cells reveals unsuspected lymphocyte responses relevant to

HIV disease. *Proc Natl Acad Sci U S A*, 105(13):5111–5116. (Cited on pages 18 and 21.)

Sato, H., Orenstein, J., Dimitrov, D., and Martin, M. (1992). Cell-to-cell spread of HIV-1 occurs within minutes and may not involve the participation of virus particles. *Virology*, 186(2):712–724. (Cited on page 93.)

Savage, V. M., Allen, A. P., Brown, J. H., Gillooly, J. F., Herman, A. B., Woodruff, W. H., and West, G. B. (2007). Scaling of number, size, and metabolic rate of cells with body size in mammals. *Proc Natl Acad Sci U S A*, 104(11):4718–4723. (Cited on page 116.)

Scheppler, J., Nicholson, J., Swan, D., Ahmed-Ansari, A., and McDougal, J. (1989). Down-modulation of MHC-I in a CD4+ T cell line, CEM-E5, after HIV-1 infection. *J Immunol*, 143(9):2858–66. (Cited on pages 96 and 98.)

Schmidt-Nielsen, K. (1984). *Scaling, Why Is Animal Size So Important?* Cambridge University Press, Cambridge. (Cited on page 116.)

Schmitz, J., Kuroda, M., Santra, S., Sasseville, V., Simon, M., Lifton, M., Racz, P., Tenner-Racz, K., Dalesandro, M., Scallon, B., Ghrayeb, J., Forman, M., Montefiori, D., Rieber, E., Letvin, N., and Reimann, K. (1999). Control of viremia in simian immunodeficiency virus infection by CD8+ lymphocytes. *Science*, 283(5403):857–60. (Cited on pages 66, 96, 104, and 105.)

Schroder, A. R. W., Shinn, P., Chen, H., Berry, C., Ecker, J. R., and Bushman, F. (2002). HIV-1 integration in the human genome favors active genes and local hotspots. *Cell*, 110(4):521–529. (Cited on page 18.)

Schwartz, O., Marechal, V., Le Gall, S., Lemonnier, F., and Heard, J. (1996). Endocytosis of major histocompatibility complex class I molecules is induced by the HIV-1 Nef protein. *Nat Med*, 2(3):338–42. (Cited on page 96.)

Sedaghat, A. R., Siliciano, R. F., and Wilke, C. O. (2008). Low-level HIV-1 replication and the dynamics of the resting CD4+ T cell reservoir for HIV-1 in the setting of HAART. *BMC Infect Dis*, 8:2. (Cited on pages 13 and 22.)

Siliciano, J., Kajdas, J., Finzi, D., Quinn, T., Chadwick, K., Margolick, J., Kovacs, C., Gange, S., and Siliciano, R. (2003). Long-term follow-up studies confirm the stability of the latent reservoir for HIV-1 in resting CD4+ T cells. *Nat Med*, 9(6):727–8. (Cited on pages 12, 13, and 20.)

Stevenson, M., Stanwick, T. L., Dempsey, M. P., and Lamonica, C. A. (1990). HIV-1 replication is controlled at the level of T cell activation and proviral integration. *EMBO J*, 9(5):1551–1560. (Cited on page 21.)

Strain, M., Gunthard, H., Havlir, D., Ignacio, C., Smith, D., Leigh-Brown, A., Macaranas, T., Lam, R., Daly, O., Fischer, M., Opravil, M., Levine, H., Bacheler, L., Spina, C., Richman, D., and Wong, J. (2003). Heterogeneous clearance rates

of long-lived lymphocytes infected with HIV: intrinsic stability predicts lifelong persistence. *Proc Natl Acad Sci U S A*, 100(8):4819–24. (Cited on pages 13 and 18.)

Strain, M., Little, S., Daar, E., Havlir, D., Gunthard, H., Lam, R., Daly, O., Nguyen, J., Ignacio, C., Spina, C., Richman, D., and Wong, J. (2005). Effect of treatment, during primary infection, on establishment and clearance of cellular reservoirs of HIV-1. *J Infect Dis*, 191(9):1410–8. (Cited on page 18.)

Swigut, T., Alexander, L., Morgan, J., Lifson, J., Mansfield, K., Lang, S., Johnson, R., Skowronski, J., and Desrosiers, R. (2004). Impact of Nef-mediated downregulation of major histocompatibility complex class I on immune response to simian immunodeficiency virus. *J Virol*, 78(23):13335–44. (Cited on pages 96 and 98.)

van Baalen, C., Guillon, C., van Baalen, M., Verschuren, E., Boers, P., Osterhaus, A., and Gruters, R. (2002). Impact of antigen expression kinetics on the effectiveness of HIV-specific cytotoxic T lymphocytes. *Eur J Immunol*, 32(9):2644–52. (Cited on pages 91, 96, 106, and 107.)

Van Stipdonk, M. J., Lemmens, E. E., and Schoenberger, S. P. (2001). Naive CTLs require a single brief period of antigenic stimulation for clonal expansion and differentiation. *Nat. Immunol.*, 2:423–429. (Cited on page 51.)

Vezys, V., Masopust, D., Kemball, C., Barber, D., O'Mara, L., Larsen, C., Pearson, T., Ahmed, R., and Lukacher, A. (2006). Continuous recruitment of naive T cells contributes to heterogeneity of antiviral CD8 T cells during persistent infection. *J Exp Med*, 203(10):2263–2269. (Cited on page 63.)

Volterra, V. (1926). Fluctuations in the abundance of a species considered mathematically. *Nature*, 118:558–560. (Cited on page 4.)

Wallinga, J. and Lipsitch, M. (2007). How generation intervals shape the relationship between growth rates and reproductive numbers. *Proc Biol Sci*, 274(1609):599–604. (Cited on pages 37 and 42.)

Wei, X., Ghosh, S. K., Taylor, M. E., Johnson, V. A., Emini, E. A., Deutsch, P., Lifson, J. D., Bonhoeffer, S., Nowak, M. A., and Hahn, B. H. (1995). Viral dynamics in human immunodeficiency virus type 1 infection. *Nature*, 373(6510):117–122. (Cited on pages 5, 28, 96, and 111.)

Weinberger, L., Burnett, J., Toettcher, J., Arkin, A., and Schaffer, D. (2005). Stochastic gene expression in a lentiviral positive-feedback loop: HIV-1 Tat fluctuations drive phenotypic diversity. *Cell*, 122(2):169–82. (Cited on pages 7, 12, 13, 21, 22, and 24.)

Weinberger, L. and Shenk, T. (2007). An HIV feedback resistor: auto-regulatory circuit deactivator and noise buffer. *PLoS Biol*, 5(1):e9. (Cited on pages 21 and 22.)

Weinberger, L. S., Dar, R. D., and Simpson, M. L. (2008). Transient-mediated fate determination in a transcriptional circuit of HIV. *Nat Genet*, 40(4):466–470. (Cited on page 22.)

West, G. B., Brown, J. H., and Enquist, B. J. (1997). A general model for the origin of allometric scaling laws in biology. *Science*, 276(5309):122–126. (Cited on page 116.)

Wherry, E., Barber, D., Kaech, S., Blattman, J., and Ahmed, R. (2004). Antigen-independent memory CD8 T cells do not develop during chronic viral infection. *Proc Natl Acad Sci U S A*, 101(45):16004–16009. (Cited on page 50.)

Wherry, E., Blattman, J., Murali-Krishna, K., van der Most, R., and Ahmed, R. (2003). Viral persistence alters CD8 T-cell immunodominance and tissue distribution and results in distinct stages of functional impairment. *J Virol*, 77(8):4911–4927. (Cited on pages 50, 51, 53, 54, 57, 59, 61, 62, 63, 64, and 113.)

Wiegel, F. W. and Perelson, A. S. (2004). Some scaling principles for the immune system. *Immunol Cell Biol*, 82(2):127–131. (Cited on page 117.)

Wodarz, D. (2007). *Killer Cell Dynamics: Mathematical and Computational Approaches to Immunology*, volume v. 32 of *Interdisciplinary applied mathematics*. Springer, New York, NY. (Cited on page 6.)

Wodarz, D. and Levy, D. N. (2007). Human immunodeficiency virus evolution towards reduced replicative fitness in vivo and the development of AIDS. *Proc Biol Sci*, 274(1624):2481–2490. (Cited on page 84.)

Wodarz, D. and Thomsen, A. (2005). Does programmed CTL proliferation optimize virus control? *Trends Immunol*, 26(6):305–310. (Cited on page 61.)

Wu, Y. (2004). HIV-1 gene expression: lessons from provirus and non-integrated DNA. *Retrovirology*, 1:13. (Cited on pages 16 and 21.)

Wu, Y. and Marsh, J. W. (2003). Early transcription from nonintegrated DNA in human immunodeficiency virus infection. *J Virol*, 77(19):10376–10382. (Cited on page 21.)

Yang, O. O. and Walker, B. D. (1997). CD8+ cells in human immunodeficiency virus type I pathogenesis: cytolytic and noncytolytic inhibition of viral replication. *Adv Immunol*, 66:273–311. (Cited on page 108.)

Yu, X., Addo, M., Rosenberg, E., Rodriguez, W., Lee, P., Fitzpatrick, C., Johnston, M., Strick, D., Goulder, P., Walker, B., and Altfeld, M. (2002). Consistent patterns in the development and immunodominance of human immunodeficiency virus type 1 (HIV-1)-specific CD8+ T-cell responses following acute HIV-1 infection. *J Virol*, 76(17):8690–701. (Cited on pages 70, 75, and 113.)

Zajac, A., Blattman, J., Murali-Krishna, K., Sourdive, D., Suresh, M., Altman, J., and Ahmed, R. (1998). Viral immune evasion due to persistence of activated T cells without effector function. *J Exp Med*, 188(12):2205–2213. (Cited on pages 50, 52, and 61.)

Zhang, L., Ramratnam, B., Tenner-Racz, K., He, Y., Vesanen, M., Lewin, S., Talal, A., Racz, P., Perelson, A., Korber, B., Markowitz, M., and Ho, D. (1999). Quantifying residual HIV-1 replication in patients receiving combination antiretroviral therapy. *N Engl J Med*, 340(21):1605–13. (Cited on page 20.)

Samenvatting

Infecties kunnen door virussen veroorzaakt worden. Binnen een besmette gastheer kunnen virussen bepaalde cellen aanvallen en zich in deze cellen vermenigvuldigen. Nadat enkele virusdeeltjes zich van de celmembraan hebben losgemaakt, kunnen ze nieuwe cellen besmetten. Het immuunsysteem van de gastheer heeft verschillende afweermechanismen om de replicatie van virussen te voorkomen. De cellulaire immuunreactie kan met zogenoemde cytotoxische T-cellen geïnfecteerde cellen herkennen en dood maken. In dit proefschrift maken we gebruik van wiskundige modellen en computersimulaties om de dynamiek van de viruspopulatie en de cellulaire immuunreactie in een besmette gastheer te beschrijven om een beter inzicht in virusinfecties te krijgen.

Allereerst houden we ons bezig met de kinetiek van HIV-replicatie. Wanneer HIV-geïnfecteerde patiënten met antiretrovirale therapie beginnen, neemt de virusconcentratie in het bloed snel af. Dit is een indicatie dat geïnfecteerde cellen korte tijd leven en één tot twee dagen na de infectie afsterven. Met een nieuwe analyse kunnen we nu laten zien, dat de levensduur van HIV-geïnfecteerde cellen afhankelijk is van de virusproductie en misschien korter is dan tot nu toe aangenomen werd.

Vervolgens analyseren we het verloop van de cellulaire immuunreactie in muizen, die met lymfocytaire choriomeningitis virus (LCMV) besmet zijn. We ontwikkelen verschillende modellen, die de dynamiek van het virus in aanwezigheid van specifieke T-cell reacties beschrijven. Daarbij onderzoeken we het vermogen van de cellulaire immuunreactie om chronische virale infecties onder controle te houden. In het geval van HIV-besmettingen kunnen we laten zien dat de replicatie van het virus sterk verminderd wordt, als cellen direct na hun infectie en nog vóór ze virus produceren door de cytotoxische T-cellen herkend worden. Bij iedere nieuwe infectie van een cel kan het virus zich door mutatie veranderen, zodat de nieuwe geïnfecteerde cellen niet meer herkend en dood gemaakt worden. Dit proces van "immune escape"geeft een indicatie van hoe sterk het virus door het immuunsysteem onderdrukt wordt. Daarom onderzoeken we met modellen hoe vaak en hoe snel deze nieuwe, door het immuunsysteem niet herkenbare virusvarianten opduiken en geselecteerd worden.

In dit proefschrift worden verschillende gastheren behandeld, zoals muizen, makaken en mensen. We bespreken in hoeverre onze inzichten in de invloed van de cellulaire immuunreacties op virale replicatie in deze gastheren gegeneraliseerd kunnen worden. We laten zien dat verschillen gedeeltelijk door allometrie, dat wil zeggen door de relatie tussen biologische processen en de lichaamsgrootte van een soort, te verklaren zijn. Verder onderzoek naar de dynamiek van virussen en cellulaire immuunreacties is nodig, om nauwkeurigere

verklaringen over het verloop van virusinfecties in verschillende soorten van gastheren te kunnen maken.

Zusammenfassung

Infektionen können durch Viren ausgelöst werden, welche innerhalb eines infizierten Wirtes bestimmte Zellen befallen. In diesen Zellen kann sich das Virus vervielfältigen und nachdem sich einzelne Viruspartikel von der Zellmembran gelöst haben, infizieren diese wiederum neue Zellen. Das Immunsystem des Wirtes besitzt jedoch ausgeklügelte Abwehrmechanismen, welche die fortlaufende Vermehrung des Virus unterbinden. Insbesondere die zelluläre Immunantwort kann durch so genannte cytotoxische T-Zellen infizierte Zellen erkennen und abtöten. In dieser Dissertation benutzen wir mathematische Modelle und Computersimulationen, um die Dynamik der Viruspopulation und der zellulären Immunantwort innerhalb eines infizierten Wirtes zu beschreiben, und damit zu einem besseren Verständnis von Virusinfektionen zu gelangen.

Zu Beginn beschäftigen wir uns mit der Kinetik der HIV-Replikation. Schon früh wurde erkannt, dass nach Beginn einer antiretroviralen Therapie in HIV-infizierten Patienten, die Viruslast im Blut rasch abnimmt. Dies liess darauf schliessen, dass infizierte Zellen sehr kurzlebig sind und ein bis zwei Tage nach ihrer Infektion absterben. Mit einer neuen Analyse zeigen wir, dass aufgrund der Kinetik der Virusproduktion, die Lebensdauer von HIV-infizierten Zellen möglicherweise noch kürzer ist als bisher angenommen wurde.

Im Weiteren analysieren wir den zeitlichen Verlauf der zellulären Immunantwort in Mäusen, die mit Lymphozytärem Choriomeningitis Virus (LCMV) infizierten sind. Wir entwickeln verschiedene Modelle, welche die Virusdynamik in Anwesenheit spezifischer T-Zell-Antworten beschreiben und untersuchen dabei die Fähigkeit der zellulären Immunantwort, chronische Virusinfektionen unter Kontrolle zu halten. Im Falle von HIV-Infektionen zeigen wir, dass die Replikation des Virus stark vermindert werden kann, wenn Zellen direkt nach ihrer Infektion und noch bevor sie neues Virus produzieren, von den cytotoxischen T-Zellen erkannt werden. Bei jeder Neuinfektion einer Zelle kann sich das HI-Virus jedoch durch Mutation verändern, sodass die neu infizierten Zellen nicht mehr erkannt und abgetötet werden können. Dieser Prozess des “immune escape” kann Hinweise darauf liefern, wie stark das Virus durch das Immunsystem supprimiert wird. Deshalb untersuchen wir anhand weiterer Modelle wie häufig und wie schnell solche neue, vom Immunsystem nicht erkennbaren Virusvarianten auftauchen und selektiert werden.

Aufgrund der unterschiedlichen Wirtsorganismen wie Mäuse, Makaken und Menschen, welche in dieser Dissertation behandelt werden, stellt sich die Frage, inwiefern sich unsere Erkenntnisse zum Einfluss der zellulären Immunantwort auf die Virusreplikation verallgemeinern lassen. Wir weisen auf Unterschiede hin, welche sich teilweise durch die Allometrie, d.h. aufgrund der Beziehung zwischen biologischen Prozessen und der Körpergrösse einer Spezies, erklären lassen. Weitere detaillierte Untersuchungen zur Dynamik von Viren und der

zellulären Immunantwort sind jedoch notwendig, um genauere Aussagen zum Ausgang von Virusinfektionen in verschiedenen Wirtsspezies machen zu können.

Curriculum Vitæ

The author of this thesis, Christian Lorenz Althaus, was born on November 2nd, 1978 in Wattwil (Switzerland). From 1993 onwards, he attended the Kantonsschule Wattwil where he graduated in 1998 with a Matura typus c (mathematically and scientifically oriented). In October 1998, he started his studies in Biology at the ETH Zurich (Switzerland) with an emphasis on Biochemistry, Immunology and Evolutionary Biology. During the study year of 2002, he spent 5 months at the Humboldt University in Berlin (Germany) as part of an Erasmus exchange programme. He became interested in the field of Theoretical Biology and followed an internship in the group of Prof. Hanspeter Herzel at the Institute for Theoretical Biology. Back at the ETH Zurich, he worked with Prof. Sebastian Bonhoeffer on modeling the effects of recombination in HIV-1 which resulted in his diploma thesis in 2004. After working at the Institute for Ecology & Evolution at the ETH Zurich, he moved to Utrecht (The Netherlands) in 2005 to start his PhD studies in the Theoretical Biology group at Utrecht University, supervised by Prof. Rob J. De Boer. The results of his thesis are described in this book. Currently, the author is working as a postdoctoral fellow at the Institute of Social and Preventive Medicine (ISPM) at the University of Bern (Switzerland).

List of Publications

Althaus, C. L. and De Boer, R. J. Intracellular delays and multiple infection of cells impede immune evasion in HIV. *in preparation.*

Althaus, C. L. and De Boer, R. J. Intracellular transactivation of HIV and its influence on the virus dynamics during drug therapy. *under review.*

Althaus, C. L. and De Boer, R. J. CTL killing mediated early during the intracellular eclipse phase explains large variations in HIV set-point levels. *under review.*

Althaus, C. L., De Vos, A.S and De Boer, R. J. Reassessing the human immunodeficiency virus type 1 life cycle through age-structured modeling: lifespan of infected cells, viral generation time and R_0. *J Virol.* in press (2009).

Althaus, C. L. and De Boer, R. J. Dynamics of immune escape during HIV/SIV infection. *PLoS Comput Biol.* 4(7): e1000103 (2008).

Althaus, C. L., Ganusov, V. V. and De Boer, R. J. Dynamics of CD8+ T Cell Responses during Acute and Chronic Lymphocytic Choriomeningitis Virus Infection. *J Immunol.* 179(5): 2944-51 (2007).

Kouyos, R. D., Althaus, C. L. and Bonhoeffer, S. Stochastic or deterministic: what is the effective population size of HIV? *Trends Microbiol.* 14(12): 507-11 (2006).

Althaus, C. L. and Bonhoeffer, S. Stochastic Interplay between Mutation and Recombination during the Acquisition of Drug Resistance Mutations in Human Immunodeficiency Virus Type 1. *J Virol.* 79(21): 13572-8 (2005).

Bretscher, M. T., Althaus, C. L., Müller, V. and Bonhoeffer, S. Recombination in HIV and the evolution of drug resistance: for better or for worse? *Bioessays.* 26(2): 180-8 (2004).